Non-Abelian Anyons in the Kitaev Honeycomb Model

Ahmet Tuna Bölükbaşı

M.Sc.

NUI MAYNOOTH

Ollscoil na hÉireann Má Nuad

Thesis presented for the degree of

Doctor of Philosophy

to the

Mathematical Physics Department

Faculty of Science

National University of Ireland Maynooth

Research Supervisor

Dr. Jiri Vala

October 2010

To my parents

TABLE OF CONTENTS

ACKNOWLEDGMENTS

First of all, I would like to thank Jiri Vala, who has been my supervisor for the past four years, for his expert guidance, generous support and advices he has given me. Also, I would like to thank Graham Kells for providing inspiring and enlightening discussions, and for sharing his enthusiasm to physics with us. I would like to express my utmost appreciation to Niall Moran for his countless helps over programming without him this work would not have been possible. I would like to thank the members of my thesis defense committee: Daniel M. Heffernan for his guidance and support and Steve Simon for his very valuable comments and inspiring discussions. I would like to recognize the hard work and affability of Daniel M. Heffernan, Jon-Ivar Skullerud and Monica Harte for the smooth running of the department.

ABSTRACT

The non-Abelian Berry phase is an essential feature of non-Abelian anyons for the realization of topological quantum computation. This thesis is primarily a study about the numerical calculation of the Berry phase of non-Abelian anyons in the Kitaev honeycomb lattice model. It is also a guide for experimental the realizations of the actual brading process.

We give an introduction to the theory of non-Abelian anyons, briefly discussing in what kind of systems they are realized, and their possible use in topological quantum computation. Non-Abelian anyons are studied within the Kitaev honeycomb model where they are realized on the plaquettes of the honeycomb lattice. The Kitaev honeycomb model can be solved exactly by using various fermionization methods. In this thesis, we review a solution based on Jordan-Wigner types of fermions which transform Hamiltonian to a fermionic quadratic form. This kind of fermionization procedure is quite general and can be applied to any trivalent spin lattice models. Moreover, we introduce Hartree-Fock-Bogoliubov method to solve general quadratic fermionic Hamiltonian and employ Bloch-Messiah theorem in order to write ground state wave function explicitly. Later, we apply these methods to honeycomb model and study the eigenstates of the model so that we can do the Berry phase calculation. The final chapter explains the details of the numerical calculation of the non-Abelian Berry phase. First, we show how to create and adiabatically move vortices in the honeycomb model. A brief review of the Berry phase is given including some discussion about a numerical approach. Later on Thouless' representation of the ground state is introduced to calculate the Berry phase. All these theoretical tools are applied to a 4 vortex configuration of the model to calculate the non-Abelian Berry phase of the system on a particular path in the parameter space.

Chapter 1

INTRODUCTION

In the chapters of quantum mechanics textbooks about identical particles [1, 2, 3, 4, 5], we encounter the arguments about how permuting the position of identical particles affects the wavefunction of the systems. Although there are a couple of different approaches in these books, in its simplest form the argument is the following: We first consider a system with N identical particles located at $r_1, r_2, ..., r_N$, and assume that swapping the positions of two particles twice P^2 does not change the wavefunction $\psi(r_1, r_2, ..., r_N)$ of the system:

$$\begin{aligned} P^2\psi(r_1, r_2, ..., r_N) &= \psi(r_1, r_2, ..., r_N) \\ P &= \pm I \end{aligned} \tag{1.1}$$

where I is the identity operator.Thus, the state functions can be either symmetric or antisymmetric with respect to the interchange of two particles. If it is symmetric then the particles are called bosons. Otherwise, they are called fermions. Although the physical consequences of this postulate were in good agreement with the experiment, there were attempts [6, 7, 8] to make theory clearer with the experimental meaning of symmetrization postulate.

Leinass and Myrheim approached [9] the problem from the quantization of the configuration space of the system and showed that the options are not restricted to bosons and fermions for 2D systems and could be any phase $e^{i\theta}$

$$P\psi(r_1, r_2, ..., r_N) = e^{i\theta}\psi(r_1, r_2, ..., r_N).$$

Later, Wilczek came across a similar kind of statistics within Aharonov-Bohm types of interaction and named these particles anyons (any-on).

A simplified version of the Leinass-Myrheim approach is the following: First, we define the configuration space $\mathcal{C}_N$ of N identical particles living on a spatial manifold $\mathcal{M}$ as

$$\mathcal{C}_N = \frac{\mathcal{M}^N \setminus \mathcal{D}}{S_N},$$

where the singular configurations $\mathcal{D}$, in which two or more particles coincide, are excluded and the quotient space of $\mathcal{M}^N \setminus \mathcal{D}$ is taken by the permutation group S_N to account for the indistinguishability of the particles.

After this configuration space is quantized via the path-integral formalism, it is not too difficult to show a one-to-one correspondence between the unitary irreducible representation (UIR) of the first homotopy group $\pi_1(\mathcal{C}_N)$ of the configuration space and the possible types of anyonic statistics [10]. These groups are known as $\pi_1(\mathcal{C}_N) = S_N$, permutation group, for 3 or higher dimensional manifolds $\mathcal{M}$, and $\pi_1(\mathcal{C}_N) = B_N$, braid group, for 2 dimensional manifolds $\mathcal{M}$ [11]. Both B_N and S_N are generated by $N-1$ generators $\mathcal{T}_1, ..., \mathcal{T}_{N-1}$, obeying the constraints

$$\mathcal{T}_i\mathcal{T}_j = \mathcal{T}_j\mathcal{T}_i, \qquad |i-j| \geq 2, \tag{1.2}$$

$$\mathcal{T}_i\mathcal{T}_{i+1}\mathcal{T}_i = \mathcal{T}_{i+1}\mathcal{T}_i\mathcal{T}_{i+1}. \tag{1.3}$$

Note that the generator $\mathcal{T}_i$ corresponds to an interchange of particles at i and $i+1$. The difference between B_N and S_N arises from the fact that for S_N, we require

$$\mathcal{T}_i^2 = 1 \tag{1.4}$$

in addition to the Eqs. 1.2 and 1.3. Although B_N is a group of infinitely many elements, the inclusion of Eq. 1.4 reduces the number of elements of S_N to $N!$.

From the particle statistics point of view, note that the process of interchanging two particles twice is topologically equivalent to the process of taking one particle around the other. In three dimensions, this process is topologically equivalent to a process in which none of the particles move at all, the wave function should be left unchanged by such two interchanges of particles. This again brings us to the standard textbook arguments given in Eq. 1.1. However, in two dimensions, a particle loop that

encircles another particle cannot be deformed to a point, so that the wave function does not necessarily come back to the same state.

There are two one-dimensional UIRs for S_N: The trivial representation 1 (for both odd and even permutation) corresponding to bosonic statistics and the anti-symmetric representation ∓ 1 (-1 for odd permutation and +1 for even permutation) corresponding to fermionic statistics. Multi-dimensional representations of S_N give rise to what is known as "parastatistics" [12]; however, it has been shown that parastatistics can be replaced by bosonic and fermionic statistics, if a hidden degree of freedom is introduced [13].

One-dimensional UIRs of the braid group B_N are labeled by an angular parameter $\theta \in [0, 2\pi)$, and they are defined by assigning the same phase factor to all generators. That is

$$\mathcal{T}_j \to e^{i\theta}$$

for all $j \in 1, ..., n-1$. These representations are Abelian since the order of braiding operations is unimportant. Note that the case $\theta = 0$ corresponds to bosons and $\theta = \pi$ corresponds to fermions.

Moreover, multi-dimensional irreducible representations of the braid group are possible and give rise to non-Abelian statistics. One of the necessary conditions for the realization of non-Abelian statistics for a systems with N well separated identical particles located at $r_1, r_2, ..., r_N$ is a D dimensional degenerate space separated by a gap from excited levels. The nature of this degenerate space is different from that of symmetry related degeneracies. More details will be given about the nature of this degenerate space later on; however note that the dimension of the degenerate space is only related to the number and types of these identical particles. The elements $\mathcal{T}_i$ of the braid group are represented by $D \times D$ unitary matrices

$$\mathcal{T}_i \to U(\mathcal{T}_i)$$

acting on the degenerate space for all $i \in 1, ..., N-1$. Since these matrices do not commute with each other, the representation is non-Abelian and the particles are called non-Abelian anyons.

The degenerate space is very special in a sense that the only way to make nontrivial operations on this space is realized by braiding the particles with each other. That is, the system is immune to any local perturbations or fluctuations that do not exceed the gap. This feature makes it very valuable for storing and processing information.

On the other hand, the statistics of several anyons combined together are again richer than that of fermionic-bosonic types. Bringing two particles together is called fusion and is denoted by the symbol $\times$. For example, two identical Abelian anyons with statistical phases $\theta = \pi/m$ combined together can be thought of as an anyon with a statistical phases $4\theta = 4\pi/m$.

Although the outcome of the fusion process for Abelian anyons is uniquely determined, non-Abelian anyons could have multiple fusion possibilities or channels. Fusion of two non-Abelian anyons of type a and b is usually written as

$$a \times b = \sum_c N_{ab}^c c$$

where the fusion multiplicities N_{ab}^c are non-negative integers which indicate the number of different ways the charges a and b can be combined to produce the charge c. For non-Abelian anyons, there is at least one a, b such that there is more than one fusion channel c with $N_{ab}^c \neq 0$. The different fusion channels are one way of accounting for the degenerate multi-particle states.

As an example, consider a simple model, the so called "Ising model", whose anyons are denoted by 1, σ and ϵ [14, 15]. Note that 1 is a trivial anyon or a vacuum. These anyons have the following fusion rules:

$$\sigma \times \sigma = 1 + \epsilon, \quad \sigma \times \epsilon = \sigma, \quad \epsilon \times \epsilon = 1,$$
$$1 \times 1 = 1, \quad 1 \times \sigma = \sigma, \quad 1 \times \epsilon = \epsilon.$$

The model is non-Abelian since two σ particles can fuse in two different ways. Consider a system with 4 well separated σs (A,B,C and D) which fuse together to give 1. That means if any of two σs (say A and B) fuse together, the fusion channel of the other two σs (C and D) is determined too. Because A and B can fuse in two different

ways, there is a two dimensional space associated with these 4 σs. It is possible to choose a basis based on the fusion result of A and B. On the other hand, another basis can be chosen based on the fusion of result A and C. The matrix parameterizing this basis change is called the $F-$matrix. It is analogous to the $6j$ symbols encountered in the couplings of three spin$-1/2$ particles.

Note also that braiding particles with each other does not change their fusion channel since their total charge (or fusion channel) can be measured along a far distant loop enclosing the two particles. The only way to change their fusion channels is to braid them with a third anyon. Therefore, when two particles fuse in a particular channel (rather than a linear superposition of channels), the effect of taking one particle around the other is just multiplication by a phase. For the Ising model, these overall phases are as follows [15]:

$$R^1_{\sigma\sigma} = e^{-i\pi/8}, \qquad R^\epsilon_{\sigma\sigma} = e^{3i\pi/8}$$
$$R^1_{\epsilon\epsilon} = 1, \qquad R^\sigma_{\sigma\epsilon} = i.$$

where R^z_{xy} is the phase resulting from a counter-clockwise exchange of particles of types x and y which fuse to a particle of type z. In order to fully specify the braiding statistics of a system of anyons, it is necessary to specify (1) the particle species, (2) the fusion rules, (3) the $F-$matrices, and (4) the $R-$matrices. These defining rules has to be consistent with each other by satisfying so called the pentagon and hexagon equations [14].

So far we have only discussed anyons from the mathematical point of view rather than their physical existence in 2D systems. Electrons, protons or atoms are all either fermions or bosons even if they are confined to two dimensions. Localized quasiparticle excitations of these systems could be a candidate for anyonic statistics. Indeed, there are several cases when these quasiparticles have Abelian or non-Abelian statistics [15]. These systems having such quasiparticles are in a topological order which is beyond the Landau symmetry-breaking description [15]. One of the most studied (both theoretically and experimentally) example is found in the fractional quantum hall (FQH) states [16, 17]. The FQH states with filling fraction $\nu = 5/2$ supports

Ising type of anyons; however it is proposed that the other filling fractions supports different types of non-Abelian anyons, too [18, 19, 20]. Together with the FQH states, $p_x + ip_y$ superconductors [21] and the Kitaev honeycomb spin lattice model [14] also support Ising anyons. However, experimental verifications of non-Abelian anyons are still challenging [22].

The studies related to non-Abelian anyons is very important not only for better theoretical and experimental understanding of the subject but also for practical applications in quantum computation [15]. Topological quantum computation (TQC) was suggested by Kitaev more than ten years ago [23] to perform fault tolerant quantum computation. Since then it has attracted the attention of the physicists, mathematicians and computer scientists to the study of non-Abelian anyons [24, 25, 15]. TQC takes advantage of the noise-free nature of the degenerate spaces of non-Abelian anyons to store information. By this way, unwanted interaction between the system and the environment, i.e. decoherence, will be prevented. In addition to that, unitary gates are more precise than any other method of quantum computation since R-matrices and F-matrices are rigid operations due to exactness of topological operations [14]. Therefore, TQC is very suitable for a precise realization of quantum computing operations.

In topological quantum computation, the initialization of the states begins with the creation of anyon pairs from the vacuum so that particle types and their fusion channels are known precisely. Separating anyons gives rise to degenerate space, which is the computational space from quantum computation perspective. Unitary gates of quantum computation are performed via braiding anyons with each other. The measurement process can be done two different ways: It can be performed by fusing anyons and measuring the energy of the state to detect the fusion channel or by an interference experiment. An interference experiment can be performed by first creating a pair of anyons and then sending one of them to the left and the other to the right side of another anyon; the anyonic charge can be detected by finally fusing the pair again and checking the fusion outcome [15].

To find out whether a system supporting non-Abelian anyons, several different approaches can be used. Moore and Read constructed a Moore-Read Pfaffian wave function for FQH states with filling fraction $\nu = 5/2$ by using the connection with conformal field theory, where non-Abelian anyons were first considered [16]. Then, Nayak and Wilczek verified the relation between degeneracy and the number of the quasiparticles of the system by showing that each quasiparticle carries a zero energy Majorana fermion [17]. Later on, this kind of Majorana fermion-quasiparticles were discovered within the p_x+ip_y superconductors context by Read and Green [21]. Ivanov revealed the statistics of its quasiparticles by using the transformation properties of the order parameters of $p_x + ip_y$ superconductors under adiabatic exchange [26]. In that way, an explicit matrix representation was given to braid group elements σ_i. Also, the braiding matrices are obtained by numerically computing the Berry integrals for the given wave functions for FQH states with filling fraction $\nu = 5/2$ [27]. On the other hand, Kitaev used a Chern number argument to show the honeycomb model supports non-Abelian anyons. The argument is that if the Chern number of the model is odd, then each vertex of the honeycomb model carries a zero energy Majorana mode [14].

Note that the essential element of the anyonic statistics is braiding. The physical process of braiding has to be adiabatic [15]. While taking one particle around another, the wave function acquires a dynamical phase depending on the time scale of the process and a Berry phase which is independent of the time. The Berry phase depends on the geometry of the path traversed (usually the area enclosed by) and the topology of the loop. If the topological part is non-zero then particles are anyons. The Berry phase is the representation of the braid group element of the corresponding motion. It is just a phase factor for Abelian anyons, since there is no degenerate space. However, for non-Abelian anyons, it is a unitary matrix whose size is the dimension of the degenerate space. Although the topological part of non-Abelian Berry phase is the most explicit way of showing the statistics of non-Abelian anyons, it requires more information about the system than any other indirect verifications. To be able to calculate

the Berry phase of a system, one first needs the position coordinate representation of its ground state. Among all non-Abelian supporting models, the Kitaev honeycomb model is the most appropriate system for this purpose. Although Kitaev's original solution has several complications, the model has several other solutions [28, 29, 30]. One of them provides an appropriate framework to calculate the Berry phase [31]. In this thesis, we are going to follow this approach to calculate the non-Abelian Berry phase of vortices of the honeycomb model by using numerical tools.

In the following chapter, all the essential parts of this appropriate solution will be reviewed together with relevant details about the Berry phase calculation. The chapter starts with a brief review of the honeycomb model and continues with the introduction of fermions within the model. This kind of fermionization procedure is quite general and can be applied to any trivalent spin lattice model. This method reduces the Hamiltonian into its quadratic fermionic form for a selected vortex configuration. Moreover, we will introduce the Hartree-Fock-Bogoliubov method to solve a general quadratic fermionic Hamiltonian and use the Bloch-Messiah theorem to write the ground state wave function explicitly. The chapter continues with the application of these methods to the honeycomb model and some discussion about the eigenstates of the model relevant to the Berry phase calculation.

Third chapter explains the detail of the numerical calculation of non-Abelian Berry phase. First, we will show how to create and adiabatically move vortices in the honeycomb model. Then, a brief review of the Berry phase will be given including some insight about numerical approaches. Later on, Thouless' representation of the ground state will be introduced. Although the Bloch-Messiah representation of the wave function is essential to work with the honeycomb model, we need Thouless' representation of the ground state to calculate the Berry phase. All these theoretical tools will be applied to a 4 vortex configuration of the model to calculate non-Abelian Berry phase of the system for a particular path.

This kind of Berry phase calculation can be used for any quadratic fermionic Hamiltonian and is easily applicable to other trivalent spin lattice models [32, 33]. It

provides an important tool for understanding the statistics of particles and gives us more insight about the nature of the topological order of the system. Moreover, it is an essential guide for the experimental realization of braiding non-Abelian anyons, and hence for topological quantum computation.

Chapter 2

THE KITAEV HONEYCOMB MODEL

The Kitaev honeycomb model [14] is an exactly solvable spin model defined on a hexagonal lattice. It was originally solved by transforming spins into free Majorana fermions. By calculating the Chern number of the model, Kitaev showed that the model supports Ising type non-Abelian anyons in the presence of a weak magnetic field.

Here we will approach the model from the perspective of a different fermionization technique which is more direct and explicit than Majorana fermionization. However, the real advantage of using this technique is in writing the eigenstates explicitly, including the precise description of the vacuum of fermions. In this way, we can calculate the degeneracy of the ground state of the system easily for toroidal configuration, although it is not a straightforward calculation if the Majorana fermionization approach is used. Also we can explicitly show how to braid non-Abelian anyons and calculate their non-Abelian Berry matrix, which is the main result of this thesis and will be discussed in the next chapter. However, in this chapter, we will first introduce this new way of fermionization of the model. Then, we will give an exact expressions for the model's eigenstates.

2.1 The Model

The Kitaev honeycomb model is a spin$-1/2$ lattice model where spins are located on the vertices of a honeycomb lattice (Fig. 2.1) with the following Hamiltonian

$$H = -\sum_{x-\text{links}} J^x_{i,j} K^x_{i,j} - \sum_{y-\text{links}} J^y_{i,j} K^y_{i,j} - \sum_{z-\text{links}} J^z_{i,j} K^z_{i,j} \tag{2.1}$$

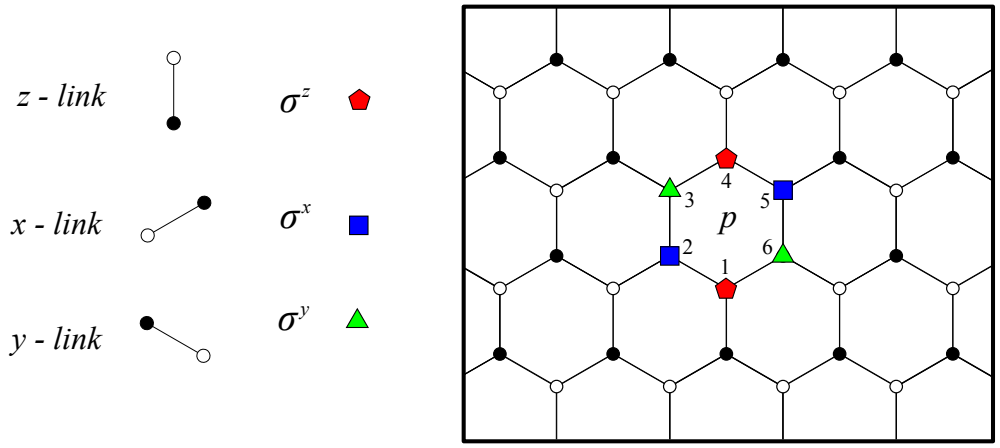

Figure 2.1: Honeycomb Lattice

where i and j are the position indices of the spins, $J_{i,j}$ is the coupling coefficients of the link (i,j), $K^x_{i,j} = \sigma^x_i \sigma^x_j, K^y_{i,j} = \sigma^y_i \sigma^y_j, K^z_{i,j} = \sigma^z_i \sigma^z_j$ and σ_i's are the Pauli operators. Note that the honeycomb lattice is bipartite and different spins are represented as empty and solid circles.

In the presence of a weak magnetic field, the following three-body potential term which breaks the time reversal symmetry is added to Hamiltonian [14];

$$V = -\sum_p \sum_{l=1}^{6} P^l_p \tag{2.2}$$

where p is the index number for each hexagon and P^l_p is

$$\begin{aligned} \sum_{l=1}^{6} P^l_p &= P^1_p + P^2_p + P^3_p + P^4_p + P^5_p + P^6_p \qquad (2.3) \\ &= \kappa^1_p\ \sigma^x_1\sigma^y_6\sigma^z_5 + \kappa^2_p\ \sigma^z_2\sigma^y_3\sigma^x_4 + \kappa^3_p\ \sigma^y_1\sigma^x_2\sigma^z_3 + \kappa^4_p\ \sigma^y_4\sigma^x_5\sigma^z_6 + \kappa^5_p\ \sigma^x_3\sigma^z_4\sigma^y_5 + \kappa^6_p\ \sigma^y_2\sigma^z_1\sigma^x_6. \end{aligned}$$

where κ^l_p is the coupling coefficient of three-body term l in hexagon p (Fig. 2.1). Originally, this term is the third order perturbation term of the magnetic potential

$$V = -\sum_j (h_x\sigma^x_j + h_y\sigma^y_j + h_z\sigma^z_j) \tag{2.4}$$

where $h = (h_x, h_y, h_z)$ is an external magnetic field acting on all spins. Note that κ coefficient is related to $h = (h_x, h_y, h_z)$ as follows

$$\kappa \sim \frac{h_x h_y h_z}{J^2}$$

for $J = J_j^x = J_j^y = J_j^z$ for all j.

The model has a commuting set of operators, called plaquette operators W_p,

$$W_p = \sigma_1^z \sigma_2^x \sigma_3^y \sigma_4^z \sigma_5^x \sigma_6^y = K_{1,2}^y K_{2,3}^z K_{3,4}^x K_{4,5}^y K_{5,6}^z K_{6,1}^x$$

defined for each hexagon p (Fig. 2.1).

These operators commute with each other since they have either no common point or 2 common anti-commuting points:

$$[W_p, W_r] = 0 \text{ for all } p \text{ and } r. \tag{2.5}$$

They also commute with the Hamiltonian since both the Hamiltonian and the plaquette operators are constructed with K operators:

$$[W_p, H] = 0 \text{ for all } p. \tag{2.6}$$

For an N spin system, there are approximately (depending on the boundary conditions) $N/2$ plaquette operators. The eigenvalues of the plaquettes are ± 1. The eigenstates with the eigenvalue -1 are called vortex. The Hilbert space of the system is divided into different sectors based on vortex configurations. The ground state of the system is the vortex-free sector i.e. all the eigenvalues of plaquettes are 1 [34]. Each vortex configuration defines a $2^{N/2}$ dimensional vector space (depending on the boundary conditions) for an N-spin system.

2.2 Effective Spin and Hardcore Boson (ES-HB) Representation

This mapping was originally proposed by Vidal *et al.* [30]; here we will restate the mapping for the sake of completeness. Let $|\uparrow\rangle$ and $|\downarrow\rangle$ denote the eigenstates of σ^z with eigenvalues 1 and -1 respectively. Two spins connected by a $z-$link can be thought

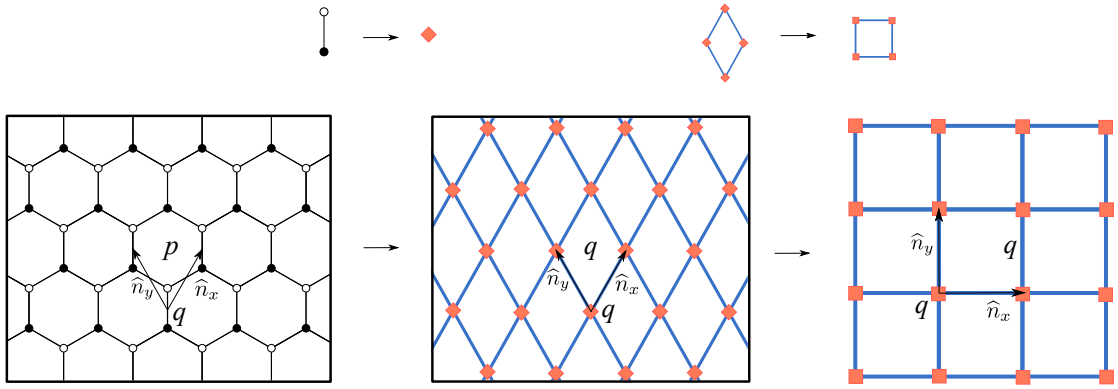

Figure 2.2: Dimers on Honeycomb Lattice: Plaquettes in the square lattice are labeled by the dimer q located at the bottom right of each square.

of as a dimer (Fig. 2.2). Two unit vectors $\widehat{n}_x$ and $\widehat{n}_y$ consist of $z-$link plus $x-$link and $z-$link plus $y-$link respectively. Note that, plaquettes in the square lattice are labeled by the dimer located at the bottom right of each square. Each dimer will have two ferromagnetic states ($|\uparrow_\bullet\uparrow_\circ\rangle$, $|\downarrow_\bullet\downarrow_\circ\rangle$) and two anti-ferromagnetic states ($|\uparrow_\bullet\downarrow_\circ\rangle$, $|\downarrow_\bullet\uparrow_\circ\rangle$), where empty and filled circles represents those spins of $z-$links. While ferromagnetic states can be thought as the eigenstates, $|\Uparrow\rangle = |\uparrow_\bullet\uparrow_\circ\rangle$ and $|\Downarrow\rangle = |\downarrow_\bullet\downarrow_\circ\rangle$, of the effective spin operator, anti-ferromagnetic states can be thought as the occupied or unoccupied states of a hard-core boson. There are various ways to define effective spin and bosonic number operators, but we are going to use the following representation

$$|\uparrow_\bullet\uparrow_\circ\rangle = |\Uparrow, 0\rangle, \qquad |\downarrow_\bullet\downarrow_\circ\rangle = |\Downarrow, 0\rangle,$$
$$|\uparrow_\bullet\downarrow_\circ\rangle = |\Uparrow, 1\rangle, \qquad |\downarrow_\bullet\uparrow_\circ\rangle = |\Downarrow, 1\rangle,$$

and the effective spin operator will take the form

$$\tau^z = \sigma^z_\bullet \otimes I, \quad \tau^x = \sigma^x_\bullet \otimes \sigma^x_\circ, \quad \tau^y = \sigma^y_\bullet \otimes \sigma^x_\circ.$$

Also, the creation, annihilation and number operators of the hard-core boson are defined as follows

$$\begin{aligned} b^\dagger &= \frac{\sigma_\circ^x - i\sigma_\bullet^z\sigma_\circ^y}{2}, \\ b &= \frac{\sigma_\circ^x + i\sigma_\bullet^z\sigma_\circ^y}{2}, \\ N &= b^\dagger b = \frac{I - \sigma_\bullet^z\sigma_\circ^z}{2}. \end{aligned}$$

It is straightforward to verify that these definitions satisfy the anti-commutation relations for each dimer q

$$\{b_q^\dagger, b_q\} = I,$$

and commutation relations for different dimers q and q' $(q \neq q')$

$$[b_q^\dagger, b_{q'}] = [b_q^\dagger, b_{q'}^\dagger] = [b_q, b_{q'}] = 0.$$

Then the Pauli spin operators read

$$\begin{aligned} \sigma_\bullet^x &= \tau^x(b^\dagger + b), & \sigma_\circ^x &= b^\dagger + b, \\ \sigma_\bullet^y &= \tau^y(b^\dagger + b), & \sigma_\circ^y &= i\tau^z(b^\dagger - b), \\ \sigma_\bullet^z &= \tau^z, & \sigma_\circ^z &= \tau^z(I - 2b^\dagger b), \end{aligned} \tag{2.7}$$

and the Hamiltonian can be written as

$$\begin{aligned} H = &-\sum_q J_q^x(b_q^\dagger + b_q)\tau_{q+\widehat{n}_x}^x(b_{q+\widehat{n}_x}^\dagger + b_{q+\widehat{n}_x}) \\ &-\sum_q J_q^y i\tau_q^z(b_q^\dagger - b_q)\tau_{q+\widehat{n}_y}^y(b_{q+\widehat{n}_y}^\dagger + b_{q+\widehat{n}_y}) \\ &-\sum_q J_q^z(I - 2b_q^\dagger b_q). \end{aligned} \tag{2.8}$$

Similarly, P_q^l term of three-body potential V (Eq. 2.2) will have the following form

$$\begin{aligned}
P_q^1 &= \kappa_q^1\ (b_q^\dagger + b_q) i\tau^x_{q+\widehat{n}_x}(b^\dagger_{q+\widehat{n}_x} - b_{q+\widehat{n}_x}) \\
P_q^2 &= \kappa_q^2\ i(b^\dagger_{q+\widehat{n}_y} - b_{q+\widehat{n}_y})\tau^x_{q+\widehat{n}_y+\widehat{n}_x}(b^\dagger_{q+\widehat{n}_y+\widehat{n}_x} + b_{q+\widehat{n}_y+\widehat{n}_x}) \\
P_q^3 &= \kappa_q^3\ \tau^z_q(b_q^\dagger - b_q)\tau^y_{q+\widehat{n}_y}(b^\dagger_{q+\widehat{n}_y} - b_{q+\widehat{n}_y}) \\
P_q^4 &= \kappa_q^4\ \tau^y_{q+\widehat{n}_x+\widehat{n}_y}(b^\dagger_{q+\widehat{n}_x+\widehat{n}_y} + b_{q+\widehat{n}_x+\widehat{n}_y})\tau^z_{q+\widehat{n}_x}(b^\dagger_{q+\widehat{n}_x} + b_{q+\widehat{n}_x}) \\
P_q^5 &= \kappa_q^5\ i(b^\dagger_{q+\widehat{n}_y} + b_{q+\widehat{n}_y})\tau^z_{q+\widehat{n}_y+\widehat{n}_x}\tau^z_{q+\widehat{n}_x}(b^\dagger_{q+\widehat{n}_x} - b_{q+\widehat{n}_x}) \\
P_q^6 &= \kappa_q^6\ \tau^y_{q+\widehat{n}_y}(b^\dagger_{q+\widehat{n}_y} + b_{q+\widehat{n}_y})\tau^z_q(I - 2b_q^\dagger b_q)\tau^x_{q+\widehat{n}_x}(b^\dagger_{q+\widehat{n}_x} + b_{q+\widehat{n}_x}).
\end{aligned}$$

2.3 ES-HB Basis of Hilbert Space

Note that the effective spin operators commute with the hard-core boson operators, and therefore both act on their own Hilbert spaces. By only using effective spin operators, we can define toric code types of plaquette operators [23] as

$$Q_q = \tau^z_q\tau^y_{q+\widehat{n}_x}\tau^y_{q+\widehat{n}_y}\tau^z_{q+\widehat{n}_x+\widehat{n}_y}.$$

It is important to note that these operators commute with each other and the honeycomb plaquette operators are related to them as follows

$$W_q = (I - 2b_q^\dagger b_q)(I - 2b^\dagger_{q+\widehat{n}_y}b_{q+\widehat{n}_y})Q_q.$$

For open boundary conditions, the eigenstates $|\lambda_{N_q}\rangle$ ($\lambda_{N_q} \in \{0,1\}$) of the number operator N_q of a hard-core boson and the eigenstates $|\lambda_{Q_q}\rangle$ ($\lambda_{Q_q} \in \{-1,1\}$) of the Q_q define a basis $B_{Q,N}$ for the full Hilbert space as

$$B_{Q,N} := \left\{ \bigotimes_q |\lambda_{Q_q}\rangle \otimes |\lambda_{N_q}\rangle \,\middle|\, \lambda_{Q_q} \in \{-1,1\}, \lambda_{N_q} \in \{0,1\} \right\}.$$

On the other hand, for the periodic boundary conditions there are constraints on the values of Q_q [30, 35]. Even-by-even lattices are bi-colorable, since their squares can be colored with two different colors consistently in a checkerboard pattern. As a result of this, there are two constraints as follow:

$$\prod_{Q_b \in Blacks} Q_b = 1, \quad \prod_{Q_w \in Whites} Q_w = 1. \tag{2.9}$$

On the other hand, odd by odd or odd by even lattices are not bi-colorable, and they have just one constraint:

$$\prod_i Q_i = 1.$$

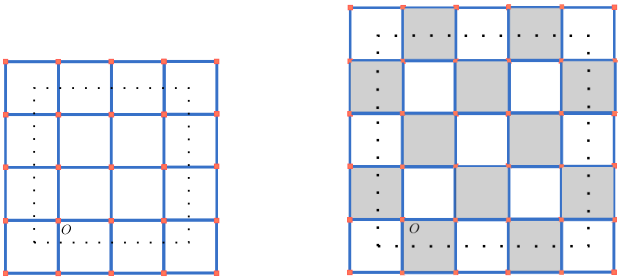

Figure 2.3: (a) Non-colorable lattice. (b) Bi-colorable lattice. The boundaries of the lattice whose opposite sites are identified are given by the dashed lines.

Note that we are only going to work with bi-colorable configurations in this thesis. There are two additional conserved quantities in bi-colorable lattices on torus. These are loop symmetry operators [35] L_x and L_y (Fig. 2.4) which commute with every Q_q and W_q and they are independent[1]. Loop symmetry operators are essential for explaining the degeneracy in toroidal configurations and have fundamental importance in the exact solution of the model.

Together with the constraints (Eq. 2.9), loop symmetry operators L_x, L_y define a basis for systems with periodic boundary condition as

$$B_{Q,N,L} := \left\{ |\lambda_{L_x}, \lambda_{L_y}\rangle \bigotimes_q |\lambda_{Q_q}\rangle \otimes |\lambda_{N_q}\rangle \;\middle|\; \begin{array}{c} \lambda_{N_q} \in \{0,1\}, \\ \lambda_{L_x}, \lambda_{L_y}, \lambda_{Q_q} \in \{-1,1\} \\ \text{satisfying} \\ \prod_{b\in B} \lambda_{Q_b} = 1, \quad \prod_{w\in W} \lambda_{Q_w} = 1 \end{array} \right\} \quad (2.10)$$

where B and W stand for the sets of black and white squares respectively.

[1] Although L_x and L_y can be defined for non-bicolorable lattices, only one of them is independent. This also effects the degeneracy of the system on the torus.

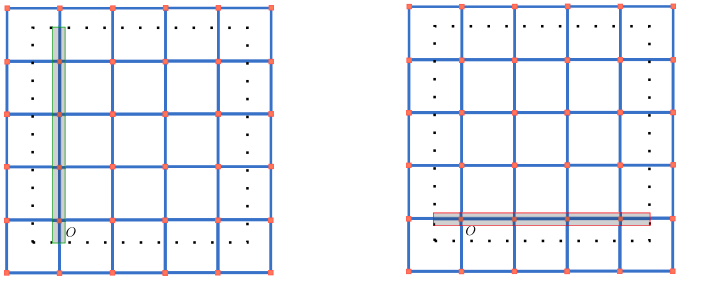

$L_y = \prod \tau^x$ (a)

$L_x = \prod -\tau^x(I - 2b^\dagger b)$ (b)

Figure 2.4: (a) L_y. (b)L_x.

2.4 Jordan-Wigner (J-W) Types of Fermionization of the Model

2.4.1 J-W Types of Fermions

Fermions satisfy the following anti–commutation relations

$$\{c_q^\dagger, c_{q'}\} = \delta_{qq'}, \quad \{c_q^\dagger, c_{q'}^\dagger\} = \{c_q, c_{q'}\} = 0.$$

Hard-core bosons already satisfy same anti-commutation relations when $q = q'$. To make them satisfy the anti-commutation relations when $q \neq q'$, a string of operators ${S'}_q$ should be compounded to them. Following the convention used in [31], we define a coordinate system by choosing a dimer as an origin O from which to start these strings. Each dimer $q = q_x\widehat{n}_x + q_y\widehat{n}_y$ will be represented as its x and y coordinates as $q = (q_x, q_y)$. Note that the coordinate system is chosen in a way that both q_x and q_y are positive integers. For systems with periodic boundary conditions, any dimer can be the origin. For plane configuration, the origin will be a dimer at the edge of the plane.

Before defining the string of operators ${S'}_q$ to be added to hard-core bosons, let's look at another string operator S_q (Fig. 2.5) which is defined between the dimer $q = (q_x, q_y)$ and the origin $O = (1, 1)$. For a dimer located at $q = (q_x, q_y)$ where $q_x \neq 1$ and $q_y \neq 1$, it consists of three parts. The first part is only the application

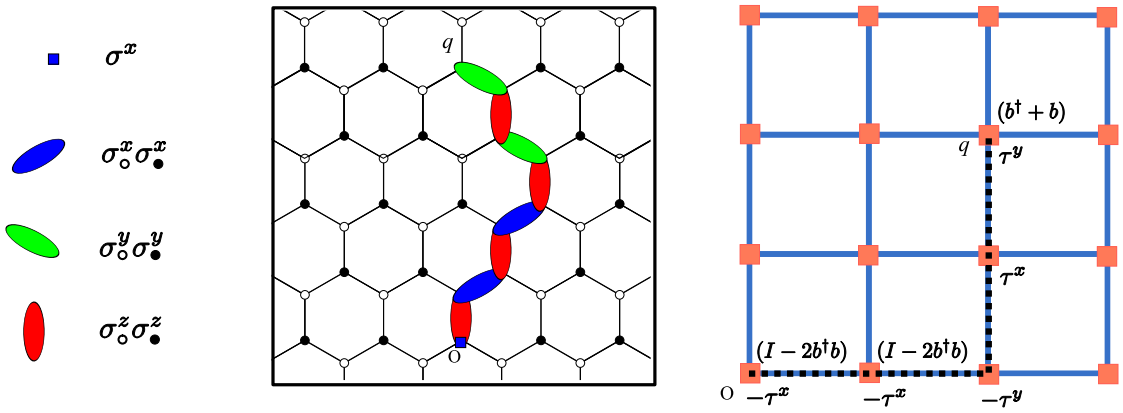

Figure 2.5: String operator S_q

of $\sigma^x_\bullet$ to the $z-$link at the origin. In the second part, $\sigma^z_\circ\sigma^z_\bullet$ and $\sigma^x_\bullet\sigma^x_\circ$ will be applied to $z-$links and $x-$links of the interval $[O, (q_x, 1))$, respectively. Similarly, in the final part $\sigma^y_\bullet\sigma^y_\circ$ and $\sigma^z_\circ\sigma^z_\bullet$ will be applied to $y-$links and $z-$links of the interval $[(q_x, 1), (q_x, q_y))$, respectively. If $q_x \neq 1$ and $q_y = 1$, the third part will be identity I, if $q_x = 1$ and $q_y \neq 1$, the second part will be I, and if $q_x = 1$ and $q_y = 1$, then both the second and the third part will be identity.

Explicitly, the string operators S_q will have the following forms in terms of the Pauli spin operators. For a dimer at (q_x, q_y) where $q_x \neq 1$ and $q_y \neq 1$

$$\begin{aligned} S_q \;=\; & \sigma^y_{(q_x,q_y),\bullet}\sigma^y_{(q_x,q_y-1),\circ}\sigma^z_{(q_x,q_y-1),\circ} \\ & \ldots\sigma^y_{(q_x,2),\bullet}\sigma^y_{(q_x,1),\circ}\sigma^z_{(q_x,1),\circ}\sigma^x_{(q_x,1),\bullet} \\ & \ldots\sigma^x_{(2,1),\bullet}\sigma^x_{(1,1),\circ}\sigma^z_{(1,1),\circ}\sigma^z_{(1,1),\bullet}, \sigma^x_{(q_x,1),\bullet}, \end{aligned}$$

and for a dimer at $(q_x, 1)$ where $q_x \neq 1$

$$\begin{aligned} S_q \;=\; & \sigma^x_{(q_x,1),\bullet}\sigma^x_{(q_x-1,1),\circ}\sigma^z_{(q_x-1,1),\circ}\sigma^z_{(q_x-1,1),\bullet} \\ & \ldots\sigma^x_{(2,1),\bullet}\sigma^x_{(1,1),\circ}\sigma^z_{(1,1),\circ}\sigma^z_{(1,1),\bullet}, \sigma^x_{(q_x,1),\bullet}, \end{aligned}$$

and for a dimer at $(1, q_y)$ where $q_y \neq 1$

$$\begin{aligned} S_q &= \sigma^y_{(1,q_y),\bullet}\sigma^y_{(1,q_y-1),\circ}\sigma^z_{(1,q_y-1),\circ} \\ &\quad ...\sigma^y_{(1,2),\bullet}\sigma^y_{(1,1),\circ}\sigma^z_{(1,1),\circ}\sigma^z_{(1,1),\bullet}\sigma^x_{(q_x,1),\bullet}, \end{aligned}$$

and for the dimer at $(1, 1)$

$$S_q = \sigma^x_{(1,1),\bullet}.$$

Note that in each case, the Pauli operator applied to the end point is either $\sigma^y_\bullet$ or $\sigma^x_\bullet$. By using the transformations (Eq. 2.7), S_q can be written as

$$S_q = (b^\dagger_q + b_q)S'_q,$$

where S'_q is the operator to be added to each hard-core boson to create fermions and has the following form

$$S'_q = S'_{(q_x,q_y)} = \begin{cases} \tau^y_q S_{(q_x,q_y-1)} & if \quad q_y \neq 1 \\ \tau^x_q S_{(q_x-1,q_y)} & if \quad q_y = 1 \end{cases}$$

Notice that $S^2_q = (S'_q)^2 = I$, and for $q \neq q'$ they satisfy

$$\{S_q, S_{q'}\} = 0 \text{ and } \{S'_q, S'_{q'}\} = 0.$$

Finally, we can define fermionic creation and annihilation operators as following

$$c^\dagger_q := b^\dagger_q S'_q, \qquad c_q := b_q S'_q,$$

we can easily verify that

$$\{c^\dagger_q, c_{q'}\} = \delta_{q,q'}, \qquad \{c^\dagger_q, c^\dagger_{q'}\} = \{c_q, c_{q'}\} = 0.$$

2.4.2 Periodic Boundary Conditions

In this section, we will work with a finite size system $N_x \times N_y$ (N_x and N_y are even) with periodic boundary condition. It is worthwhile to transform the Hamiltonian (Eq. 2.8) into its fermionic representation. To do that it would be handy to list some basic properties satisfied by fermions and hard-core bosons.

First of all, notice that the attached string operator S'_q commutes with the creation and annihilation operators of the hard-core bosons

$$[b_q^\dagger, S'_q] = [b_q, S'_q] = 0$$

so that

$$b_q^\dagger = c_q^\dagger S'_q = S'_q c_q^\dagger, \qquad b_q = c_q S'_q = S'_q c_q.$$

By taking into account of the following simple algebraic relations

$$\begin{aligned}
(b^\dagger + b)^2 &= I, \qquad (b^\dagger - b)^2 = -I, \qquad (I - 2b^\dagger b)^2 = I, \\
(c^\dagger + c)^2 &= I, \qquad (c^\dagger - c)^2 = -I, \qquad (I - 2c^\dagger c)^2 = I,
\end{aligned}$$

$$\begin{aligned}
(b^\dagger + b)(I - 2b^\dagger b) &= (b^\dagger - b), \qquad (c^\dagger + c)(I - 2c^\dagger c) = (c^\dagger - c), \\
(I - 2b^\dagger b)(b^\dagger + b) &= -(b^\dagger - b), \quad (I - 2c^\dagger c)(c^\dagger + c) = -(c^\dagger - c),
\end{aligned}$$

$$(I - 2b^\dagger b) = (I - 2c^\dagger c),$$

we can write the fermionic representation of the Hamiltonian (Eq. 2.8) as

$$\begin{aligned}
H &= \sum_q J_q^x X_q (c_q^\dagger - c_q)(c_{q+\widehat{n}_x}^\dagger + c_{q+\widehat{n}_x}) \\
&\quad + \sum_q J_q^y Y_q (c_q^\dagger - c_q)(c_{q+\widehat{n}_y}^\dagger + c_{q+\widehat{n}_y}) \\
&\quad + \sum_q J_q^z (2c_q^\dagger c_q - I),
\end{aligned} \tag{2.11}$$

where X and Y are defined as

$$X_{(q_x,q_y)} = \begin{cases}
\prod_{i_y=1}^{q_y-1} W_{(q_x,i_y)} & if \quad q_y \neq 1 \text{ and } q_x \neq N_x \\
-L_x \prod_{i_y=1}^{q_y-1} W_{(q_x,i_y)} & if \quad q_y \neq 1 \text{ and } q_x = N_x \\
1 & if \quad q_y = 1 \text{ and } q_x \neq N_x \\
-L_x & if \quad q_y = 1 \text{ and } q_x = N_x,
\end{cases} \tag{2.12}$$

$$Y_{(q_x,q_y)} = \begin{cases}
1 & if \;\; q_y \neq N_y \\
-L_y \prod_{i_x=1}^{q_x-1} \prod_{i_y=1}^{N_y} W_{(i_x,i_y)} & if \;\; q_y = N_y.
\end{cases}$$

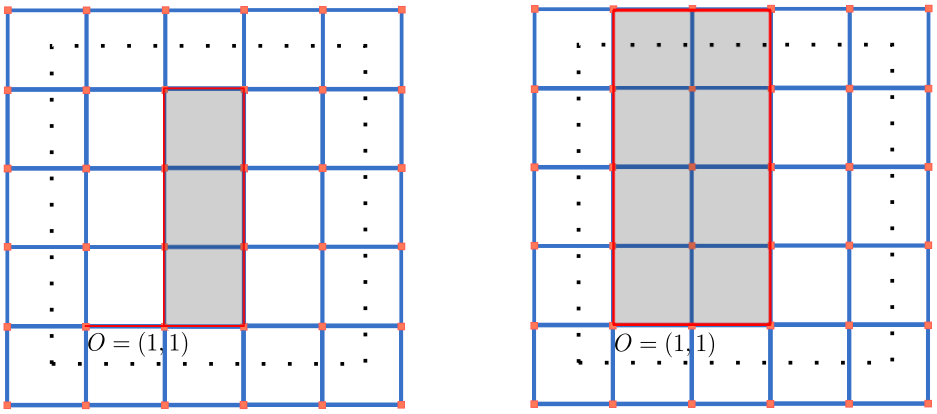

$$X_{(2,4)} = \prod_{i_y=1}^{3} W_{(2,i_y)} \qquad Y_{(3,4)} = -L_y \prod_{i_x=1}^{2} \prod_{i_y=1}^{4} W_{(i_x,i_y)}$$

(a) (b)

Figure 2.6: Examples: (a) $X_{(2,4)}$ and (b) $Y_{(3,4)}$.

Similarly, fermionic representation of P_q^l terms of V will be in the following form:

$$P_q^1 = -\kappa_q^1 \, iX_q(c_q^\dagger - c_q)(c_{q+\widehat{n}_x}^\dagger - c_{q+\widehat{n}_x}) \tag{2.13}$$

$$P_q^2 = -\kappa_q^2 \, iX_{q+\widehat{n}_y}(c_{q+\widehat{n}_y}^\dagger + c_{q+\widehat{n}_y})(c_{q+\widehat{n}_y+\widehat{n}_x}^\dagger + c_{q+\widehat{n}_y+\widehat{n}_x}) \tag{2.14}$$

$$P_q^3 = -\kappa_q^3 \, iY_q(c_q^\dagger - c_q)(c_{q+\widehat{n}_y}^\dagger - c_{q+\widehat{n}_y}) \tag{2.15}$$

$$P_q^4 = -\kappa_q^4 \, iY_{q+\widehat{n}_x}(c_{q+\widehat{n}_x}^\dagger + c_{q+\widehat{n}_x})(c_{q+\widehat{n}_x+\widehat{n}_y}^\dagger + c_{q+\widehat{n}_x+\widehat{n}_y}) \tag{2.16}$$

$$P_q^5 = \kappa_q^5 \, iX_{q+\widehat{n}_y}Y_{q+\widehat{n}_x}(c_{q+\widehat{n}_y}^\dagger - c_{q+\widehat{n}_y})(c_{q+\widehat{n}_x}^\dagger - c_{q+\widehat{n}_x}) \tag{2.17}$$

$$P_q^6 = \kappa_q^6 \, iX_qY_q(c_{q+\widehat{n}_y}^\dagger + c_{q+\widehat{n}_y})(c_{q+\widehat{n}_x}^\dagger + c_{q+\widehat{n}_x}) \tag{2.18}$$

By summing P_q^1 with $P_{q-\widehat{n}_y}^2$, we define $P_q^x := P_q^1 + P_{q-\widehat{n}_y}^2$ as

$$P_q^x := -\kappa_q^x \, i2X_q(c_q^\dagger c_{q+\widehat{n}_x}^\dagger + c_q c_{q+\widehat{n}_x}) \tag{2.19}$$

where $\kappa_q^x = \kappa_q^1 = \kappa_{q-\widehat{n}_y}^2$ and by summing P_q^3 with $P_{q-\widehat{n}_x}^4$, we define $P_q^y := P_q^3 + P_{q-\widehat{n}_x}^4$ as

$$P_q^y := -\kappa_q^y \, i2Y_q(c_q^\dagger c_{q+\widehat{n}_y}^\dagger + c_q c_{q+\widehat{n}_y}) \tag{2.20}$$

where $\kappa_q^y = \kappa_q^3 = \kappa_{q-\widehat{n}_x}^4$. Finally, we can write the V term as

$$V = -\sum_q (P_q^x + P_q^y + P_q^5 + P_q^6). \tag{2.21}$$

2.5 Diagonalization of Quadratic Hamiltonian

2.5.1 General Theory

It is possible to write every quadratic fermionic Hamiltonian in terms of non-interacting free fermions which are linear combinations of the original fermions [36]. Free fermionic systems are exactly solvable in terms of their energy eigenvalues and eigenstates. Before writing our Hamiltonian in terms of free fermions let us go through the general solving method of the quadratic fermionic Hamiltonians.

Every quadratic fermionic Hamiltonian of a system with N fermions can be written in the following form:

$$H = \frac{1}{2}\sum_{jk}\left(\xi_{jk}c_j^\dagger c_k - \xi_{jk}^* c_j c_k^\dagger + \Delta_{jk}c_j c_k - \Delta_{jk}^* c_j^\dagger c_k^\dagger\right),$$

where ξ is Hermitian and Δ is antisymmetric.

It would be handier to use the following representation

$$H = \frac{1}{2}\begin{bmatrix} c_\leftrightarrow^\dagger & c_\leftrightarrow \end{bmatrix}\begin{bmatrix} \xi & \Delta \\ -\Delta^* & -\xi^* \end{bmatrix}\begin{bmatrix} c_\updownarrow \\ c_\updownarrow^\dagger \end{bmatrix}, \tag{2.22}$$

where for convenience we defined row and column vectors as

$$\begin{aligned} \begin{bmatrix} c_\leftrightarrow^\dagger & c_\leftrightarrow \end{bmatrix} &:= \begin{bmatrix} c_1^\dagger \ldots c_i^\dagger \ldots c_N^\dagger & c_1 \ldots c_i \ldots c_N \end{bmatrix}, \\ \begin{bmatrix} c_\updownarrow \\ c_\updownarrow^\dagger \end{bmatrix} &:= \begin{bmatrix} c_1 \ldots c_i \ldots c_N & c_1^\dagger \ldots c_i^\dagger \ldots c_N^\dagger \end{bmatrix}^T. \end{aligned} \tag{2.23}$$

Let us denote the middle part of the right hand side of Eq. 2.22 with M as

$$M := \begin{bmatrix} \xi & \Delta \\ -\Delta^* & -\xi^* \end{bmatrix}, \tag{2.24}$$

and notice that M is Hermitian. Moreover, M has a symmetric spectrum. To see that, let's assume that E_r is an eigenvalue of M with the following eigenvalue equation,

$$\begin{bmatrix} \xi & \Delta \\ -\Delta^* & -\xi^* \end{bmatrix} \begin{bmatrix} U_r \\ V_r \end{bmatrix} = E_r \begin{bmatrix} U_r \\ V_r \end{bmatrix}.$$

By expanding this equation, we get

$$\begin{aligned} \xi U_r + \Delta V_r &= E_r U_r, \\ -\Delta^* U_r - \xi^* V_r &= E_r V_r, \end{aligned}$$

after negation and conjugation they will appear as

$$\begin{aligned} -\xi^* U_r^* - \Delta^* V_r^* &= -E_r U_r^*, \\ \Delta U_r^* + \xi V_r^* &= -E_r V_r^*, \end{aligned}$$

since E_r is real. Now it is apparent that $-E_r$ is also an eigenvalue of M with the following eigenvalue equation

$$\begin{bmatrix} \xi & \Delta \\ -\Delta^* & -\xi^* \end{bmatrix} \begin{bmatrix} V_r^* \\ U_r^* \end{bmatrix} = -E_r \begin{bmatrix} V_r^* \\ U_r^* \end{bmatrix}.$$

Let's denote the unitary transformation that diagonalize M as T. The similarity transformation will have the form

$$M_D = T^\dagger M T,$$

where M_D is a diagonal matrix. The above equation also means that we can replace M with $TM_DT^\dagger$ and then Hamiltonian (Eq. 2.22) takes the following form

$$H = \frac{1}{2} \begin{bmatrix} c_\leftrightarrow^\dagger & c_\leftrightarrow \end{bmatrix} \; TM_DT^\dagger \begin{bmatrix} c_\updownarrow \\ c_\updownarrow^\dagger \end{bmatrix}. \tag{2.25}$$

To make the discussion more concrete, let us work with a definite description of M_D. By taking advantage of the symmetric spectrum of M, we can write M_D as follows:

$$M_D = \begin{bmatrix} E & \\ & -E \end{bmatrix},$$

where E is a diagonal matrix with positive entries which are placed in an increasing order

$$E = \begin{bmatrix} E_1 & & \\ & \ddots & \\ & & E_N \end{bmatrix}, \quad E_1 < ... < E_N.$$

Then T will have the following form

$$T = \begin{bmatrix} U & V^* \\ V & U^* \end{bmatrix} = \begin{bmatrix} U_1 & ... & U_N & V_1^* & ... & V_N^* \\ V_1 & ... & V_N & U_1^* & ... & U_N^* \end{bmatrix}, \tag{2.26}$$

and $T^\dagger$ will be

$$T^\dagger = \begin{bmatrix} U^\dagger & V^\dagger \\ V^T & U^T \end{bmatrix}.$$

Now, by inserting given forms of M_D, T and $T^\dagger$ into Eq. 2.25, the Hamiltonian will be transformed into

Since T and $T^\dagger$ are unitary matrices, their action on $\begin{bmatrix} c_\leftrightarrow^\dagger & c_\leftrightarrow \end{bmatrix}$ and $\begin{bmatrix} c_\updownarrow \\ c_\updownarrow^\dagger \end{bmatrix}$ defines a new set of fermions as the following:

$$\begin{aligned} \begin{bmatrix} \gamma_\leftrightarrow^\dagger & \gamma_\leftrightarrow \end{bmatrix} &:= \begin{bmatrix} c_\leftrightarrow^\dagger & c_\leftrightarrow \end{bmatrix} \begin{bmatrix} U & V^* \\ V & U^* \end{bmatrix}, \\ &= \begin{bmatrix} c_\leftrightarrow^\dagger U + c_\leftrightarrow V & c_\leftrightarrow^\dagger V^* + c_\leftrightarrow U^* \end{bmatrix}, \end{aligned} \tag{2.27}$$

or, equally,

$$\begin{aligned} \begin{bmatrix} \gamma_\updownarrow \\ \gamma_\updownarrow^\dagger \end{bmatrix} &:= \begin{bmatrix} U^\dagger & V^\dagger \\ V^T & U^T \end{bmatrix} \begin{bmatrix} c_\updownarrow \\ c_\updownarrow^\dagger \end{bmatrix}, \\ &= \begin{bmatrix} U^\dagger c_\updownarrow + V^\dagger c_\updownarrow^\dagger \\ V^T c_\updownarrow + U^T c_\updownarrow^\dagger \end{bmatrix}. \end{aligned}$$

Explicitly, $\begin{bmatrix} \gamma_\leftrightarrow^\dagger & \gamma_\leftrightarrow \end{bmatrix} := [\gamma_1^\dagger ... \gamma_i^\dagger ... \gamma_N^\dagger \ \gamma_1 ... \gamma_i ... \gamma_N]$ with

$$\begin{aligned} \gamma_i^\dagger &:= \sum_r c_r^\dagger U_{ri} + c_r V_{ri}, \\ \gamma_i &:= \sum_r c_r^\dagger V_{ri}^* + c_r U_{ri}^*. \end{aligned} \tag{2.28}$$

This type of transformations is called generalized Bogoliubov transformation [37]. It is straightforward to show these two definitions are compatible. Every γ satisfies the same anti-commutation relations as fermions if T is unitary. The unitarity constraint restricts U and V to satisfy the following equations:

$$\begin{aligned} U^\dagger U + V^\dagger V = 1, \qquad & UU^\dagger + V^* V^T = 1, \\ U^T V + V^T U = 0, \qquad & UV^\dagger + V^* U^T = 0, \end{aligned} \tag{2.29}$$

and allows us to invert Eq. 2.28

$$\begin{aligned} c_i^\dagger &:= \sum_r \gamma_r^\dagger U_{ri}^\dagger + \gamma_r V_{ri}^T, \\ c_i &:= \sum_r \gamma_r^\dagger V_{ri}^\dagger + \gamma_r U_{ri}^T. \end{aligned} \tag{2.30}$$

With these new fermions, Hamiltonian will have the following free fermionic form

$$\begin{aligned} H &= \frac{1}{2}\begin{bmatrix}\gamma_\leftrightarrow^\dagger & \gamma_\leftrightarrow\end{bmatrix}\begin{bmatrix}E & \\ & -E\end{bmatrix}\begin{bmatrix}\gamma_\updownarrow \\ \gamma_\updownarrow^\dagger\end{bmatrix} \\ &= \frac{1}{2}\sum_i E_i\gamma_i^\dagger\gamma_i - E_i\gamma_i\gamma_i^\dagger \\ &= \frac{1}{2}\sum_i 2E_i\left(\gamma_i^\dagger\gamma_i - \frac{I_i}{2}\right) \\ &= \sum_i E_i\gamma_i^\dagger\gamma_i - \sum_i \frac{E_i}{2}. \end{aligned} \tag{2.31}$$

2.5.2 Application to the Kitaev Honeycomb Model

In our case, we first write H (Eq. 2.11) in the following symmetric form:

$$\begin{aligned} H &= \frac{1}{2}\sum_q J_q^x X_q\left(c_q^\dagger c_{q+\widehat{n}_x} + c_{q+\widehat{n}_x}^\dagger c_q\right) + J_q^y Y_q\left(c_q^\dagger c_{q+\widehat{n}_y} + c_{q+\widehat{n}_y}^\dagger c_q\right) + 2J_q^z c_q^\dagger c_q \\ &+ J_q^x X_q\left(c_q^\dagger c_{q+\widehat{n}_x}^\dagger - c_{q+\widehat{n}_x}^\dagger c_q^\dagger\right) + J_q^y Y_q\left(c_q^\dagger c_{q+\widehat{n}_y}^\dagger - c_{q+\widehat{n}_y}^\dagger c_q^\dagger\right) \\ &- J_q^x X_q\left(c_q c_{q+\widehat{n}_x} - c_{q+\widehat{n}_x} c_q\right) - J_q^y Y_q\left(c_q c_{q+\widehat{n}_y} - c_{q+\widehat{n}_y} c_q\right) \\ &- J_q^x X_q\left(c_q c_{q+\widehat{n}_x}^\dagger + c_{q+\widehat{n}_x} c_q^\dagger\right) - J_q^y Y_q\left(c_q c_{q+\widehat{n}_y}^\dagger + c_{q+\widehat{n}_y} c_q^\dagger\right) - 2J_q^z c_q c_q^\dagger, \end{aligned}$$

then ξ^H and Δ^H are defined as

$$\begin{aligned}
\xi^H_{i(q),i(q')}(X,Y) &:= J^x_q X_q \delta_{i(q),i(q'-\widehat{n}_x)} + J^x_{q'} X_{q'} \delta_{i(q-\widehat{n}_x),i(q')} \\
&\quad + J^y_q Y_q \delta_{i(q),i(q'-\widehat{n}_y)} + J^y_{q'} Y_{q'} \delta_{i(q-\widehat{n}_y),i(q')} + 2J^z_q \delta_{i(q),i(q')} \\
\Delta^H_{i(q),i(q')}(X,Y) &:= J^x_q X_q \delta_{i(q),i(q'-\widehat{n}_x)} - J^x_{q'} X_{q'} \delta_{i(q-\widehat{n}_x),i(q')} \\
&\quad + J^y_q Y_q \delta_{i(q),i(q'-\widehat{n}_y)} - J^y_{q'} Y_{q'} \delta_{i(q-\widehat{n}_y),i(q')},
\end{aligned}$$

where i is a one-to-one mapping between $q = (q_x, q_y)$ and integers between $1, ..., N$, to be able to use the notation introduced in Eq. 2.23, and it is defined as

$$i(q) := q_x + (q_y - 1)N_x.$$

Finally, M_H will have the following form

$$M_H = \begin{bmatrix} \xi^H & \Delta^H \\ -\Delta^H & -\xi^H \end{bmatrix}.$$

Similarly, we first write V (Eq. 2.21) in the following symmetric form

$$\begin{aligned}
V &= \frac{1}{2}\sum_q -i\left[\kappa^5_q\, X_{q+\widehat{n}_y} Y_{q+\widehat{n}_x} - \kappa^6_q\, X_q Y_q\right]\left[c^\dagger_{q+\widehat{n}_x} c_{q+\widehat{n}_y} - c^\dagger_{q+\widehat{n}_y} c_{q+\widehat{n}_x}\right] \\
&\quad + 2i\kappa^x_q\, X_q\left[c^\dagger_q c^\dagger_{q+\widehat{n}_x} - c^\dagger_{q+\widehat{n}_x} c^\dagger_q\right] + 2i\kappa^y_q\, Y_q\left[c^\dagger_q c^\dagger_{q+\widehat{n}_y} - c^\dagger_{q+\widehat{n}_y} c^\dagger_q\right] \\
&\quad + i\left[\kappa^5_q\, X_{q+\widehat{n}_y} Y_{q+\widehat{n}_x} + \kappa^6_q\, X_q Y_q\right]\left[c^\dagger_{q+\widehat{n}_x} c^\dagger_{q+\widehat{n}_y} - c^\dagger_{q+\widehat{n}_y} c^\dagger_{q+\widehat{n}_x}\right] \\
&\quad + 2i\kappa^x_q\, X_q\left[c_q c_{q+\widehat{n}_x} - c_{q+\widehat{n}_x} c_q\right] + 2i\kappa^y_q\, Y_q\left[c_q c_{q+\widehat{n}_y} - c_{q+\widehat{n}_y} c_q\right] \\
&\quad + i\left[\kappa^5_q\, X_{q+\widehat{n}_y} Y_{q+\widehat{n}_x} + \kappa^6_q\, X_q Y_q\right]\left[c_{q+\widehat{n}_x} c_{q+\widehat{n}_y} - c_{q+\widehat{n}_y} c_{q+\widehat{n}_x}\right] \\
&\quad - i\left[\kappa^5_q\, X_{q+\widehat{n}_y} Y_{q+\widehat{n}_x} - \kappa^6_q\, X_q Y_q\right]\left[c_{q+\widehat{n}_x} c^\dagger_{q+\widehat{n}_y} - c_{q+\widehat{n}_y} c^\dagger_{q+\widehat{n}_x}\right],
\end{aligned}$$

then ξ^V and Δ^V are defined as

$$\begin{aligned}
\xi^V_{i(q),i(q')}(X,Y) &:= -i\left(\kappa^5_{q-\widehat{n}_x}\, X_{q'} Y_q - \kappa^6_{q-\widehat{n}_x}\, X_{q-\widehat{n}_x} Y_{q-\widehat{n}_x}\right)\delta_{i(q-\widehat{n}_x),i(q'-\widehat{n}_y)} \\
&\quad + i\left(\kappa^5_{q'-\widehat{n}_x}\, X_q Y_{q'} - \kappa^6_{q'-\widehat{n}_x}\, X_{q'-\widehat{n}_x} Y_{q'-\widehat{n}_x}\right)\delta_{i(q-\widehat{n}_y),i(q'-\widehat{n}_x)}, \\
\Delta^V_{i(q),i(q')}(X,Y) &:= 2i\left[\kappa^x_q X_q \delta_{i(q),i(q'-\widehat{n}_x)} - \kappa^x_{q'} X_{q'} \delta_{i(q-\widehat{n}_x),i(q')}\right. \\
&\quad \left. + \kappa^y_q Y_q \delta_{i(q),i(q'-\widehat{n}_y)} - \kappa^y_{q'} Y_{q'} \delta_{i(q-\widehat{n}_y),i(q')}\right] \\
&\quad + i\left(\kappa^5_{q-\widehat{n}_x}\, X_{q'} Y_q + \kappa^6_{q-\widehat{n}_x}\, X_{q-\widehat{n}_x} Y_{q-\widehat{n}_x}\right)\delta_{i(q-\widehat{n}_x),i(q'-\widehat{n}_y)} \\
&\quad + i\left(\kappa^5_{q'-\widehat{n}_x}\, X_q Y_{q'} + \kappa^6_{q'-\widehat{n}_x}\, X_{q'-\widehat{n}_x} Y_{q'-\widehat{n}_x}\right)\delta_{i(q-\widehat{n}_y),i(q'-\widehat{n}_x)},
\end{aligned}$$

and M_V has the following form:

$$M_V = \begin{bmatrix} \xi^V & \Delta^V \\ -\left(\Delta^V\right)^* & -\left(\xi^V\right)^* \end{bmatrix},$$

and for the total system, ξ and Δ are defined as

$$\begin{aligned} \xi &:= \xi^H + \xi^V, \\ \Delta &:= \Delta^H + \Delta^V, \end{aligned}$$

and M has the following form

$$M := \begin{bmatrix} \xi & \Delta \\ -\Delta^* & -\xi^* \end{bmatrix}. \tag{2.32}$$

To work with eigenvalues and eigenvectors of M, we have to fix the values of ξ and Δ and this is done by fixing the values of X and Y i.e. fixing $\{W_p, L_x, L_y\}$ configuration.

2.6 Eigenstates of Quadratic Hamiltonians

2.6.1 General Theory

We will to take advantage of the Bloch-Messiah theorem [38, 37], to write the ground state of the system explicitly. Bloch and Messiah showed that a unitary matrix of the form (Eq. 2.26) can always be decomposed into three matrices of very special form:

$$T = \begin{bmatrix} D & \\ & D^* \end{bmatrix} \begin{bmatrix} \overline{U} & \overline{V} \\ \overline{V} & \overline{U} \end{bmatrix} \begin{bmatrix} C & \\ & C^* \end{bmatrix},$$

or

$$U = D\overline{U}C, \qquad V = D^*\overline{V}C,$$

where D and C are unitary matrices and $\overline{U}$ and $\overline{V}$ are real matrices of the general form

$$\overline{U} = \begin{bmatrix}
0 & & & & & & & & & & & \\
& \ddots & & & & & & & & & & \\
& & 0 & & & & & & 0 & & & \\
& & & u_1 & 0 & & & & & & & \\
& & & 0 & u_1 & & & & & & & \\
& & & & & \ddots & & & & & & \\
& & & & & & u_n & 0 & & & & \\
& & & & & & 0 & u_n & & & & \\
& & 0 & & & & & & 1 & & & \\
& & & & & & & & & \ddots & & \\
& & & & & & & & & & 1
\end{bmatrix}, \tag{2.33}$$

and

$$\overline{V} = \begin{bmatrix}
1 & & & & & & & & & & & \\
& \ddots & & & & & & & & & & \\
& & 1 & & & & & & 0 & & & \\
& & & 0 & v_1 & & & & & & & \\
& & & -v_1 & 0 & & & & & & & \\
& & & & & \ddots & & & & & & \\
& & & & & & 0 & v_n & & & & \\
& & & & & & -v_n & 0 & & & & \\
& & 0 & & & & & & 0 & & & \\
& & & & & & & & & \ddots & & \\
& & & & & & & & & & 0
\end{bmatrix}, \tag{2.34}$$

where zero-block-matrices and identity-block-matrices are the same size.

Now we go back to the transformation (Eq. 2.27):

$$\begin{aligned}
\begin{bmatrix} \gamma^\dagger_\leftrightarrow & \gamma_\leftrightarrow \end{bmatrix} &:= \begin{bmatrix} c^\dagger_\leftrightarrow & c_\leftrightarrow \end{bmatrix} \begin{bmatrix} U & V^* \\ V & U^* \end{bmatrix}, \\
&= \begin{bmatrix} c^\dagger_\leftrightarrow & c_\leftrightarrow \end{bmatrix} \begin{bmatrix} D & \\ & D^* \end{bmatrix} \begin{bmatrix} \overline{U} & \overline{V} \\ \overline{V} & \overline{U} \end{bmatrix} \begin{bmatrix} C & \\ & C^* \end{bmatrix}.
\end{aligned}$$

First D transforms particle operators $c^\dagger$ and c among themselves into $a^\dagger$ and a:

$$\begin{bmatrix} a^\dagger_\leftrightarrow & a_\leftrightarrow \end{bmatrix} := \begin{bmatrix} c^\dagger_\leftrightarrow & c_\leftrightarrow \end{bmatrix} \begin{bmatrix} D & \\ & D^* \end{bmatrix} = \begin{cases} a^\dagger_\leftrightarrow = c^\dagger_\leftrightarrow D \\ a_\leftrightarrow = c_\leftrightarrow D^* \end{cases},$$

or explicitly,

$$a^\dagger_k = \sum_l D_{lk} c^\dagger_l, \qquad a_k = \sum_l D^*_{lk} c_l.$$

Then there is a special Bogoliubov transformation,

$$\begin{bmatrix} \alpha^\dagger_\leftrightarrow & \alpha_\leftrightarrow \end{bmatrix} := \begin{bmatrix} a^\dagger_\leftrightarrow & a_\leftrightarrow \end{bmatrix} \begin{bmatrix} \overline{U} & \overline{V} \\ \overline{V} & \overline{U} \end{bmatrix} = \begin{cases} \alpha^\dagger_\leftrightarrow = a^\dagger_\leftrightarrow \overline{U} + a_\leftrightarrow \overline{V} \\ \alpha_\leftrightarrow = a^\dagger_\leftrightarrow \overline{V} + a_\leftrightarrow \overline{U} \end{cases},$$

which defines three types of energy levels: the "paired" levels with $u_p > 0, v_p > 0$)

$$\begin{aligned} \alpha^\dagger_p &= u_p a^\dagger_p - v_p a_{\overline{p}}, \\ \alpha^\dagger_{\overline{p}} &= u_p a^\dagger_{\overline{p}} + v_p a_p, \end{aligned}$$

$$\begin{aligned} \alpha_p &= -v_p a^\dagger_{\overline{p}} + u_p a_p, \\ \alpha_{\overline{p}} &= v_p a^\dagger_p + u_p a_{\overline{p}}, \end{aligned}$$

where $(p, \overline{p})$ are defined by the 2×2 boxes in Eqs. 2.33 - 2.34, the "occupied" levels $(v_i = 1; u_i = 0)$ and the "empty" levels $(v_m = 0; u_m = 1)$

$$\begin{aligned} \alpha^\dagger_i &= a_i, & \alpha^\dagger_m &= a^\dagger_m, \\ \alpha_i &= a^\dagger_i, & \alpha_m &= a_m. \end{aligned}$$

Finally the unitary transformation of the $\alpha^\dagger$ and α among themselves

$$\begin{bmatrix} \gamma^\dagger_\leftrightarrow & \gamma_\leftrightarrow \end{bmatrix} := \begin{bmatrix} \alpha^\dagger_\leftrightarrow & \alpha_\leftrightarrow \end{bmatrix} \begin{bmatrix} C & \\ & C^* \end{bmatrix} = \begin{cases} \gamma^\dagger_\leftrightarrow = \alpha^\dagger_\leftrightarrow C \\ \gamma_\leftrightarrow = \alpha_\leftrightarrow C^* \end{cases},$$

or explicitly

$$\gamma^\dagger_k = \sum_l C_{lk} \alpha^\dagger_l, \qquad \gamma_k = \sum_l C^*_{lk} \alpha_l. \tag{2.35}$$

In a general quadratic fermionic Hamiltonian, the ground state wavefunction is defined as a non-zero wavefunction $|\phi\rangle$ such that $\gamma_k|\phi\rangle = 0$ for all k. It can be easily verified that the following wavefunction satisfies these criteria:

$$|\phi\rangle = \prod_i a_i^\dagger \prod_p (u_p + v_p a_p^\dagger a_{\bar{p}}^\dagger)|-\rangle, \tag{2.36}$$

where $|-\rangle$ represents the vacuum of $c-$fermions. We will refer to first product as $i-$part and second product as $p-$part of the Eq. 2.36.

2.6.2 Eigenstates of the Kitaev Honeycomb Model

For the Kitaev honeycomb model, there are a few things to consider when dealing with its eigenstates. First of all, recall that the Hamiltonian (Eq. 2.31)

$$H = \sum_i E_i \gamma_i^\dagger \gamma_i - \sum_i \frac{E_i}{2}$$

is brought to this form after a particular configuration of vortices and loop symmetry operators $\{W_p, L_x, L_y\}$ was selected.

Note that, the single fermionic operators c and $c^\dagger$ commute with all plaquette operators except two plaquettes located to the left of the origin which they anti-commute. Therefore, c and $c^\dagger$ flip the values of those plaquettes. In other words, they do not preserve the $\{W_p, L_x, L_y\}$ configuration. This is also true for γ, $\gamma^\dagger$, a and $a^\dagger$, since they are superpositions of c and $c^\dagger$. Only quadratic applications of γ's ($\gamma_i^\dagger\gamma_j^\dagger$, $\gamma_i^\dagger\gamma_j$, etc.) or c's ($c_i^\dagger c_j^\dagger$, $c_i^\dagger c_j$, etc.) preserve $\{W_p, L_x, L_y\}$ configurations. In this respect, although the p-part (i.e. paired levels) of Eq. 2.36 always preserves the $\{W_p, L_x, L_y\}$ configuration of $|-\rangle$, the i-part (occupied levels) only preserves it when the number of i is even.

On the other hand, we have to be careful when we deal with some particular vortex configuration $\{W_p, L_x, L_y\}$ because it may not be possible to choose a vacuum $|-\rangle$ whose vortex configuration matches with $\{W_p, L_x, L_y\}$. To see that, we should have a closer look into the properties of $|-\rangle$.

The vacuum $|-\rangle$ vanishes under the application of any annihilation operator c. This means that $|-\rangle$ does not have any $c-$fermions or $b-$hard-core bosons. More

formally it is only composed of basis elements $B_{Q,N,L}$ (Eq. 2.10) with $\lambda_{N_q} = 0$. On the other hand, some $\{W_p, L_x, L_y\}$ configurations *match* with $\{Q_q, L_x, L_y\}$ configurations (Fig. 2.7(a)), whereas some others (Fig. 2.7(b)) don't because of the constraints (Eq. 2.9) on the values of Q_q. For those *unmatched configurations,* we can take advantage of two Q_q's which are on the left of the origin (Fig. 2.7(b′)) to satisfy these constraints. Those are the same two plaquettes whose values get flipped by any application of a single fermionic operators c and $c^\dagger$.

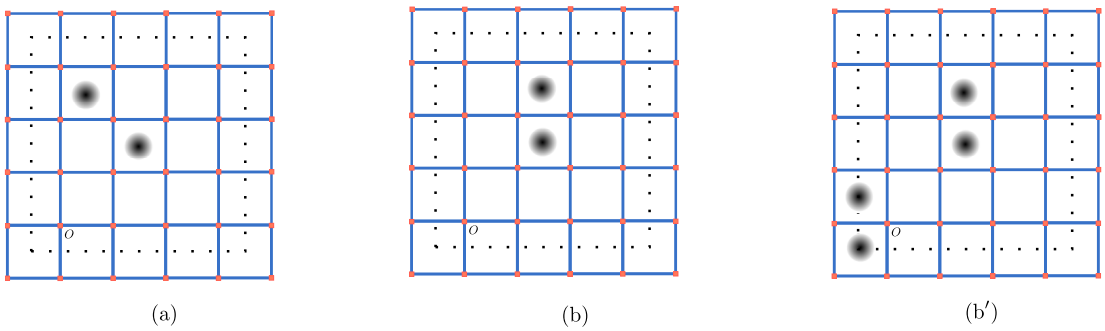

Figure 2.7: Various Q_q configurations. (a) Matched configuration: Appropriate choice for $|-\rangle$. (b) Unmatched configuration: There is no such Toric code configuration so there is no ES-HB basis. (b′) Fixed unmatched configuration: Unmatched configurations can be fixed by adding two vortices onto the left side of origin and can be a valid choice for $|-\rangle$.

Therefore, the definition of a ground state $|\Phi\rangle$ for Kitaev's honeycomb model must satisfy two conditions: (1) $|\Phi\rangle$ is in the same $\{W_p, L_x, L_y\}$ configuration as the M (Eq. 2.32) and (2) applications of $\gamma_k\gamma_l$ for any k, l $(k \neq l)$ should annihilate it.

Notice that there are two cases in which the state $|\phi\rangle$ (Eq. 2.36) may not be in the same $\{W_p, L_x, L_y\}$ configuration as the M (Eq. 2.32): (a) an odd number of occupied levels (i.e. odd number of i) with matched configurations and (b) an even number of occupied levels with unmatched configurations. In both cases the resulting state $|\phi\rangle$ is not an eigenstate of the systems. There are two different approaches to resolve these types of situations.

First, we can apply $\gamma_1^\dagger$, the minimum energy fermionic creation operator, to the

state $|\phi\rangle$ to find the actual ground state $|\Phi\rangle$ of the system:

$$|\Phi\rangle = \gamma_1^\dagger |\phi\rangle. \tag{2.37}$$

That will bring it back to the same $\{W_p, L_x, L_y\}$ configuration as the M, and will be the eigenstate with minimum energy which is

$$E_{GS} = -\sum_i \frac{E_i}{2} + E_1.$$

Applications of any $\gamma_k \gamma_l$ $(k \neq l)$ vanish it

$$\gamma_k \gamma_l |\Phi\rangle = 0, \text{ for any } k, l \text{ with } k \neq l.$$

In this respect, only the half of the Hilbert space for each $\{W_p, L_x, L_y\}$ configuration are spanned by the eigenvectors of system. The other half belongs to different $\{W_p, L_x, L_y\}$ configurations, therefore they are *not* eigenstates. So, starting with the ground state of the right $\{W_p, L_x, L_y\}$ configurations, the *excited states* can only be achieved by the applications of even number of $\gamma-$fermions.

On the other hand, the second way of dealing with these two cases is to exchange the roles of γ_1 and $\gamma_1^\dagger$ before we use the Bloch-Messiah theorem for the second time. The practical purpose of this approach will be seen in the next chapter when we need to calculate the overlap between two ground states of different systems. This role exchange can be done via exchanging the first column of T (Eq. 2.26) with the first column of its second half. With this approach, it is also possible to write higher excited levels as in the form of Eq. 2.36 once the appropriate column exchange operations were performed. This approach makes the connection between eigenstates and U, V more apparent, since there is no need for a correction (Eq. 2.37). In other words, there is a one-to-one correspondence between U, V matrices and the ground state. We will use this correspondence to calculate the Berry phase with the help of Thouless' theorem which will be explained in section 3.3.2.

2.7 Vortices in the Kitaev Honeycomb Model

One of the signatures of the existence of non-Abelian anyons is the degeneracy of the ground state of the system. Depending on types of non-Abelian anyons, there are different relations between the number of well-separated non-Abelian anyons and the degeneracy of the ground state. For Ising anyons this relation is like $2M$ well-separated σ-anyons results in $2^{M-1}-$fold degeneracy in the ground state. [17]

Numerical results show that separating two vortices in the honeycomb model makes one of the $\gamma-$fermions's energy converge to zero (Fig. 2.8).

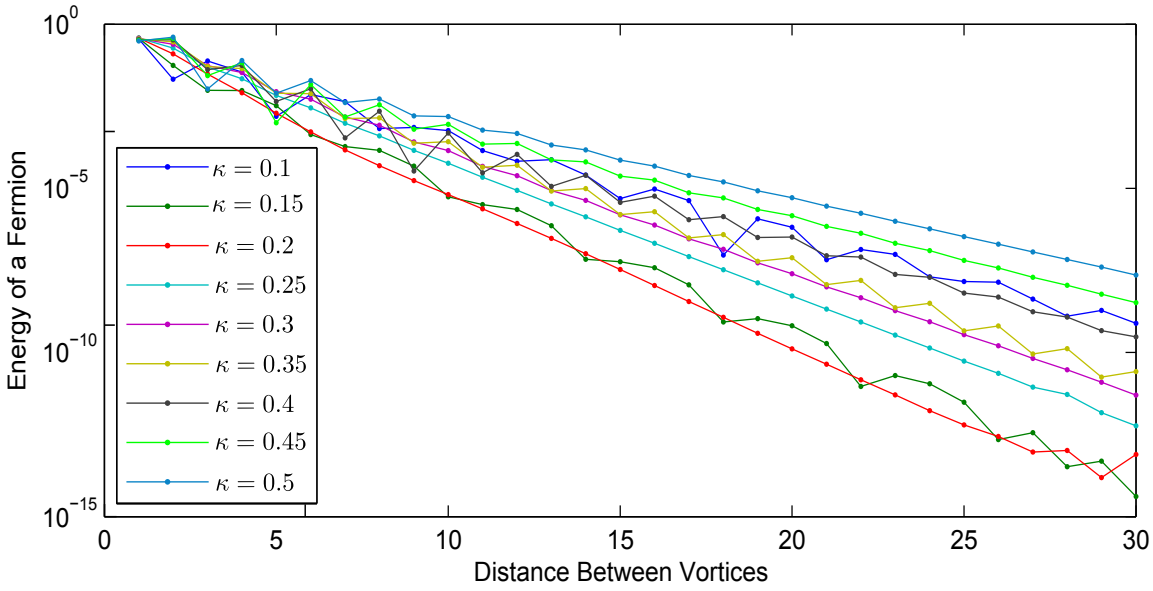

Figure 2.8: A plot showing the energy of a lowest energy fermion for various distances between two vortices separated vertically from each other in a 40×80 dimer lattice for different magnetic field strength κ. Note that, $J_q^x = J_q^y = J_q^z = 1$ for all q and $\kappa_p^l = \kappa$ for all p and l (Eq. 2.3).

For a $2-$vortex configuration this does not result in any degeneracy, since, to get an excited state, an even number of $\gamma^\dagger$ need to be applied. Therefore, a configuration of 4 well-separated vortices have two zero energy fermions, hence a $2-$fold degenerate ground state. Similarly, a configuration with 6 well-separated vortices have three zero energy fermions and a $4-$fold degenerate ground state. In general, $2M$ well-separated

vortices have M zero energy fermions and a 2^{M-1} degenerate ground state.

Chapter 3

NON-ABELIAN ANYONS IN THE KITAEV HONEYCOMB MODEL

Non-Abelian anyons are defined in terms of their non-trivial evolution under their position exchange. This evolution happens in the degenerate ground state of the system that we described in the previous chapter. In this chapter we are going to investigate how this evolution happens. In other words, we will calculate the non-Abelian Berry phase of the model on a path in the parameter space. Physically, this path swaps the position of two vortices. Because a degenerate space is needed to have non-Abelian Berry phase, we work with the systems having four vortices to get $2-$fold degenerate space. In addition to that, vortices have to follow the path adiabatically to calculate non-Abelian Berry phase. Therefore, we start the chapter by explaining how to move vortices adiabatically.

3.1 Simulation of Adiabatic Vortex Motion

Simulation of vortex creation and motion is first discussed in [39], and here we will adapt it into our formalism. Recall that, the Hamiltonian H of the Kitaev honeycomb model depends continuously on J and κ parameters. To see the fundamental relation between these coefficients and vortex excitations let's focus on an $x-$link of the fermionic representation of H (Eq. 2.11):

$$J_q^x X_q (c_q^\dagger - c_q)(c_{q+\widehat{n}_x}^\dagger + c_{q+\widehat{n}_x})$$

The effect of changing the value of J_q^x to its negative $-J_q^x$ slowly is the same as that of changing the value of corresponding X_q to its negative $-X_q$. Moreover, if $q_y \neq 1$, this action can be considered as negating the eigenvalues of both $W_{q-\widehat{n}_y}$ and

W_q (Fig. 3.1 and Fig.3.1); we denote these new values by $\widetilde{W}_{q-\widehat{n}_y}$ and $\widetilde{W}_q$. Therefore, the fermionic spectrum of H for $(-J_q^x, W_{q-\widehat{n}_y}, W_q)-$configuration is the same as that of H for $(J_q^x, \widetilde{W}_{q-\widehat{n}_y}, \widetilde{W}_q)-$configuration. However, notice that changing the value of J_q^x to its negative $-J_q^x$ does not actually change the value of $W_{q-\widehat{n}_y}$ and W_q, because H commutes with any W_p for all values of J_q^x:

$$[H, W_p] = 0.$$

The vortex configuration of an actual eigenstate of H is only related to the choice of vacuum $|-\rangle$, and the evenness or oddness of the number of i (i.e. the number of the occupied levels) in Eq. 2.36 as discussed in section 2.6.2.

For systems with the magnetic field, the slow changes in J_q^x from its original value to its negative should be accompanied by the slow changes in $\kappa^5_{q-\widehat{n}_y}$, κ^6_q and κ^x_q (Eqs. 2.17, 2.18 and 2.19) from their original value to their negatives to simulate the creation or motion of the vortices as in Fig. 3.1 and Fig.3.1. Let us denote the set of the coefficients needed to be changed to move a vortex vertically between the plaquettes sharing $x-$link of the dimer q as

$$[J\kappa]^x_q := \{J^x_q, \kappa^5_{q-\widehat{n}_y}, \kappa^6_q, \kappa^x_q\}$$

.

Similarly, the effect of slowly changing the value of J_q^y to its negative $-J_q^y$ is the same as that of changing the value of the corresponding Y_q to its negative $-Y_q$. Moreover, when q_y is equal to N_y, this change can be considered as a negating the eigenvalues of both $W_{q-\widehat{n}_x}$ and W_q. As in the $x-$links, under magnetic field, the slow changes in J_q^y should be accompanied by the slow changes in $\kappa^5_{q-\widehat{n}_x}, \kappa^6_q$ and κ^y_q (Eqs. 2.17, 2.18 and 2.20) to simulate the creation or motion of the vortices. Let us denote the set of the coefficients needed to be changed to move a vortex horizontally between the plaquettes sharing $y-$link of the dimer q as

$$[J\kappa]^y_q := \{J^y_q, \kappa^5_{q-\widehat{n}_x}, \kappa^6_q, \kappa^y_q\}$$

.

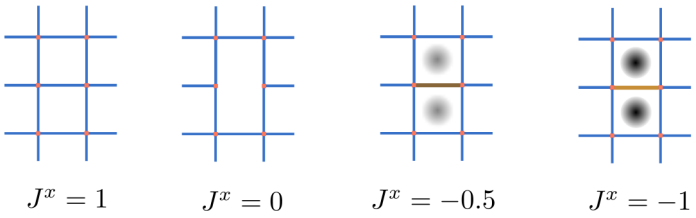

Figure 3.1: Example: Vortex Creation by changing J^x (no magnetic field)

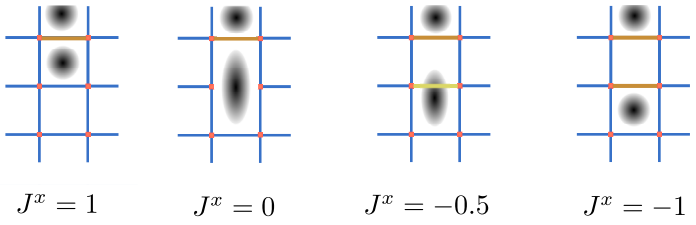

Figure 3.2: Example: Vortex Motion by changing J^x (no magnetic field)

As a result, we can simulate the effect of creating or moving vortices just by changing some local values of the J and κ coefficients together. Since we change them together, let us represent them as a single variable $J\kappa$ and these vortices as $J\kappa-$vortices.

The motion of the $J\kappa-$vortices does not effect the gap between the ground state and the excited states as long as vortices are well-separated based on the numerical observation which will be discussed more in section 3.4. Therefore the slow vortex motion is also adiabatic, as long as vortices are kept far apart.

3.2 Numerical Evaluation of Berry Phase

3.2.1 Brief Review of General Theory of Berry Phase

In this part, a brief review of the Berry phase will be given based on the approach discussed in the book [40]. Let's assume that we have a time-dependent finite dimensional Hamiltonian $H(\lambda)$ which is a smooth and single valued function of some

external parameters λ on a parameter manifold $\mathcal{M}$.

Abelian Berry Phase

For any value of λ, one may choose an orthonormal basis of eigenstates $|\phi^n\rangle$. Suppose that a non-degenerate eigenstate $|\varphi^n(\lambda(0))\rangle$ is the initial state of the system. A change in the parameters $\lambda(t)$ will change the initial state. The adiabatic approximation states that if

$$\langle\varphi^m(\lambda(t))|\frac{d}{dt}\varphi^n(\lambda(t))\rangle \cong 0, \text{ for all } m \neq n \tag{3.1}$$

the system will be in $|\varphi^n(\lambda(t))\rangle$ at any time t. We can also express this statement in terms of the matrix elements of the time derivative of the Hamiltonian. In order to show this, let us take the time derivative of both sides of the eigenvalue equation $H(\lambda)|\varphi^n(\lambda)\rangle = E^n(\lambda)|\varphi^n(\lambda)\rangle$

$$\frac{dH(\lambda)}{dt}|\varphi^n(\lambda)\rangle + H(\lambda)|\frac{d}{dt}\varphi^n(\lambda)\rangle = \frac{dE(\lambda)}{dt}|\varphi^n(\lambda)\rangle + E(\lambda)|\frac{d}{dt}\varphi^n(\lambda)\rangle$$

and take the overlap of both sides of this equation with $|\varphi^m(\lambda)\rangle$ for $m \neq n$. This yields

$$\langle\varphi^m(\lambda)|\frac{dH(\lambda)}{dt}|\varphi^n(\lambda)\rangle + E^m(\lambda)\langle\varphi^m(\lambda)|\frac{d}{dt}\varphi^n(\lambda)\rangle = E^n(\lambda)\langle\varphi^m(\lambda)|\frac{d}{dt}\varphi^n(\lambda)\rangle$$

where orthogonality of the eigenstates $\langle\varphi^j(\lambda)|\varphi^k(\lambda)\rangle = \delta_{jk}$ have been used. We can express above equation in the following form

$$\langle\varphi^m(\lambda)|\frac{d}{dt}\varphi^n(\lambda)\rangle = \frac{\langle\varphi^m(\lambda(t))|\frac{d}{dt}H(\lambda)|\varphi^n(\lambda)\rangle}{E_n(\lambda) - E_m(\lambda)}.$$

In view of the adiabatic approximation (Eq. 3.1), above equation can be expressed as

$$\langle\varphi^m(\lambda)|\frac{d}{dt}\varphi^n(\lambda)\rangle = \frac{\langle\varphi^m(\lambda(t))|\frac{d}{dt}H(\lambda)|\varphi^n(\lambda)\rangle}{E_n(\lambda) - E_m(\lambda)} \cong 0. \tag{3.2}$$

Notice that the validity of the adiabatic approximation is correlated with the slowness of the changes and the gap between the eigenvalues of the system.

By expressing the evolving state vector together with the phase dependencies as $|\psi(t)\rangle = c(t)|\varphi^n(\lambda(t))\rangle$ such that $c(0) = 1$, the Schrödinger equation will admit the

following solution under the adiabatic approximation

$$c(t) = \exp\left\{-\frac{i}{\hbar}\int_0^t E_n(t')dt'\right\}\exp\left\{-\int_0^t \langle\varphi^n(\lambda(t'))|\frac{d}{dt'}\varphi^n(\lambda(t'))\rangle dt'\right\}$$

where the first part of the right-hand side is called the *dynamical phase factor* and the second is called the *Berry phase* $e^{i\gamma_n(t)}$ where

$$\gamma_n(t) := i\int_0^t \langle\varphi^n(\lambda(t'))|\frac{d}{dt'}\varphi^n(\lambda(t'))\rangle dt'$$

is a real phase angle. Notice that $\gamma_n(t)$ does not depend on the time dependence of the integrand and it can be calculated directly as

$$\gamma_n(t) := i\int_{\lambda(0)}^{\lambda(t)} \langle\varphi^n(\lambda)|\frac{\partial}{\partial\lambda^i}\varphi^n(\lambda)\rangle d\lambda^i,$$

where λ^i are indexed representation of the external parameters. On a closed curve $\mathbf{C}$ in the parameter space it takes the following form

$$\gamma(\mathbf{C}) := i\oint_{\mathbf{C}} \langle\varphi^n(\lambda)|\frac{\partial}{\partial\lambda^i}\varphi^n(\lambda)\rangle\ d\lambda^i$$

and, as easily verified, $\gamma(\mathbf{C})$ is an invariant quantity under the gauge transformation $|\varphi^n(\lambda)\rangle \to e^{i\alpha_n(\lambda)}|\varphi^n(\lambda)\rangle$.

Non-Abelian Berry Phase

Suppose that the eigenvalue $E_n(\lambda)$ of the Hamiltonian $H(\lambda)$ is D_n-fold degenerate, and D_n does not depend on λ. We can introduce the orthonormal eigenvectors $|\varphi^{(n,a)}(\lambda)\rangle$ satisfying

$$H(\lambda)|\varphi^{(n,a)}(\lambda)\rangle = E_n(\lambda)|\varphi^{(n,a)}(\lambda)\rangle \text{ for all } a = 1, ..., D_n.$$

Let the system with the initial state

$$|\psi(\lambda(0))\rangle = \sum_{a=1}^{D_n} c_a^n(\lambda(0))|\varphi^{(n,a)}(\lambda(0))\rangle$$

evolve on a trajectory $\lambda(t)$ given as a function of time in the parameter space. The adiabatic approximation for degenerate eigenvalues states that if

$$\langle\varphi^{(m,b)}(\lambda(t))|\frac{d}{dt}\varphi^{(n,a)}(\lambda(t))\rangle \cong 0, \text{ for all } m \neq n \text{ and for all } a, b$$

the state will always be in the degenerate subspace $\text{Span}\{|\varphi^{(n,a)}(\lambda(t))\rangle\}$ at any time t

$$|\psi(\lambda(t))\rangle = \sum_{a=1}^{D_n} c_a^n(\lambda(t))|\varphi^{(n,a)}(\lambda(t))\rangle.$$

Substituting this into the Schrödinger equation and by taking the inner product with $\langle\varphi^{(m,b)}(\lambda(t))|$ we get the following differential equation under the adiabatic approximation:

$$\frac{dc_b^n(\lambda(t))}{dt} + \sum_{a=1}^{D_n}\left[\frac{i}{\hbar}E_n(\lambda(t))\delta_{ab} + \langle\varphi^{(n,b)}(\lambda(t))|\frac{d}{dt}\varphi^{(n,a)}(\lambda(t))\rangle\right] c_a^n(\lambda(t)) = 0.$$

The solution of this equation is as follows

$$c_b^n(\lambda(t)) = \sum_{a=1}^{D_n}\left[\mathcal{T}\exp\left\{i\int_0^t\left(-\frac{i}{\hbar}E_n(\lambda(t'))I + \mathcal{A}_{D_n}^n(\lambda(t'))\right)dt'\right\}\right]^{ba} c_a^n(\lambda(0)) \quad (3.3)$$

where I is an identity operator and $\mathcal{A}_{D_n}^n(\lambda(t'))$ is a Hermitian matrix defined in terms of its matrix elements as

$$\left[\mathcal{A}_{D_n}^n\right]^{ba}(\lambda(t')) = i\langle\varphi^{(n,b)}(\lambda(t'))|\frac{d}{dt'}\varphi^{(n,a)}(\lambda(t'))\rangle \quad (3.4)$$

and $\mathcal{T}$ is the time-ordering operator whose action on $\exp\left\{i\int_{\lambda(0)}^{\lambda(t)}\mathcal{A}_{D_n}^n(\lambda(t'))dt'\right\}$ is defined as

$$\mathcal{T}\exp\left\{i\int_0^t\mathcal{A}_{D_n}^n(\lambda(t'))dt'\right\} := \lim_{M\to\infty}\prod_{i=0}^{M-1}\exp\left\{i\mathcal{A}_{D_n}^n(\lambda(t_i))\Delta t\right\}$$

where $\lambda(t_0)$ and $\lambda(t_M)$ are coinciding points denoting the beginning and end point of the closed trajectory whose curve length is given by $\textbf{length}(\lambda(t_M),\lambda(t_0))$, and Δt is given as $\Delta t = \textbf{length}(\lambda(t_M),\lambda(t_0))/M$.

Note that the first term in the integrand of Eq. 3.3 commutes with the all $\mathcal{A}_{D_n}^n$ and allow us to write Eq. 3.3 as

$$c_b^n(\lambda(t)) = \exp\left\{-\int_{\lambda(0)}^{\lambda(t)}\frac{i}{\hbar}E_n(\lambda')d\lambda'\right\}\sum_{a=1}^{D_n}\left[\mathcal{P}\exp\left\{i\int_{\lambda(0)}^{\lambda(t)}\mathcal{A}_{D_n}^n(\lambda')d\lambda'\right\}\right]^{ba} c_a^n(\lambda(0)) \quad (3.5)$$

where $\mathcal{P}$ is the path-ordering operator. The first part of the right hand-side of Eq. 3.5 is the dynamical phase, and second part is the non-Abelian Berry matrix

$$B(\lambda(t),\lambda(0)) = \mathcal{P}\exp\left\{i\int_{\lambda(0)}^{\lambda(t)}\mathcal{A}_{D_n}^n(\lambda')d\lambda'\right\}.$$

Under the gauge transformation

$$|\phi^{(n,a)}(\lambda)\rangle \to U_{ab}(\lambda)|\varphi^{(n,b)}(\lambda)\rangle$$

$\mathcal{A}^n_{D_n}(\lambda)$ transforms as $U_{ab}(\lambda)\mathcal{A}^n_{D_n}(\lambda)U^\dagger_{ab}(\lambda) + i\frac{dU_{ab}(\lambda)}{d\lambda}U^\dagger_{ab}(\lambda)$ [41, 42] and the non-Abelian Berry matrix transforms as

$$B(\lambda(t),\lambda(0)) \to U_{ab}(\lambda)B(\lambda(t),\lambda(0))U^\dagger_{ab}(0).$$

If the path is closed $\mathcal{C}$ ($\lambda(T) = \lambda(0)$), the transformation is given as

$$B(\lambda(0)) \to B'(\lambda(0)) = U_{ab}(\lambda(0))B(\lambda(0))U^\dagger_{ab}(\lambda(0)). \tag{3.6}$$

However, its trace stays invariant:

$$\mathrm{tr}B(\lambda) = \mathrm{tr}B'(\lambda).$$

3.2.2 Numerical Evaluation of Berry Phases

There are a couple of different ways [43] for approximating the derivative of a function, but we are going to use "the central-difference formula" which says

$$f'(x)\Delta x \simeq \frac{f(x+\Delta x) - f(x-\Delta x)}{2} + O((\Delta x)^3) \tag{3.7}$$

as long as the third derivative of f is a continuous function. Its proof is very simple. Note that, the second-degree Taylor expansion of $f(x)$ about x for $f(x+\Delta x)$ and $f(x-\Delta x)$ are as follows

$$f(x+\Delta x) = f(x) + f'(x)\Delta x + \frac{f''(x)\,(\Delta x)^2}{2} + \frac{f'''(c_1)\,(\Delta x)^3}{6} \tag{3.8}$$

and

$$f(x-\Delta x) = f(x) - f'(x)\Delta x + \frac{f''(x)\,(\Delta x)^2}{2} - \frac{f'''(c_2)\,(\Delta x)^3}{6}. \tag{3.9}$$

By subtracting Eq. 3.9 from Eq. 3.8, we get

$$f(x+\Delta x) - f(x-\Delta x) = 2f'(x)\Delta x + \frac{f'''(c_1) + f'''(c_2)}{6}\,(\Delta x)^3\,.$$

By the intermediate value theorem, there exists a c between c_1 and c_2 such that $f'''(c) = \frac{f'''(c_1)+f'''(c_2)}{2}$, and we can write $O((\Delta x)^3) = \frac{f'''(c)}{3}(\Delta x)^3$ and complete the proof.

It is also possible to get higher level approximations using similar approach, such as

$$f'(x)\Delta x \simeq \frac{-f(x+2\Delta x)+8f(x+\Delta x)-8f(x-\Delta x)+f(x-2\Delta x)}{12}+O((\Delta x)^5)$$

by using the fourth degree Taylor expansion $f(x)$ about x both for $f(x+\Delta x)$ and $f(x-\Delta x)$ and for $f(x+2\Delta x)$ and $f(x-2\Delta x)$.

Applying Eq. 3.7 to $\left[\mathcal{A}^n_{D_n}\right]^{ba}(\lambda')\Delta\lambda$ results in

$$\begin{aligned}\left[\mathcal{A}^n_{D_n}\right]^{ba}(\lambda')\Delta\lambda &= i\langle\varphi^{(n,b)}(\lambda')|\frac{d}{d\lambda'}\varphi^{(n,a)}(\lambda')\rangle\Delta\lambda \\ &= i\frac{\langle\varphi^{(n,b)}(\lambda')|\varphi^{(n,a)}(\lambda'+\Delta\lambda)\rangle-\langle\varphi^{(n,b)}(\lambda')|\varphi^{(n,a)}(\lambda'-\Delta\lambda)\rangle}{2}\end{aligned}$$

which will reduce the calculation of the Berry phase to simply getting of the overlaps between adjacent points on the trajectory.

3.3 Overlap between the Eigenstates of the Quadratic Hamiltonians

3.3.1 Onishi Formula

The overlap between the eigenstates of quadratic Hamiltonians is needed in several context in many-body problems [37]. The Onishi formula [44] provides the norm of this overlap.

Consider the following Bogoliubov transformations for $\gamma(0)$ and $\gamma(i)-$fermions

$$\begin{bmatrix}\gamma^\dagger_\leftrightarrow(0) & \gamma_\leftrightarrow(0)\end{bmatrix} := \begin{bmatrix}c^\dagger_\leftrightarrow & c_\leftrightarrow\end{bmatrix}\begin{bmatrix}U(0) & V^*(0)\\ V(0) & U^*(0)\end{bmatrix}$$

$$\begin{bmatrix}\gamma^\dagger_\leftrightarrow(i) & \gamma_\leftrightarrow(i)\end{bmatrix} := \begin{bmatrix}c^\dagger_\leftrightarrow & c_\leftrightarrow\end{bmatrix}\begin{bmatrix}U(i) & V^*(i)\\ V(i) & U^*(i)\end{bmatrix}$$

with ground states (or vacuums) $|\phi_0\rangle$, $|\phi_i\rangle$ respectively. We would like to calculate the overlap $\langle\phi_0|\phi_i\rangle$ between these states.

By using the inverse relation between $\gamma(0)-$fermions and $c-$fermions

$$\begin{bmatrix} c^\dagger_\leftrightarrow & c_\leftrightarrow \end{bmatrix} = \begin{bmatrix} \gamma^\dagger_\leftrightarrow(0) & \gamma_\leftrightarrow(0) \end{bmatrix} \begin{bmatrix} U^\dagger(0) & V^\dagger(0) \\ V^T(0) & U^T(0) \end{bmatrix}$$

we can re-write $\gamma(i)-$fermions in terms of $\gamma(0)-$fermions as

$$\begin{aligned} \begin{bmatrix} \gamma^\dagger_\leftrightarrow(i) & \gamma_\leftrightarrow(i) \end{bmatrix} &= \begin{bmatrix} \gamma^\dagger_\leftrightarrow(0) & \gamma_\leftrightarrow(0) \end{bmatrix} \begin{bmatrix} U^\dagger(0) & V^\dagger(0) \\ V^T(0) & U^T(0) \end{bmatrix} \begin{bmatrix} U(i) & V^*(i) \\ V(i) & U^*(i) \end{bmatrix} \\ &= \begin{bmatrix} \gamma^\dagger_\leftrightarrow(0) & \gamma_\leftrightarrow(0) \end{bmatrix} \begin{bmatrix} U(i,0) & V^*(i,0) \\ V(i,0) & U^*(i,0) \end{bmatrix} \end{aligned}$$

explicitly,

$$\gamma^\dagger_\leftrightarrow(i) = \gamma^\dagger_\leftrightarrow(0)U(i,0) + \gamma_\leftrightarrow(0)V(i,0) \tag{3.10}$$

$$\gamma_\leftrightarrow(i) = \gamma^\dagger_\leftrightarrow(0)V^*(i,0) + \gamma_\leftrightarrow(0)U^*(i,0) \tag{3.11}$$

where $U(i,0)$ and $V(i,0)$ are defined as

$$\begin{aligned} U(i,0) &= U^\dagger(0)\ U(i) + V^\dagger(0)\ V(i) \\ V(i,0) &= V^T(0)\ U(i) + U^T(0)\ V(i). \end{aligned} \tag{3.12}$$

By applying the Bloch-Messiah theorem, we can write

$$\begin{bmatrix} U(i,0) & V^*(i,0) \\ V(i,0) & U^*(i,0) \end{bmatrix} = \begin{bmatrix} D(i,0) & \\ & D^*(i,0) \end{bmatrix} \begin{bmatrix} \overline{U}(i,0) & \overline{V}(i,0) \\ \overline{V}(i,0) & \overline{U}(i,0) \end{bmatrix} \begin{bmatrix} C(i,0) & \\ & C^*(i,0) \end{bmatrix}.$$

Let us define $\overline{\gamma}(0)-$fermions as

$$\overline{\gamma}^\dagger_k(0) = \sum_{k'} D_{k'k}(i,0)\gamma^\dagger_{k'}(0)$$

Now, we can write the vacuum $|\phi_{(i,0)}\rangle$ of $\gamma(i)-$fermions in terms of the vacuum $|\phi_0\rangle$ of $\gamma(0)-$fermions as

$$|\phi_{(i,0)}\rangle = \prod_i \overline{\gamma}^\dagger_i(0) \prod_p \Big(u_p(i,0) + v_p(i,0)\ \overline{\gamma}^\dagger_p(0)\ \overline{\gamma}^\dagger_{\overline{p}}(0)\Big)\ |\phi_0\rangle \tag{3.13}$$

Note that if the ground state of $\gamma(i)-$fermions is non-degenerate then $|\phi_i\rangle$ and $|\phi_{(i,0)}\rangle$ is same up to an overall phase.

Now $\langle\phi_0|\phi_{(i,0)}\rangle$ reads

$$\langle\phi_0|\phi_{(i,0)}\rangle = \langle\phi_0| \prod_i \overline{\gamma}_i^\dagger \prod_p \Big(u_p(i,0) + v_p(i,0)\, \overline{\gamma}_p^\dagger(0)\, \overline{\gamma}_{\overline{p}}^\dagger(0)\Big)\ |\phi_0\rangle$$

$\langle\phi_0|\phi_{(i,0)}\rangle$ is only non-zero if there are no occupied levels (i.e. $i-$part) and it is equal to

$$\langle\phi_0|\phi_{(i,0)}\rangle = \langle\phi_0| \prod_p u_p(i,0)\ |\phi_0\rangle = \prod_p u_p(i,0) = \sqrt{\det \overline{U}(i,0)} = \sqrt{|\det U(i,0)|}$$

recall that $\overline{U}(i,0)$ is diagonal. Therefore, we can state the Onishi formula as

$$|\langle\phi_0|\phi_i\rangle| = \sqrt{|\det U(i,0)|}$$

Remark: *Notice that* $\langle\phi_0|\phi_{(i,0)}\rangle \neq 0$ *if and only if* $\det U(i,0) \neq 0$. *In other words,* $\langle\phi_0|\phi_{(i,0)}\rangle \neq 0$ *if* $U^{-1}(i,0)$ *exists.*

However, this overlap is not enough for calculating the Berry phase. In the Berry phase calculation, we need to determine the overlap between the states $|\phi_{(0)}\rangle$ and $|\phi_{(i)}\rangle$ in terms of both magnitude and phase. On the other hand, the Onishi formula only gives us the magnitude of the overlap. This is due to fact that the Bloch-Messiah method used to get Eq. 3.13 does not preserve the relative phases between the ground states $|\phi_{(0)}\rangle$ and $|\phi_{(i)}\rangle$. However, we are going to use the above remark in Thouless' theorem which will eventually lead us to a more precise description of the overlap.

3.3.2 Thouless' Theorem

For the Bogoliubov transformations given in the previous part, we can state the Thouless' theorem [45] as follows:

Theorem 1 *Let* $|\phi_0\rangle, |\phi_i\rangle$ *be the vacuum of* $\gamma(0)$ *and* $\gamma(i)-$*fermions respectively such that* $\langle\phi_i|\phi_0\rangle \neq 0$. *Then* $|\phi_i\rangle$ *may be expressed in the following form* $|\psi_{(i,0)}\rangle$

$$|\psi_{(i,0)}\rangle = \mathcal{N} e^{\mathbf{Z}(i,0)} |\phi_0\rangle \tag{3.14}$$

where

$$\mathbf{Z}(i,0) = \frac{1}{2}\sum_{k,k'} Z_{kk'}(i,0)\gamma_k^\dagger(0)\gamma_{k'}^\dagger(0),$$

$\mathcal{N}$ *is a normalization constant and* $Z(i,0)$ *is a skew symmetric matrix given as*

$$Z(i,0) = \left(V(i,0)U^{-1}(i,0)\right)^*. \tag{3.15}$$

Note that the ground state of the $\gamma-$fermions will be denoted by either ϕ or ψ depending on whether we use the Bloch-Messiah representation or the Thouless representation respectively. Also note that, $|\phi_i\rangle$ and $|\psi_{(i,0)}\rangle$ are just different way of representing the same ground state of $\gamma(i)-$fermions; the former is written in terms of the vacuum $|-\rangle$ of $c-$fermions, the latter is written in terms of vacuum $|\phi_0\rangle$ of $\gamma(0)-$fermions.

By using the remark from the previous section we can define $\widetilde{\gamma}(i)-$fermions as following:

$$\widetilde{\gamma}_k^\dagger(i) := \sum_{k'} U^{-1}_{k'k}(i,0)\gamma_{k'}^\dagger(i)$$

By expressing $\gamma_{k'}^\dagger(i)$ in terms of $\gamma(0)-$fermions as in Eq. 3.10, we get

$$\widetilde{\gamma}_k^\dagger(i) = \gamma_k^\dagger(0) + \sum_{k'} Z^*_{k'k}(i,0)\gamma_{k'}(0).$$

Note that $\widetilde{\gamma}(i)-$fermions share the same vacuum $|\phi_i\rangle$ with $\gamma(i)-$fermions, since $\widetilde{\gamma}^\dagger(i)$ $(\widetilde{\gamma}(i))$ is just a linear combination of creation $\gamma^\dagger(i)$(or annihilation $\gamma(i)$) operators.

If we show that $\widetilde{\gamma}_k(i)e^{\mathbf{Z}(i,0)}|\phi_0\rangle = 0$ for all k, then $e^{\mathbf{Z}(i,0)}|\phi_0\rangle$ will be equivalent to the ground state of $\gamma(i)-$fermions $|\phi_i\rangle$ up to normalization factor and a phase.

By noting that

$$\widetilde{\gamma}_k(i) = \gamma_k(0) + \sum_{k'} Z_{k'k}(i,0)\gamma_{k'}^\dagger(0)$$

$\widetilde{\gamma}_k(i)e^{\mathbf{Z}(i,0)}|\phi_0\rangle$ can be written as

$$\widetilde{\gamma}_k(i)e^{\mathbf{Z}(i,0)}|\phi_0\rangle = e^{\mathbf{Z}(i,0)}\left\{e^{-\mathbf{Z}(i,0)}\gamma_k(0)e^{\mathbf{Z}(i,0)} + \sum_{k'} Z_{k'k}(i,0)\gamma_{k'}^\dagger(0)\right\}|\phi_0\rangle \tag{3.16}$$

since $\left[\sum_{k'} Z_{k'k}(i,0)\gamma^{\dagger}_{k'}(0), e^{\mathbf{Z}(i,0)}\right] = 0$.

By using the Baker–Campbell–Hausdorff formula

$$e^{A}Be^{-A} = B + [A,B] + \frac{1}{2!}[A,[A,B]] + \frac{1}{3!}[A,[A,[A,B]]] + \cdots$$

$e^{-\mathbf{Z}(i,0)}\gamma_k(0)e^{\mathbf{Z}(i,0)}$ can be written as

$$e^{-\mathbf{Z}(i,0)}\gamma_k(0)e^{\mathbf{Z}(i,0)} = \gamma_k(0) - \sum_{k'} Z_{k'k}(i,0)\gamma^{\dagger}_{k'}(0). \tag{3.17}$$

Combining this result with Eq. 3.16 shows that $\widetilde{\gamma}_k(i)e^{\mathbf{Z}(i,0)}|\phi_0\rangle = 0$, and completes the proof of the theorem.

Notice that the normalization constant $\mathcal{N}$ is, up to a phase, given as the following

$$\mathcal{N} = \langle\phi_0|\psi_{(i,0)}\rangle = \langle\phi_0|\phi_{(i,0)}\rangle = \sqrt{|\det U(i,0)|}.$$

Finally, we can represent $|\psi_{(i,0)}\rangle$ up to a phase as:

$$|\psi_{(i,0)}\rangle = \sqrt{|\det U(i,0)|}\; e^{\mathbf{Z}(i,0)}|\phi_0\rangle. \tag{3.18}$$

Remark: *Although the columns of U and V (Eq. 2.26) are defined up to a phase, Z is a unique matrix for all M given as in Eq. 2.24. A general gauge transformation $\mathcal{A}$ for the columns of U and V act as*

$$\begin{aligned} U &\longrightarrow U\mathcal{A} \\ V &\longrightarrow V\mathcal{A} \end{aligned}$$

where $\mathcal{A}$ is a block diagonal matrix

$$\begin{pmatrix} \mathcal{A}_1 & & \\ & \ddots & \\ & & \mathcal{A}_N \end{pmatrix}$$

where the $\mathcal{A}_i$'s are just phase factors for nondegenerate eigenvalues of M and can be unitary matrices for degenerate eigenvalues of M. As can be easily verified, Z stays invariant for different gauges

$$Z = \left(VU^{-1}\right)^{*} \longrightarrow \left(VA\,(UA)^{-1}\right)^{*} = \left(VU^{-1}\right)^{*}.$$

3.3.3 Overlap

In this section, the overlap between the ground states of a quadratic Hamiltonians is discussed. Recall that by using the column exchange operation explained in section 2.6.2, all eigenstates of a quadratic Hamiltonian can be written as the ground state of the set of newly defined fermions. Therefore this discussion can be extended to other eigenstates too.

The overlap between the ground states $|\psi_{(j,0)}\rangle$ and $|\psi_{(i,0)}\rangle$ where $i \neq j \neq 0$, is equal to

$$\langle\psi_{(j,0)}|\psi_{(i,0)}\rangle = \sqrt{|\det U(j,0)|}\ \sqrt{|\det U(i,0)|}\langle\phi_0|e^{\mathbf{Z}^\dagger(j,0)}e^{\mathbf{Z}(i,0)}|\phi_0\rangle.$$

Moreover, the overlap $\langle\phi_0|e^{\mathbf{Z}^\dagger(j,0)}e^{\mathbf{Z}(i,0)}|\phi_0\rangle$ has been calculated with the correct sign factor in the recent paper [46]. Here we are going to re-derive it within our formulation.

We start the derivation by introducing the coherent states $|z\rangle$

$$|z\rangle := \exp\left\{\sum_{k=1}^{N}\gamma_k^\dagger(0)z_k\right\}|\phi_0\rangle$$

where z_k and z_k^* are anti-commuting elements of a Grassmann algebra (* represents conjugation on Grassmann algebra) satisfying the following equations

$$\gamma_k(0)|z\rangle = z_k|z\rangle \text{ and } \langle z|\gamma_k^\dagger(0) = \langle z|z_k^*.$$

The coherent states satisfy a completeness relation

$$I = \int d\mu(z)\ |z\rangle\langle z|$$

where the measure of the integral is given by $d\mu(z) = \exp\{\sum_k -z_k^* z_k\}\prod_k dz_k^* dz_k$.

By taking the advantage of this completeness relation, we can express the general

overlap as

$$\begin{aligned}
\langle\phi_0|e^{\mathbf{Z}^\dagger(j,0)}e^{\mathbf{Z}(i,0)}|\phi_0\rangle &= \int d\mu(z)\ \langle\phi_0|e^{\mathbf{Z}^\dagger(j,0)}|z\rangle\ \langle z|e^{\mathbf{Z}(i,0)}|\phi_0\rangle \\
&= \int d\mu(z)\ \langle\phi_0|\exp\left\{\frac{1}{2}\sum_{k,k'} Z^*_{kk'}(j,0)\gamma_{k'}(0)\gamma_k(0)\right\}|z\rangle \\
&\quad \times\langle z|\exp\left\{\frac{1}{2}\sum_{k,k'} Z_{kk'}(i,0)\gamma^\dagger_k(0)\gamma^\dagger_{k'}(0)\right\}|\phi_0\rangle \\
&= \int d\mu(z)\quad \exp\left\{\frac{1}{2}\sum_{k,k'} Z^*_{kk'}(j,0)z_{k'}z_k\right\}\times \\
&\quad \exp\left\{\frac{1}{2}\sum_{k,k'} Z_{kk'}(i,0)z^*_k z^*_{k'}\right\}
\end{aligned}$$

where $|\langle\phi_0|z\rangle|^2 = 1$ is used. The above integral can be written in a more compact way by introducing the skew-symmetric matrix

$$\mathcal{Z}(j,0;i,0) = \begin{bmatrix} Z(i,0) & -I \\ I & -Z^*(j,0) \end{bmatrix}$$

and the vector of Grassmann variables $z^*_{\leftrightarrow} = \begin{bmatrix} z^*_1 & z^*_2 & \cdots & z^*_N \end{bmatrix}$ and $z^*_{\updownarrow} = \begin{bmatrix} z^*_1 \\ z^*_2 \\ \vdots \\ z^*_N \end{bmatrix}$

$$\langle\phi_0|e^{\mathbf{Z}^\dagger(j,0)}e^{\mathbf{Z}(i,0)}|\phi_0\rangle = \int\prod_k dz^*_k dz_k\ \exp\left\{\frac{1}{2}\begin{bmatrix} z^*_{\leftrightarrow} & z_{\leftrightarrow}\end{bmatrix}\mathcal{Z}(i,j)\begin{bmatrix} z^*_{\updownarrow} \\ z_{\updownarrow}\end{bmatrix}\right\} \tag{3.19}$$

The skew-symmetric matrix $\mathcal{Z}$ can always be written in its canonical form with the

help of the unitary transformation $\mathcal{U}$ [47]

$$\begin{aligned}\mathcal{Z}(j,0;i,0) &= \mathcal{U}(j,0;i,0)\begin{pmatrix} 0 & \cdots & 0 & \zeta_1 & 0 & 0 \\ \vdots & \ddots & \vdots & 0 & \ddots & 0 \\ 0 & \cdots & 0 & 0 & 0 & \zeta_N \\ -\zeta_1 & 0 & 0 & 0 & \cdots & 0 \\ 0 & \ddots & 0 & \vdots & \ddots & \vdots \\ 0 & 0 & -\zeta_N & 0 & \cdots & 0 \end{pmatrix}\mathcal{U}^T(j,0;i,0) \\ &= \mathcal{U}(j,0;i,0)\mathcal{Z}_C(j,0;i,0)\mathcal{U}^T(j,0;i,0)\end{aligned}$$

where ζ_i are real and positive. By introducing new Grassmann variables

$$\begin{bmatrix}\eta^*_{\leftrightarrow} & \eta_{\leftrightarrow}\end{bmatrix} = \begin{bmatrix}z^*_{\leftrightarrow} & z_{\leftrightarrow}\end{bmatrix}\mathcal{U}(i,j)$$

the exponential in the integral becomes

$$\exp\left\{\frac{1}{2}\begin{bmatrix}\eta^*_{\leftrightarrow} & \eta_{\leftrightarrow}\end{bmatrix}\mathcal{Z}_C(j,0;i,0)\begin{bmatrix}\eta^*_{\updownarrow} \\ \eta_{\updownarrow}\end{bmatrix}\right\} = \exp\left\{\sum_{k=1}^{N}\zeta_k\,\eta^*_k\eta_k\right\}$$

and the measure becomes

$$\prod_k dz^*_k dz_k = \det J^{-1}\prod_k d\eta^*_k d\eta_k$$

where J is the Jacobian

$$J = \begin{pmatrix} \frac{\partial}{\partial\eta^*_1}z^*_1 & \cdots & \frac{\partial}{\partial\eta^*_N}z^*_1 & \frac{\partial}{\partial\eta_1}z^*_1 & \cdots & \frac{\partial}{\partial\eta_N}z^*_1 \\ \vdots & \ddots & \vdots & \vdots & \ddots & \vdots \\ \frac{\partial}{\partial\eta^*_1}z^*_N & \cdots & \frac{\partial}{\partial\eta^*_N}z^*_N & \frac{\partial}{\partial\eta_1}z^*_N & \cdots & \frac{\partial}{\partial\eta_N}z^*_N \\ \frac{\partial}{\partial\eta^*_1}z_1 & \cdots & \frac{\partial}{\partial\eta^*_N}z_1 & \frac{\partial}{\partial\eta_1}z_1 & \cdots & \frac{\partial}{\partial\eta_N}z_1 \\ \vdots & \ddots & \vdots & \vdots & \ddots & \vdots \\ \frac{\partial}{\partial\eta^*_1}z_N & \cdots & \frac{\partial}{\partial\eta^*_N}z_N & \frac{\partial}{\partial\eta_1}z_N & \cdots & \frac{\partial}{\partial\eta_N}z_N \end{pmatrix} = \mathcal{U}^*(i,j)$$

Note that $\det J^{-1} = \det\mathcal{U}^T(i,j) = \det\mathcal{U}(i,j)$.

Now we can write the integral (Eq. 3.19) as

$$\langle\phi_0|e^{\mathbf{Z}^\dagger(j,0)}e^{\mathbf{Z}(i,0)}|\phi_0\rangle = \int \det\mathcal{U}(i,j)\prod_k d\eta^*_k d\eta_k \exp\left\{\sum_{k=1}^{N}\zeta_k\,\eta^*_k\eta_k\right\}$$

We can easily evaluate this multivariable Gaussian integral in Grassmann variables as

$$\langle\phi_0|e^{\mathbf{Z}^\dagger(j,0)}e^{\mathbf{Z}(i,0)}|\phi_0\rangle = (-1)^N \det\mathcal{U}(i,j)\prod_{k=1}^{N}\zeta_k \tag{3.20}$$

by using the properties

$$\int d\eta^* d\eta e^{\zeta\,\eta^*\eta} = -\zeta.$$

By using the following properties of Pfaffian

$$\mathrm{Pf}\begin{pmatrix} 0 & R \\ -R & 0 \end{pmatrix} = (-1)^{N(N-1)/2}\det R$$

and

$$\mathrm{Pf}(P^T R P) = \det P\ \mathrm{Pf}(R)$$

for any $N\times N$ matrices R and P, Eq. 3.20 can be expressed in terms of the Pfaffian of $\mathcal{Z}(j,0;i,0)$ as

$$\langle\phi_0|e^{\mathbf{Z}^\dagger(j,0)}e^{\mathbf{Z}(i,0)}|\phi_0\rangle = (-1)^{N(N+1)/2}\ \mathrm{Pf}(\mathcal{Z}(j,0;i,0))$$

Now we are going to write Pfaffian in terms of the determinant of some simpler matrices. Now note that $\mathrm{Pf}(\mathcal{Z}(j,0;i,0)) = (\pm 1)\sqrt{\det\mathcal{Z}(j,0;i,0)}$ and by using the following theorem [48] we can reduce $\det\mathcal{Z}(j,0;i,0)$ into a simpler form.

Theorem 2 *If* $M = \begin{pmatrix} A & B \\ C & D \end{pmatrix}$, *where* A, B, C, D *are* $n\times n$ *matrices with complex coefficients and* $CD = DC$, *then*

$$\det M = \det(AD - BC).$$

Now, we can write $\det(\mathcal{Z}(j,0;i,0))$ as

$$\det(\mathcal{Z}(j,0;i,0)) = \det\left(I - Z(i,0)Z^*(j,0)\right). \tag{3.21}$$

Recall that $Z(i,0) = [V(i,0)U^{-1}(i,0)]^*$ and since it is skew-symmetric it is also true that $Z(i,0) = -\left(U^\dagger(i,0)\right)^{-1}V^\dagger(i,0)$. Therefore, we have

$$\begin{aligned} I - Z(i,0)Z^*(j,0) &= I + (U^\dagger(i,0))^{-1}V^\dagger(i,0)V(j,0)U^{-1}(j,0) \\ &= (U^\dagger(i,0))^{-1}\left(U^\dagger(i,0)U(j,0) + V^\dagger(i,0)V(j,0)\right)U^{-1}(j,0) \end{aligned}$$

By using Eq. 3.12, it is easy to show

$$U^{\dagger}(i,0)U(j,0)+V^{\dagger}(i,0)V(j,0)=U\left(i,j\right).$$

where $U\left(i,j\right)$ is defined as

$$U(i,j):=U^{\dagger}(j)U(i)+V^{\dagger}(j)V(i) \tag{3.22}$$

as a generalized version of Eq. 3.12.

Therefore we have

$$\det\left(I-Z(i,0)Z^{*}(j,0)\right)=\det\left(\left(U^{\dagger}(i,0)\right)^{-1}U\left(j,i\right)U^{-1}(j,0)\right)$$

Finally, we can express $\langle\phi_0|e^{\mathbf{Z}^{\dagger}(j,0)}e^{\mathbf{Z}(i,0)}|\phi_0\rangle$ in its final form as

$$\langle\phi_0|e^{\mathbf{Z}^{\dagger}(j,0)}e^{\mathbf{Z}(i,0)}|\phi_0\rangle=(-1)^{N(N+1)/2}\left[(\pm1)\sqrt{\frac{\det U\left(j,i\right)}{\det U^{\dagger}(i,0)\det U(j,0)}}\right] \tag{3.23}$$

Moreover, if we fix the general phase of Eq. 3.18 as 1, we can express the overlap between $|\psi_{(i,0)}\rangle$ and $|\psi_{(j,0)}\rangle$ as

$$\begin{aligned}\langle\psi_{(j,0)}|\psi_{(i,0)}\rangle &= \sqrt{|\det U(j,0)|}\ \sqrt{|\det U(i,0)|}\ \langle\phi_0|e^{\mathbf{Z}^{\dagger}(j,0)}e^{\mathbf{Z}(i,0)}|\phi_0\rangle\\ &= \sqrt{|\det U(j,0)|}\ \sqrt{|\det U(i,0)|}\ (-1)^{N(N+1)/2}\times\\ &\quad\left[(\pm1)\sqrt{\frac{\det U\left(j,i\right)}{\det U^{\dagger}(i,0)\det U(j,0)}}\right]\\ &= (-1)^{N(N+1)/2}\left[(\pm1)\sqrt{\exp\left\{i\theta_0\left(j,i\right)\right\}\ |\det U\left(j,i\right)|}\right]\end{aligned} \tag{3.24}$$

where

$$\theta_0\left(j,i\right)=\arg\left\{\det U(i,0)\det U^{\dagger}(j,0)\det U\left(j,i\right)\right\}.$$

By taking phase out of the square root, $\langle\psi_{(j,0)}|\psi_{(i,0)}\rangle$ is equal to one of the following

$$\langle\psi_{(j,0)}|\psi_{(i,0)}\rangle=\begin{cases}(-1)^{N(N+1)/2}\exp\left\{\frac{i\theta_0(j,i)}{2}\right\}\sqrt{|\det U\left(j,i\right)|}\\ (-1)^{N(N+1)/2}\exp\left\{\frac{i\theta_0(j,i)}{2}+\pi\right\}\sqrt{|\det U\left(j,i\right)|}.\end{cases} \tag{3.25}$$

where

$$-\pi<\theta_0\left(j,i\right)\leq\pi$$

and

$$\sqrt{|\det U\left(j,i\right)|}\geq0.$$

3.4 Non-Abelian Berry Phase of the Honeycomb Model

In this section, numerical results of the non-Abelian Berry phase of a particular type of configuration (Fig. 3.3) with various sizes of the honeycomb model will be presented. Note that, all configurations that has been studied are even-by-even lattices with periodic boundary condition. Vortices are created by making a series of adiabatic changes in the J and κ values of a zero-vortex configuration so they are $J\kappa-$vortices. Recall that, 4 well-separated $J\kappa-$vortices provides 2 zero-energy $\gamma-$fermions (two zero modes), which results in a $2-$fold degenerate ground state with the basis states[1] $|\Phi^1(\lambda_0)\rangle$ and $|\Phi^2(\lambda_0)\rangle$, where λ_0 denote the beginning point of the trajectory on which Berry phase to be calculated. Note that the Berry phase is given as

$$\begin{aligned}\mathcal{B}(\mathbf{C}) &:= \mathcal{P}\exp\left\{i\oint \mathcal{A}_2(\lambda)d\lambda\right\} \\ &:= \lim_{M\to\infty}\exp\left\{i\mathcal{A}_2(\lambda_{M-1})\Delta\lambda\right\}\cdots\exp\left\{i\mathcal{A}_2(\lambda_0)\Delta\lambda\right\} \qquad (3.26)\end{aligned}$$

where

$$[\mathcal{A}_2(\lambda_k)]^{ba} = \langle\Phi^b(\lambda)|\frac{d}{d\lambda}\Phi^a(\lambda)\rangle\Big|_{\lambda=\lambda_k},$$

and where λ_0 and λ_M are coinciding points denoting the beginning and end point of the closed trajectory whose curve length is given by $\mathbf{length}(\lambda_M,\lambda_0)$, and $\Delta\lambda$ is given as $\Delta\lambda = \mathbf{length}(\lambda_M,\lambda_0)/M$. Note that, the third-order central-difference-formula (Eq. 3.7) is used for evaluating numerical value of the derivatives in our calculations.

The Berry matrix 3.26 is calculated for the path shown in Fig. 3.3 by moving $J\kappa-$vortices slowly as described in Section 3.1. However, for the sake of calculating Berry matrix the motion has to be adiabatic as well, which means the degenerate ground-state space has to be separated from the first excited state by a gap. For the sake of precision, it is better to do this discussion with the help of the non-Abelian version of the adiabatic approximation given in Eq.3.2

$$\langle\varphi^{(m,b)}(\lambda)|\frac{d}{dt}\varphi^{(n,a)}(\lambda)\rangle = \frac{\langle\varphi^{(m,b)}(\lambda(t))|\frac{d}{dt}H(\lambda)|\varphi^{(n,a)}(\lambda)\rangle}{E_n(\lambda)-E_m(\lambda)} \cong 0, \qquad (3.27)$$

[1]The ground state of the Kitaev honeycomb model will be denoted by Φ or Ψ in the Bloch-Messiah representation or Thouless representation respectively, in contrast to the use of ϕ and ψ for the ground state of the quadratic Hamiltonians.

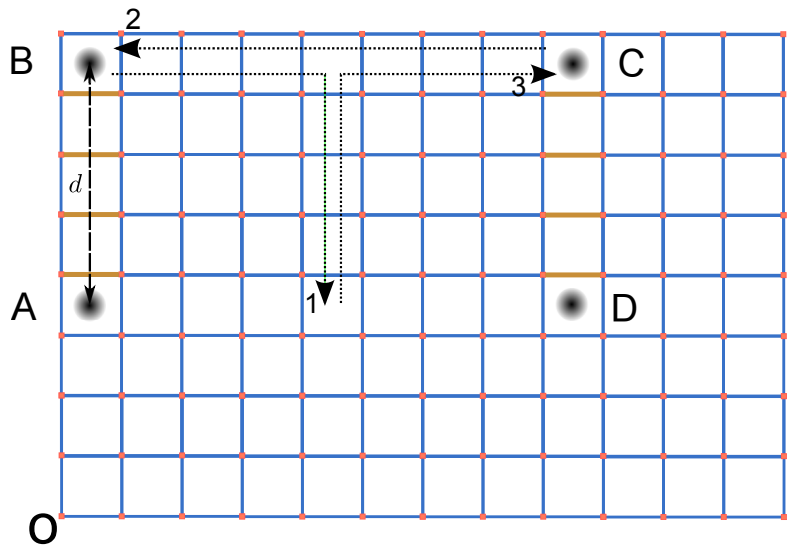

Figure 3.3: A configuration of 4 $J\kappa-$vortices with minimum distance $d = 4$. Note that the size of the system changes with the minimum distance d such that $N_x = 3d$, $N_y = 2d$ for even d and $N_x = 3d + 1$, $N_y = 2d$ for odd d. The arrows point out the trajectory of swapping the vortex **B** with the vortex **C**. Yellow colored links between **A** and **B** (and **C** and **D**) highlight changed links while creating and bringing the vortices to their shown positions. System has periodic boundary conditions so that opposite sides of the lattices are identified.

for all $m \neq n$ and for all a, b, where m, n denotes different degenerate energy spaces and a, b labels different basis states within each degenerate space. According to Eq. 3.27, the adiabatic approximation for the degenerate space n is valid when the change in the Hamiltonian is very slow and the gap $G_{m,n}(\lambda) := E_m(\lambda) - E_n(\lambda)$ is very large for $m \neq n$. However, when the system is nearly degenerate, a scaled version of the gap between nearly-degenerate space and higher excited states is a more meaningful quantity. For this reason, the smallness of the ratio $G_{(n,b),(n,a)}(\lambda)/G_{m,n}(\lambda)$ where $G_{(n,a),(n,b)}(\lambda)$ is the gap between the nearly degenerate levels $G_{(n,b),(n,a)}(\lambda) := E_{(n,b)}(\lambda) - E_{(n,a)}(\lambda)$ for $a \neq b$, is a more relevant quantity to check the validity of the adiabatic approximation.

In our case, $|\Phi^1(\lambda)\rangle$ and $|\Phi^2(\lambda)\rangle$ are nearly degenerate states along the trajectory, and they are separated by a gap from higher excited states $|\Phi^m(\lambda)\rangle$, $m \geq 3$. Fig. 3.4

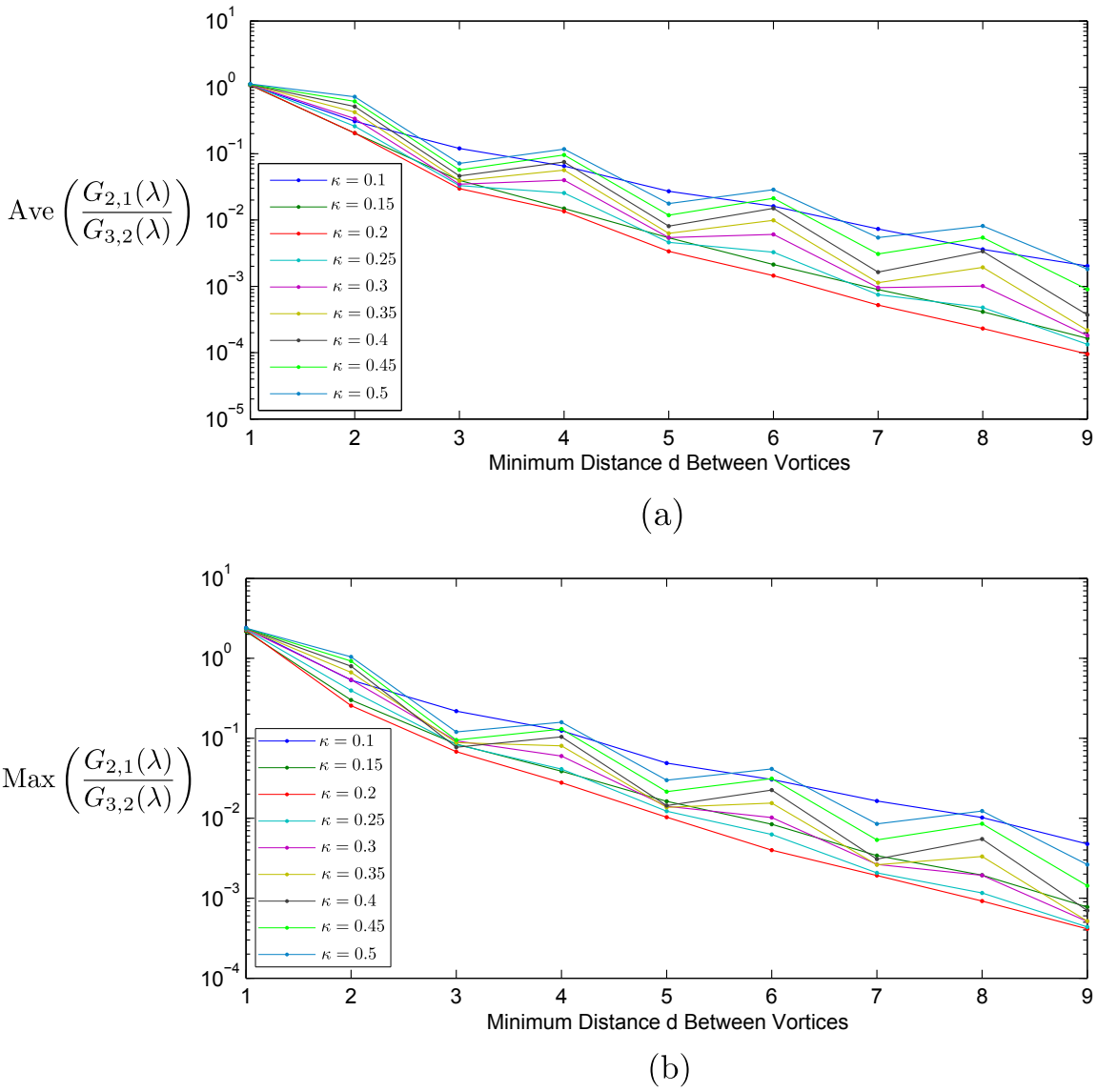

Figure 3.4: (a) Average value of the ratio $G_{2,1}(\lambda)/G_{3,2}(\lambda)$ along the trajectory vs. Minimum distance between vortices ($G_{2,1}(\lambda)$ is the gap between nearly-degenerate states, and $G_{3,2}(\lambda)$ is the gap between nearly-degenerate space and higher excited states). (b) Maximum value of the ratio $G_{2,1}(\lambda)/G_{3,2}(\lambda)$ along the trajectory vs. Minimum distance between vortices. Maximum value of the ratio corresponds to the smallest (scaled) gap between nearly-degenerate space and higher excited states. Note that, in our calculations $J = J_q^x = J_q^y = J_q^z = 1$ for all q and $\kappa = \kappa_q^x = \kappa_q^y = \kappa_q^5 = \kappa_q^6$ for all q (Eqs. 2.17−2.20) where κ have various values between 0.1 and 0.5.

shows both the average and the maximum value of the ratio of $G_{2,1}(\lambda)/G_{3,2}(\lambda)$ along the trajectory where $G_{2,1}(\lambda) = E_{|\Phi^2\rangle}(\lambda) - E_{|\Phi^1\rangle}(\lambda)$ and $G_{3,2}(\lambda) = E_{|\Phi^3\rangle}(\lambda) - E_{|\Phi^2\rangle}(\lambda)$. Maximum value of the ratio corresponds to the smallest (scaled) gap between nearly-degenerate space and higher excited states, in other words the worst gap (scaled) values to apply adiabatic approximation along the trajectory. As it seen from the Fig. 3.4, the adiabatic approximation becomes more meaningful as the minimum distance d between vortices increases. We will also have a closer look to this plot in following pages, but for now it is important for the justification of the adiabatic approximation.

On the other hand, to be able to calculate the non-Abelian Berry phase, the basis states of the degenerate space have to follow a smooth trajectory. Since we don't have the analytical solutions for eigenstates and have to work with numerical tools, we must pay attention to three crucial steps to satisfy that. First of all, we have to distinguish degenerate states from each other along the trajectory to be able to use them as basis states for each point. This is easy to achieve since the energy of the zero modes in the honeycomb model are not exactly zero unless vortices are infinitely apart as it is seen from Fig.3.5 which shows the minimum value of the gap between nearly degenerate states along each point on the trajectory.

Secondly, we need to choose a reference state $|\Phi(0)\rangle$ which is not orthogonal to degenerate space for all points along the trajectory, so that we can represent all the states with respect to this reference state. This ensures that the Thouless representations[2] of the states change smoothly along the trajectory. Note that, the ground state of a point which is near to any point of the trajectory could be used as a reference state.[3] However, numerical verification of non-orthogonality is still needed. Once the reference state $|\Phi(0)\rangle$ has been fixed, $Z(k, 0)$ (Eq. 3.15) is unique for each point k on the trajectory. Therefore, fixing the overall phase of the data points is enough to assure

[2]Note that, Thouless representation can also be used to represent excited states by using the column exchange operation mentioned in section 2.6.2.

[3]Note that if we use the ground state of a point on the trajectory as reference state we can not represent nearly degenerate state of the same point in Thouless' formalism since they are orthogonal to each other.

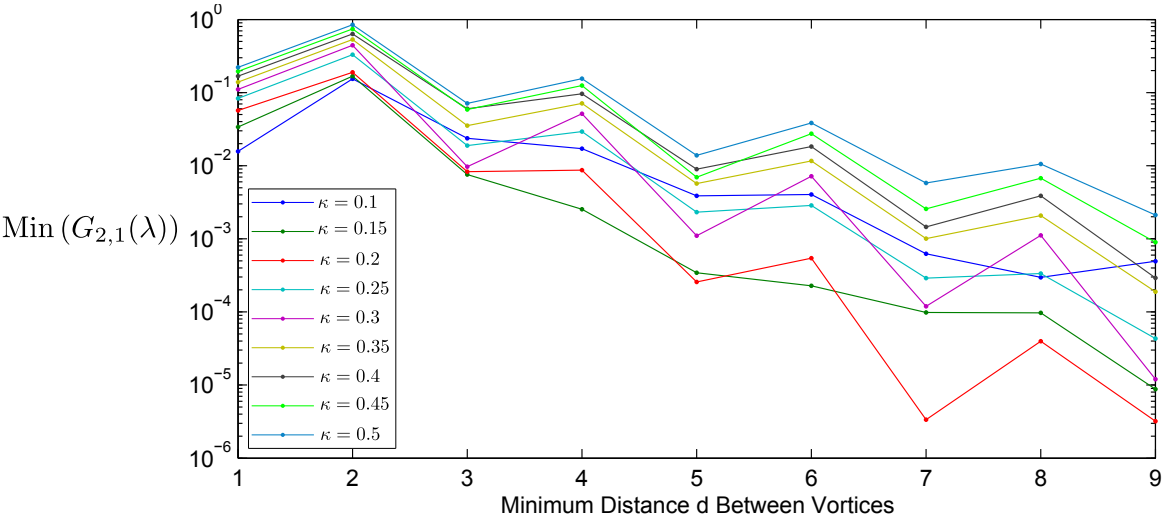

Figure 3.5: Minimum value of the gap $G_{2,1}(\lambda)$ along the trajectory vs. Minimum distance between vortices. Note that, in our calculations $J = J_q^x = J_q^y = J_q^z = 1$ for all q and $\kappa = \kappa_q^x = \kappa_q^y = \kappa_q^5 = \kappa_q^6$ for all q (Eqs. 2.17−2.20) where κ have various values between 0.1 and 0.5.

the smoothness of the representation of the state along the trajectory.[4]

Finally, while we are moving the $J\kappa-$vortices by changing the $[J\kappa]$ values for each link on the trajectory of links (Fig. 3.3) we have to do it in such a way that resulting trajectory in the parameter space is smooth. Note that changing one link after another gives us a curve with square edges (Fig. 3.6(a)). Therefore to ensure smoothness we need to start changing the next coupling coefficient when we are about to stop changing that of present one (Fig. 3.6(b)). For example, let $[J\kappa]_q^y$ and $[J\kappa]_{q+\widehat{n}_x}^y$ be two coupling coefficients of two successive links on the trajectory (Fig. 3.6). Say that we need to change $[J\kappa]_q^y$ from a^5 to $-a$ to move a vortex. To be able to do it smoothly, we need to start changing $[J\kappa]_{q+\widehat{n}_x}^y$ before $[J\kappa]_q^y$ reaches $-a$. We will refer

[4]The overall phases of the states between each numerical data points can be considered so that the smoothness of the trajectory is granted since the characteristic properties (e.g. trace, eigenvalues) of the Berry phase do not depend on overall phases of the states on the trajectory as Berry matrix changes as Eq. 3.6 under gauge transformations.

[5]Note that a could be different for J and κ. In our calculations, a was set as 1 for $J = J^x = J^y = J^z$ and some various values, between 0.1 and 0.5, for κ ($\kappa = \kappa_q^x = \kappa_q^y = \kappa_q^5 = \kappa_q^6$ for all q (Eqs. 2.17−2.20)).

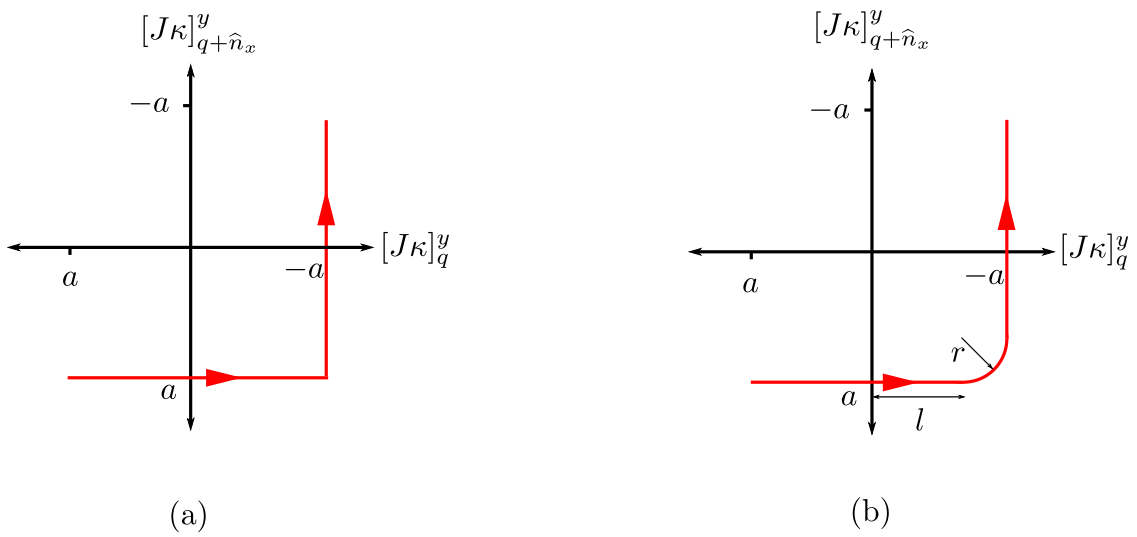

Figure 3.6: (a) Changing the J and κ values of a link after another gives us a trajectory with square edges. (b) Changing the J and κ values of the next link before stopping to change that of the present one gives us smooth trajectory.

to the part where only single $[J\kappa]$ changes as *linear part* and where two $[J\kappa]$ changes as *circular part*, because of the shape of the curve in parameter space. Note that, for this reason a vortex is never located on a particular plaquette with its 100% presence.

Our numerical Berry matrix calculations have been done for two different trajectories in terms of their linear and circular parts. In both calculations, every link on the trajectory has been covered in 4000 steps which all have *equal length* Δs in the parameter space. Let l be the total length of the linear part from 0 to the start of the circular part (Fig. 3.6) and r is the radius of the circular part then $r + l = a$ and $\Delta s = \Delta l = r\Delta\theta$ where $\Delta l = l/$*number of linear steps* and $\Delta\theta = \frac{\pi}{2}/$*number of circular steps*. In one calculation the number of linear steps was set to 3991 whereas the number of circular steps was 9 for all links. This corresponds to changing both links at $-0.997a$, hence we refer to this calculation as $0.997[J\kappa]$. In the other calculation the number of linear steps was 3801 whereas the number of circular steps was 199 for all links, and this corresponds to changing both links at $-0.937a$. Similarly we refer to this calculation as $0.937[J\kappa]$

Berry matrix $\mathcal{B}$ resulting from the exchange of **B** and **C** (Fig. 3.3) is diagonal for the orthonormal basis $\{|\Omega^I\rangle, |\Omega^\epsilon\rangle\}$ formed by the fusion channels I and ϵ of **B** and **C**[6]

$$\mathcal{B}_\Omega = \begin{pmatrix} R^1_{\sigma\sigma} & \\ & R^\epsilon_{\sigma\sigma} \end{pmatrix}. \tag{3.28}$$

The diagonal entries $R^1_{\sigma\sigma}, R^\epsilon_{\sigma\sigma}$ are found by solving the pentagon and hexagon equation [14] are as follows

$$R^1_{\sigma\sigma} = \theta e^{i\alpha\pi/8}, \qquad R^\epsilon_{\sigma\sigma} = \theta e^{-i\alpha\pi/8}$$

with the possible combinations of θ and α are

$$\theta = e^{i\pi\nu/8}, \quad \alpha = (-1)^{(\nu+1)/2}$$

where ν is the Chern number only having odd values.

Moreover, the states $\left\{|\Phi^I\rangle, |\Phi^\epsilon\rangle\right\}$ corresponding to the fusion channels I and ϵ of vortices **A** and **B** also form an orthonormal basis for the same space. The transformation rule between these basis states are as follows

$$\begin{aligned} |\Omega^I\rangle &= \frac{1}{\sqrt{2}}\left(|\Phi^I\rangle + e^{i\varphi}|\Phi^\epsilon\rangle\right) \\ |\Omega^\epsilon\rangle &= \frac{1}{\sqrt{2}}\left(|\Phi^I\rangle - e^{i\varphi}|\Phi^\epsilon\rangle\right) \end{aligned}$$

up to a relative phase $e^{i\varphi}$ between $|\Phi^I\rangle$ and $|\Phi^\epsilon\rangle$. Therefore, the Berry matrix $\mathcal{B}$ in the basis $\left\{|\Phi^I\rangle, |\Phi^\epsilon\rangle\right\}$ is as follows

$$\begin{aligned} \mathcal{B}_\Phi &= \begin{pmatrix} \langle\Phi^I|\mathcal{B}_\Omega|\Phi^I\rangle & \langle\Phi^I|\mathcal{B}_\Omega|\Phi^\epsilon\rangle \\ \langle\Phi^\epsilon|\mathcal{B}_\Omega|\Phi^I\rangle & \langle\Phi^\epsilon|\mathcal{B}_\Omega|\Phi^\epsilon\rangle \end{pmatrix} \\ &= \frac{1}{2}\begin{pmatrix} R^1_{\sigma\sigma} + R^\epsilon_{\sigma\sigma} & e^{-i\varphi}(R^1_{\sigma\sigma} - R^\epsilon_{\sigma\sigma}) \\ e^{i\varphi}(R^1_{\sigma\sigma} - R^\epsilon_{\sigma\sigma}) & R^1_{\sigma\sigma} + R^\epsilon_{\sigma\sigma} \end{pmatrix}. \end{aligned} \tag{3.29}$$

On the other hand, the matrix elements of the Berry matrices Eq. 3.26 calculated for closed paths depends on the basis that we started with (i.e. the basis

[6]They also correspond to **A** and **D**. However determining fusion channel of **B** and **C** fixes the fusion channel for **A** and **D** since they all fuse into vacuum 1.

that $\mathcal{A}_2(\lambda_0)$ is written). In our calculations two nearly degenerate energy eigenstates $\{|\Phi^1(\lambda_0)\rangle, |\Phi^2(\lambda_0)\rangle\}$ are used to define a basis. Remarkably, numerical results suggest that

$$|\Phi^1(\lambda_0)\rangle \cong |\Phi^I\rangle \quad \text{and} \quad |\Phi^2(\lambda_0)\rangle \cong |\Phi^\epsilon\rangle.$$

This may be due to the way we separate **A** and **B**, and **C** and **D** preserves the symmetry of the relative positions of the vortices with respect to each other, however it still deserves further explanation.

For a configuration showed in Fig. 3.3, numerical results show that $\theta = e^{i\pi/8}$, $\alpha = -1$ and $\nu = 1$ with various accuracies depending on minimum distances d and the values of κ. These results are summarized in Fig. 3.7 and Table 3.1 where Frobenius norm (metric) has been used to measure the proximity of the numerical Berry matrix $\mathcal{B}_N$ to $\mathcal{B}_\Phi$.

Note that, Frobenius norm of an $n \times n$ matrix A defined as

$$|A| = \left(\sum_{i,j} |a_{ik}|^2 \right)^{1/2} = \sqrt{\mathrm{tr}(AA^\dagger)}. \tag{3.30}$$

Here, we calculate that norm $|\Delta|$ of $\Delta = \mathcal{B}_\Phi - \mathcal{B}_N$ to measure the distance between $\mathcal{B}_N$ and $\mathcal{B}_\Phi$. It is not difficult to show that the maximum Frobenius distance between two unitary matrix is equal to 2. Therefore, the half of the values in Fig. 3.7 and Table 3.1 express the difference within the range [0,1].

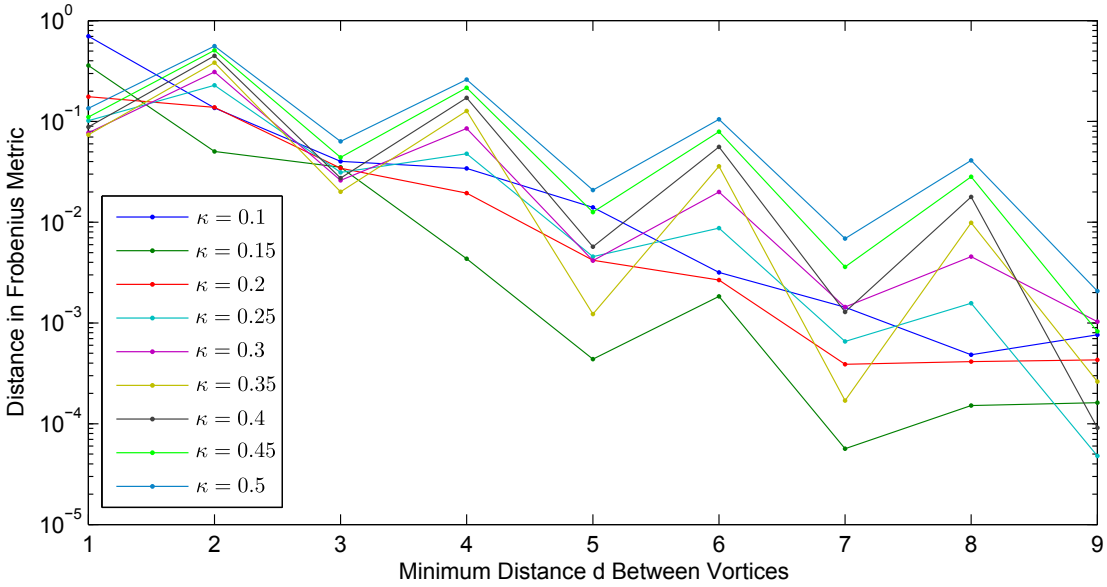

Figure 3.7: Calculation $0.997[J\kappa]$: Frobenious distance between $\mathcal{B}_N$ and $\mathcal{B}_\Phi$ vs. Minimum distance between vortices. The number of steps taken to cover the change in the value of $[J\kappa]$ of the link as follows: 3991 linear step and 9 circular steps. Note that, in our calculations $J = J_q^x = J_q^y = J_q^z = 1$ for all q and $\kappa = \kappa_q^x = \kappa_q^y = \kappa_q^5 = \kappa_q^6$ for all q (Eqs. 2.17−2.20) where κ have various values between 0.1 and 0.5.

	$\kappa = 0.1$	$\kappa = 0.15$	$\kappa = 0.2$	$\kappa = 0.25$	$\kappa = 0.3$	$\kappa = 0.35$	$\kappa = 0.4$	$\kappa = 0.45$	$\kappa = 0.50$
$d = 1$	6.1229×10^{-1}	3.5892×10^{-1}	1.7653×10^{-1}	1.0187×10^{-1}	7.6684×10^{-2}	7.4006×10^{-2}	8.8460×10^{-2}	1.1089×10^{-1}	1.3520×10^{-1}
$d = 2$	1.3611×10^{-1}	5.0328×10^{-2}	1.3823×10^{-1}	2.2908×10^{-1}	3.1060×10^{-1}	3.8354×10^{-1}	4.4895×10^{-1}	5.0783×10^{-1}	5.6099×10^{-1}
$d = 3$	4.0278×10^{-2}	3.5064×10^{-2}	3.4368×10^{-2}	3.1306×10^{-2}	2.6074×10^{-2}	2.0051×10^{-2}	2.7451×10^{-2}	4.4035×10^{-2}	6.3432×10^{-2}
$d = 4$	3.4217×10^{-2}	4.3510×10^{-3}	1.9470×10^{-2}	4.7854×10^{-2}	8.5127×10^{-2}	1.2727×10^{-1}	1.7159×10^{-1}	2.1638×10^{-1}	2.6055×10^{-1}
$d = 5$	1.4016×10^{-2}	4.3713×10^{-4}	4.1949×10^{-3}	4.5575×10^{-3}	4.1523×10^{-3}	1.2235×10^{-3}	5.7176×10^{-3}	1.2580×10^{-2}	2.0881×10^{-2}
$d = 6$	3.1718×10^{-3}	1.8359×10^{-3}	2.6673×10^{-3}	8.7248×10^{-3}	1.9958×10^{-2}	3.5956×10^{-2}	5.5987×10^{-2}	7.9227×10^{-2}	1.0488×10^{-1}
$d = 7$	1.4360×10^{-3}	5.6627×10^{-5}	3.8841×10^{-4}	6.5684×10^{-4}	1.4374×10^{-3}	1.6981×10^{-4}	1.2869×10^{-3}	3.5955×10^{-3}	6.8772×10^{-3}
$d = 8$	4.8331×10^{-4}	1.5179×10^{-4}	4.1290×10^{-4}	1.5690×10^{-3}	4.5531×10^{-3}	9.8876×10^{-3}	1.7800×10^{-2}	2.8280×10^{-2}	4.1164×10^{-2}
$d = 9$	7.6262×10^{-4}	1.6211×10^{-4}	4.2982×10^{-4}	4.7970×10^{-5}	1.0286×10^{-3}	2.6166×10^{-4}	9.1137×10^{-5}	8.2510×10^{-4}	2.0739×10^{-3}

Table 3.1: Calculation $0.997[J\kappa]$: Frobenious distance between $\mathcal{B}_N$ and $\mathcal{B}_\Phi$ vs. Minimum distance between vortices. The number of steps taken to cover the change in the value of $[J\kappa]$ of the link as follows: 3991 linear step and 9 circular steps. Note that, in our calculations $J = J_q^x = J_q^y = J_q^z = 1$ for all q and $\kappa = \kappa_q^x = \kappa_q^y = \kappa_q^5 = \kappa_q^6$ for all q (Eqs. 2.17−2.20) where κ have various values between 0.1 and 0.5.

As an example, for a vortex configuration illustrated in Fig. 3.3 with $d = 9$ and $\kappa = 0.25$, the numerical value of the Berry matrix $\mathcal{B}_N$ as follows

$$\mathcal{B}_N = \begin{pmatrix} 0.653270 + 0.270630i & 0.653280 + 0.270598i \\ -0.653280 - 0.270598i & 0.653296 + 0.270568i \end{pmatrix}$$

whose Frobenious distance to $\mathcal{B}_\Phi$

$$\mathcal{B}_\Phi = \frac{1}{\sqrt{2}} \begin{pmatrix} e^{i\pi/8} & e^{i\pi/8} \\ e^{-7i\pi/8} & e^{i\pi/8} \end{pmatrix} = \begin{pmatrix} 0.653281 + 0.270598i & 0.653281 + 0.270598i \\ -0.653281 - 0.270598i & 0.653281 + 0.270598i \end{pmatrix}$$

is equal 4.7970×10^{-5}. In other words, $\mathcal{B}_N$ is 0.0024% different from $\mathcal{B}_\Phi$. Note that, matrices were written for $e^{i\varphi} = -i$ (Eq. 3.29), which is an arbitrary phase factor that has been chosen to express $\mathcal{B}_\Phi$. There is also a similar relative phase chosen to work with the basis states $|\Phi^1(\lambda_0)\rangle$ and $|\Phi^2(\lambda_0)\rangle$ when calculating the Berry phase. Therefore, the matrix representation of both $\mathcal{B}_N$ and $\mathcal{B}_\Phi$ are written up to some relative phases between the elements of their basis $\{|\Phi^1(\lambda_0)\rangle, |\Phi^2(\lambda_0)\rangle\}$ and $\{|\Phi^I\rangle, |\Phi^\epsilon\rangle\}$ respectively.

Recall that to satisfy the smoothness condition, the trajectory consists of linear and circular parts. This condition also affects the beginning point of the closed trajectory as shown in Fig. 3.8. In our calculation, we started to change the first link $[J\kappa]^y_{2,N_y}$ from $0.997[J\kappa]$. Recall that, $[J\kappa]^y_{2,N_y} = \{J^y_{2,N_y}, \kappa^5_{1,N_y}, \kappa^6_{2,N_y}, \kappa^y_{2,N_y}\}$ denotes the set of the coupling coefficients of the first link of the trajectory to be changed to move the vortex **B** to the right plaquette (for more details *see* section 3.1) and $[J\kappa]$ denotes the general J and κ values used for every links, in our calculations $J = J^x_q = J^y_q = J^z_q = 1$ for all q and $\kappa = \kappa^x_q = \kappa^y_q = \kappa^5_q = \kappa^6_q$ for all q (Eqs. 2.17−2.20) where κ have various values between 0.1 and 0.5 as shown in the legends of the plots. Therefore the basis states of the calculated Berry matrices is slightly different than the energy eigenstates of the configuration in Fig. 3.3, where coupling coefficients of all links are $[J\kappa]$. This difference results in a little decrease in the accuracy. However, we can also compare the eigenvalues of $\mathcal{B}_N$ with that of $\mathcal{B}_\Phi$, to compensate for this difference of two basis. Fig. 3.9 and Table 3.2 show the distances of between diagonalized $\mathcal{B}_N$ and $\mathcal{B}_\Phi$ for the calculation $0.997[J\kappa]$ with improved values.

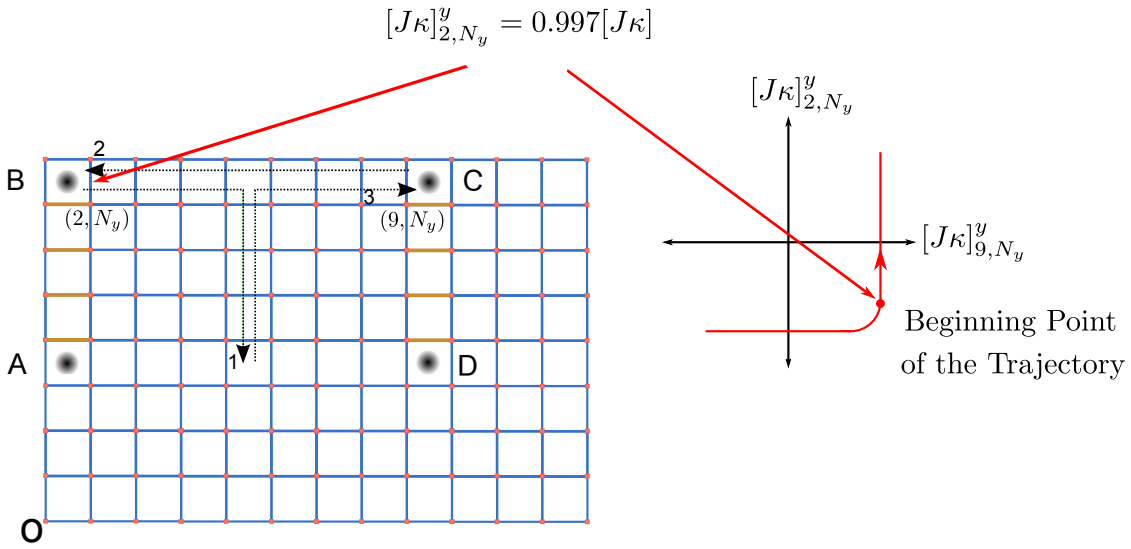

Figure 3.8: At the beginning point of the trajectory, the coupling coefficients of the first link is slightly smaller than other links. Note that, in our calculations $J = J^x_q = J^y_q = J^z_q = 1$ for all q and $\kappa = \kappa^x_q = \kappa^y_q = \kappa^5_q = \kappa^6_q$ for all q (Eqs. 2.17−2.20) where κ have various values between 0.1 and 0.5.

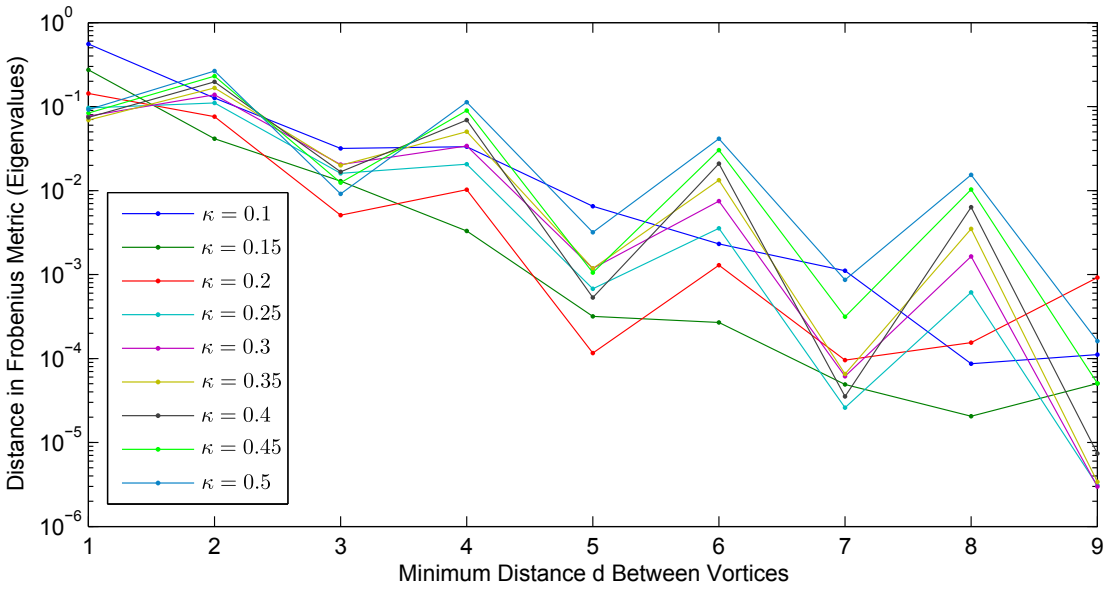

Figure 3.9: Calculation $0.997[J\kappa]$: Frobenious distance between diagonalized $\mathcal{B}_N$ and $\mathcal{B}_\Phi$ vs. Minimum distance between vortices. The number of steps taken to cover the change in the value of $[J\kappa]$ of the link as follows: 3991 linear step and 9 circular steps. Note that, in our calculations $J = J_q^x = J_q^y = J_q^z = 1$ for all q and $\kappa = \kappa_q^x = \kappa_q^y = \kappa_q^5 = \kappa_q^6$ for all q (Eqs. 2.17−2.20) where κ have various values between 0.1 and 0.5.

	$\kappa = 0.1$	$\kappa = 0.15$	$\kappa = 0.2$	$\kappa = 0.25$	$\kappa = 0.3$	$\kappa = 0.35$	$\kappa = 0.4$	$\kappa = 0.45$	$\kappa = 0.50$
$d = 1$	5.5738×10^{-1}	2.7392×10^{-1}	1.4299×10^{-1}	9.6641×10^{-2}	7.6584×10^{-2}	6.9092×10^{-2}	7.4138×10^{-2}	8.3580×10^{-2}	9.1824×10^{-2}
$d = 2$	1.2662×10^{-1}	4.1486×10^{-2}	7.5703×10^{-2}	1.1028×10^{-1}	1.3841×10^{-1}	1.6647×10^{-1}	1.9701×10^{-1}	2.3013×10^{-1}	2.6511×10^{-1}
$d = 3$	3.1792×10^{-2}	1.2955×10^{-2}	5.1021×10^{-3}	1.5992×10^{-2}	2.0370×10^{-2}	1.9933×10^{-2}	1.6693×10^{-2}	1.2420×10^{-2}	9.1366×10^{-3}
$d = 4$	3.3331×10^{-2}	3.3007×10^{-3}	1.0239×10^{-2}	2.0566×10^{-2}	3.4002×10^{-2}	5.0170×10^{-2}	6.8884×10^{-2}	8.9835×10^{-2}	1.1258×10^{-1}
$d = 5$	6.5033×10^{-3}	3.1676×10^{-4}	1.1610×10^{-4}	6.7643×10^{-4}	1.1835×10^{-3}	1.1826×10^{-3}	5.3189×10^{-4}	1.0549×10^{-3}	3.1860×10^{-3}
$d = 6$	2.3197×10^{-3}	2.6920×10^{-4}	1.2901×10^{-3}	3.5587×10^{-3}	7.4854×10^{-3}	1.3264×10^{-2}	2.0912×10^{-2}	3.0344×10^{-2}	4.1412×10^{-2}
$d = 7$	1.1075×10^{-3}	4.9014×10^{-5}	9.5535×10^{-5}	2.5933×10^{-5}	6.1463×10^{-5}	6.5410×10^{-5}	3.5362×10^{-5}	3.1350×10^{-4}	8.6554×10^{-4}
$d = 8$	8.6440×10^{-5}	2.0579×10^{-5}	1.5489×10^{-4}	6.1193×10^{-4}	1.6392×10^{-3}	3.4906×10^{-3}	6.3448×10^{-3}	1.0299×10^{-2}	1.5378×10^{-2}
$d = 9$	1.1129×10^{-4}	5.0269×10^{-5}	3.9419×10^{-4}	3.0784×10^{-6}	2.9750×10^{-6}	3.4057×10^{-6}	7.3888×10^{-6}	5.0728×10^{-5}	1.6157×10^{-4}

Table 3.2: Calculation $0.997[J\kappa]$: Frobenious distance between diagonalized $\mathcal{B}_N$ and $\mathcal{B}_\Phi$ vs. Minimum distance between vortices. The number of steps taken to cover the change in the value of $[J\kappa]$ of the link as follows: 3991 linear step and 9 circular steps. Note that, in our calculations $J = J_q^x = J_q^y = J_q^z = 1$ for all q and $\kappa = \kappa_q^x = \kappa_q^y = \kappa_q^5 = \kappa_q^6$ for all q (Eqs. 2.17−2.20) where κ have various values between 0.1 and 0.5.

As an example, for a vortex configuration showed in Fig. 3.3 with $d = 9$ and $\kappa = 0.30$ the eigenvalues of $\mathcal{B}_N$ and $\mathcal{B}_\Phi$ are as follows

$$\begin{aligned} 0.3826813 + 0.9238804i &\simeq 0.3826834 + 0.9238795i = e^{3i\pi/8} \\ 0.9238802 - 0.3826817i &\simeq 0.9238795 - 0.3826834i = e^{-i\pi/8} \end{aligned}$$

so that the Frobenious distance between diagonalized $\mathcal{B}_N$ and diagonalized $\mathcal{B}_\Phi$ is equal to 2.9750×10^{-6}. In other words, diagonalized $\mathcal{B}_N$ is 0.00015% different from the diagonalized $\mathcal{B}_\Phi$.

The eigenvalues of the Berry matrix is less sensitive to the changes in the numbers of linear and circular steps taken to cover every link on the trajectory of the links show in Fig. 3.3. In this respect, Fig. 3.10 summarize the results of the Berry matrix analysis where all links on the trajectory were covered in 4000 steps consisting of 3801 linear step and 199 circular steps, all having equal curve length. This also means that the beginning point of the trajectory in the parameter space corresponds to a coupling coefficient configuration where coupling coefficients of all links are $[J\kappa]$ except $[J\kappa]^y_{2,N_y} = 0.937[J\kappa]$ with $J = J^x_q = J^y_q = J^z_q = 1$ for all q and $\kappa = \kappa^x_q = \kappa^y_q = \kappa^5_q = \kappa^6_q$ for all q (Eqs. 2.17−2.20) where κ have various values between 0.1 and 0.5.

In addition to that, Table 3.3 shows the Frobenius norm between two diagonalized $\mathcal{B}_N$ which were got from the calculations $0.997[J\kappa]$ and $0.937[J\kappa]$. Values are relatively small so we can say that comparing the eigenvalues of the Berry matrices is more meaningful measure than comparing the matrices. This can also be seen when we compare Fig. 3.10(b) with Fig. 3.9. Whereas, the comparison of Fig. 3.10(a) with Fig. 3.7 shows how a slight change of the beginning points from $[J\kappa]^y_{2,N_y} = 0.997[J\kappa]$ to $[J\kappa]^y_{2,N_y} = 0.937[J\kappa]$ affects the comparison between $\mathcal{B}_N$ and $\mathcal{B}_\Phi$.

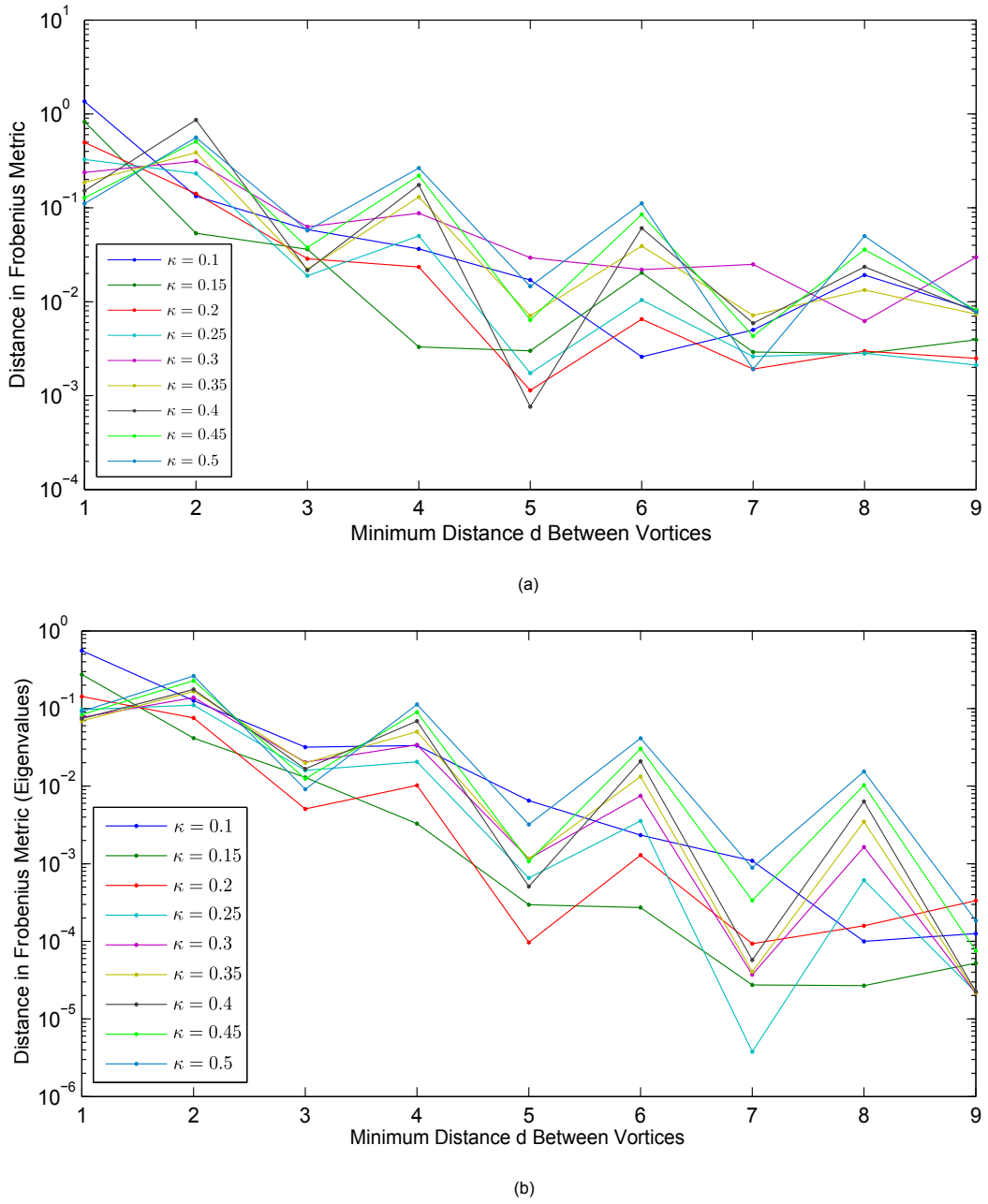

Figure 3.10: Calculation $0.937[J\kappa]$: (a) Frobenious distance between $\mathcal{B}_N$ and $\mathcal{B}_\Phi$ vs. Minimum distance between vortices. (b) Frobenious distance between diagonalized $\mathcal{B}_N$ and $\mathcal{B}_\Phi$ vs. Minimum distance between vortices. The number of steps taken to cover the change in the value of $[J\kappa]$ of the link as follows: 3801 linear step and 199 circular steps. Note that, in our calculations $J = J_q^x = J_q^y = J_q^z = 1$ for all q and $\kappa = \kappa_q^x = \kappa_q^y = \kappa_q^5 = \kappa_q^6$ for all q (Eqs. 2.17−2.20) where κ have various values between 0.1 and 0.5.

	$\kappa = 0.1$	$\kappa = 0.15$	$\kappa = 0.2$	$\kappa = 0.25$	$\kappa = 0.3$	$\kappa = 0.35$	$\kappa = 0.4$	$\kappa = 0.45$	$\kappa = 0.50$
$d = 1$	1.2190×10^{-4}	1.6614×10^{-4}	1.9593×10^{-4}	2.2233×10^{-4}	2.3136×10^{-4}	2.4317×10^{-4}	2.5189×10^{-4}	2.5736×10^{-4}	2.5975×10^{-4}
$d = 2$	1.9291×10^{-5}	1.1039×10^{-5}	1.5527×10^{-5}	1.5831×10^{-5}	1.5084×10^{-5}	1.4544×10^{-5}	1.4523×10^{-5}	1.4530×10^{-5}	1.4684×10^{-5}
$d = 3$	3.0497×10^{-5}	2.3390×10^{-5}	2.1893×10^{-5}	2.1993×10^{-5}	2.1891×10^{-5}	2.1470×10^{-5}	2.1378×10^{-5}	2.1999×10^{-5}	2.1096×10^{-5}
$d = 4$	1.0803×10^{-5}	1.8707×10^{-5}	2.1116×10^{-5}	2.1922×10^{-5}	2.1914×10^{-5}	2.1163×10^{-5}	1.9764×10^{-5}	1.7942×10^{-5}	1.5958×10^{-5}
$d = 5$	1.2365×10^{-5}	2.3273×10^{-5}	2.1318×10^{-5}	2.2960×10^{-5}	2.3807×10^{-5}	2.3957×10^{-5}	2.3419×10^{-5}	2.2257×10^{-5}	2.0597×10^{-5}
$d = 6$	1.5335×10^{-5}	1.8441×10^{-5}	2.1371×10^{-5}	2.3242×10^{-5}	2.4252×10^{-5}	2.4768×10^{-5}	2.4749×10^{-5}	2.4221×10^{-5}	2.3240×10^{-5}
$d = 7$	1.4292×10^{-5}	4.3371×10^{-5}	1.9460×10^{-5}	2.3194×10^{-5}	2.4370×10^{-5}	2.5124×10^{-5}	2.5205×10^{-5}	2.5067×10^{-5}	2.4338×10^{-5}
$d = 8$	1.4150×10^{-5}	1.8447×10^{-5}	2.1457×10^{-5}	2.3204×10^{-5}	2.4398×10^{-5}	2.5070×10^{-5}	2.5332×10^{-5}	2.5253×10^{-5}	2.4867×10^{-5}
$d = 9$	1.4961×10^{-5}	1.8489×10^{-5}	6.8265×10^{-5}	2.3067×10^{-5}	2.4430×10^{-5}	2.5096×10^{-5}	1.8562×10^{-5}	2.5352×10^{-5}	2.5106×10^{-5}

Table 3.3: Frobenious distance between two diagonalized $\mathcal{B}_N$ which were got from the calculations $0.997[J\kappa]$ and $0.937[J\kappa]$ vs Minimum distance between vortices. Note that, in our calculations $J = J_q^x = J_q^y = J_q^z = 1$ for all q and $\kappa = \kappa_q^x = \kappa_q^y = \kappa_q^5 = \kappa_q^6$ for all q (Eqs. 2.17−2.20) where κ have various values between 0.1 and 0.5.

Note that, the validity of the adiabatic approximation is essential for understanding oscillations seen in Fig. 3.7 and Fig. 3.9. Let us restate the non-Abelian version of the adiabatic approximation

$$\langle\varphi^{(m,b)}(\lambda)|\frac{d}{dt}\varphi^{(n,a)}(\lambda)\rangle = \frac{\langle\varphi^{(m,b)}(\lambda(t))|\frac{d}{dt}H(\lambda)|\varphi^{(n,a)}(\lambda)\rangle}{E_n(\lambda) - E_m(\lambda)} \cong 0, \tag{3.31}$$

for all $m \neq n$ and for all a, b, where m, n denotes different degenerate energy spaces and a, b labels different states within each degenerate space. Recall that, when the system is nearly degenerate then the smallness of the ratio $G_{(n,b),(n,a)}(\lambda)/G_{m,n}(\lambda)$ determines the validness of the adiabatic approximation. Let us have closer look into the nature of the these gaps in our system.

For each point of the trajectory shown in Fig. 3.3, the vortices are always separated by at least d plaquettes, therefore the system have two nearly-zero-energy fermions namely γ_1, γ_2[7], which generates two fold degenerate ground-state space with basis elements $|\Phi^1\rangle, |\Phi^2\rangle$. This ground-state space is separated from the first excite state $|\Phi^3\rangle$ by a gap. The energy difference between the lowest three energy eigenstates $|\Phi^1\rangle, |\Phi^2\rangle, |\Phi^3\rangle$ are related to whether the system contains odd or even number of fermions (i.e. whether the number elements in $i-$part of Eq. 2.36 is odd or even[8]). Table 3.4 explicitly shows the lowest three energy eigenstates $|\Phi^1\rangle, |\Phi^2\rangle, |\Phi^3\rangle$ and their energies $E_{|\Phi^1\rangle}, E_{|\Phi^2\rangle}, E_{|\Phi^3\rangle}$ of the systems containing odd/even number of fermions.

According to Table 3.4, the gap $G_{3,2}$ between nearly-degenerate space and higher excited states is always equal to $E_3 - E_2$ irrespective of whether system is odd or even, although the gap $G_{2,1}$ between nearly-degenerate states is either $E_1 + E_2$ or $E_2 - E_1$ for even and odd systems, respectively.

It is remarkable that a system could change from even to odd (or vica versa) while we move along the trajectory. By assigning, 1 and 0 to the even and odd systems respectively, we can calculate the average evenness/oddness of each configuration

[7]Recall that fermions are indexed according to their energies, from lowest to the highest.

[8]Recall that we only simulate the vortex excitation by adopting the J and κ values, so $X_q = Y_q = 1$ for all q. Therefore, $\{W_p, L_x, L_y\}$ always matches with $\{Q_q, L_x, L_y\}$ (*see* section 2.6.2 for more details).

Even/Odd	Eigenstates	Energies
Even	$\|\Phi^1\rangle = \|\phi\rangle$	$E_{\|\Phi^1\rangle} = E_{\|\phi\rangle}$
	$\|\Phi^2\rangle = \gamma_2^\dagger\gamma_1^\dagger\|\phi\rangle$	$E_{\|\Phi^2\rangle} = E_{\|\phi\rangle} + E_1 + E_2$
	$\|\Phi^3\rangle = \gamma_3^\dagger\gamma_1^\dagger\|\phi\rangle$	$E_{\|\Phi^3\rangle} = E_{\|\phi\rangle} + E_1 + E_3$
Odd	$\|\Phi^1\rangle = \gamma_1^\dagger\|\phi\rangle$	$E_{\|\Phi^1\rangle} = E_{\|\phi\rangle} + E_1$
	$\|\Phi^2\rangle = \gamma_2^\dagger\|\phi\rangle$	$E_{\|\Phi^2\rangle} = E_{\|\phi\rangle} + E_2$
	$\|\Phi^3\rangle = \gamma_3^\dagger\|\phi\rangle$	$E_{\|\Phi^3\rangle} = E_{\|\phi\rangle} + E_3$

Table 3.4: The lowest three energy eigenstates $|\Phi^1\rangle, |\Phi^2\rangle, |\Phi^3\rangle$ and their energies $E_{|\Phi^1\rangle}, E_{|\Phi^2\rangle}, E_{|\Phi^3\rangle}$ of the system are given explicitly for systems having odd/even number of fermions. Note that, E_i is the energy of γ_i-fermion, and $\gamma_i|\phi\rangle = 0$ for all i where $|\phi\rangle$ is given explicitly in Eq. 2.36 as $|\phi\rangle = \prod_i a_i^\dagger \prod_p (u_p + v_p a_p^\dagger a_{\bar{p}}^\dagger)|-\rangle$ having the energy $E_{|\phi\rangle} = \sum_i E_i/2$.

which depends on d, κ values. Fig. 3.11(a) shows this average value against d for various κ values. Similar type of oscillation as in Fig. 3.7 and Fig. 3.9 can be seen in this figure too, and this oscillations also affect the gap $G_{2,1}$. Recall that, $G_{2,1}/G_{3,2}$ is an essential quantity for the validity of the adiabatic approximation. Again, Fig. 3.11(b) shows the average value of the ratio $G_{2,1}/G_{3,2}$ along the trajectory for various κ values and minimum distances d between vortices. These oscillations in Fig. 3.11(b) could be the reason for the oscillations seen in Fig. 3.7 and Fig. 3.9.

Moreover, Fig. 3.11(a) also shows that when d is even, the system almost always contains even number of fermions, although when d is odd the system is almost half even and half odd. This is especially true for large κ values. The underlying relation between minimum distance d between vortices and evenness/oddness of the system needs further analysis. For this analysis, it could be helpful to restate the relation between the size of the systems and d

$$\begin{aligned} N_x = 3d+1, \quad N_y &= 2d \quad \text{for odd } d \\ N_x = 3d, \qquad N_y &= 2d \quad \text{for even } d \end{aligned}$$

which was discussed under Fig.3.3 before.

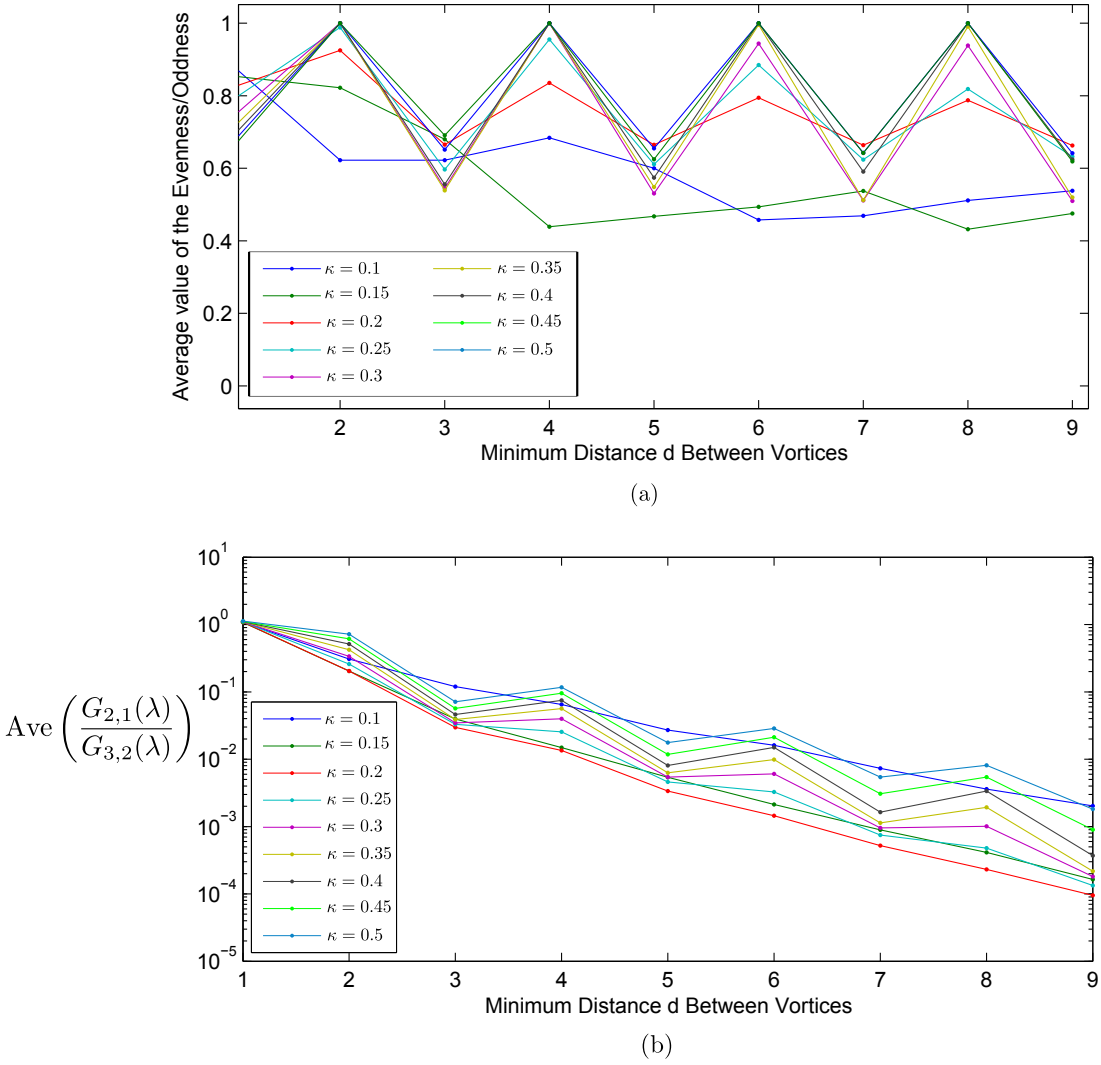

Figure 3.11: (a) Average evenness/oddness of the configurations along the trajectory vs. Minimum distance d between vortices for various κ values. Average evenness/oddness along the trajectory is calculated after assigning 1 and 0 to the even and odd systems respectively. (b) Average of the ratio $G_{2,1}/G_{3,2}$ along the trajectory vs. Minimum distance between vortices ($G_{2,1}$ is the gap between nearly-degenerate states, and $G_{3,2}$ is the gap between nearly-degenerate space and higher excited states). As a general note, the number of steps taken to cover the change in the value of $[J\kappa]$ of the link as follows: 3991 linear step and 9 circular steps. Note that, in our calculations $J = J_q^x = J_q^y = J_q^z = 1$ for all q and $\kappa = \kappa_q^x = \kappa_q^y = \kappa_q^5 = \kappa_q^6$ for all q (Eqs. 2.17−2.20) where κ have various values between 0.1 and 0.5.

As a final result, we will present an analysis on the unitarity of calculated Berry matrix. The unitarity of the calculated Berry matrices can be investigated by checking the Frobenius distance between $\mathcal{B}_N\mathcal{B}_N^\dagger$ and 2-by-2 identity matrix I. These results are summarized in Table 3.5 and Table 3.6 respectively for calculations $0.997[J\kappa]$ and $0.937[J\kappa]$. These analysis could also be considered as a measure for the accuracy of the Berry matrix calculations.

	$\kappa = 0.1$	$\kappa = 0.15$	$\kappa = 0.2$	$\kappa = 0.25$	$\kappa = 0.3$	$\kappa = 0.35$	$\kappa = 0.4$	$\kappa = 0.45$	$\kappa = 0.50$
$d = 1$	4.1267×10^{-10}	4.3663×10^{-10}	3.8781×10^{-10}	2.8238×10^{-10}	1.3563×10^{-10}	4.4136×10^{-11}	2.2331×10^{-10}	3.9918×10^{-10}	5.5852×10^{-10}
$d = 2$	2.0115×10^{-11}	2.4115×10^{-11}	7.4814×10^{-11}	3.3293×10^{-10}	1.4185×10^{-11}	4.7546×10^{-10}	4.7153×10^{-10}	4.3423×10^{-10}	4.2256×10^{-10}
$d = 3$	1.2784×10^{-10}	1.3386×10^{-12}	1.2917×10^{-11}	8.1709×10^{-11}	3.6136×10^{-10}	2.2017×10^{-10}	3.6572×10^{-11}	4.1213×10^{-11}	8.2458×10^{-11}
$d = 4$	2.6521×10^{-10}	1.4256×10^{-11}	4.8390×10^{-11}	4.5252×10^{-10}	8.0272×10^{-12}	9.8229×10^{-10}	6.0448×10^{-10}	4.8537×10^{-10}	4.3817×10^{-10}
$d = 5$	8.3661×10^{-12}	2.3711×10^{-9}	5.3036×10^{-12}	3.9197×10^{-11}	3.0126×10^{-10}	1.0288×10^{-9}	2.4533×10^{-10}	9.7242×10^{-11}	1.0874×10^{-10}
$d = 6$	3.1791×10^{-11}	6.2327×10^{-12}	2.8182×10^{-11}	4.6115×10^{-10}	2.6187×10^{-11}	1.4386×10^{-9}	8.1385×10^{-10}	6.4016×10^{-10}	5.4648×10^{-10}
$d = 7$	4.6333×10^{-11}	9.3927×10^{-11}	7.9391×10^{-10}	5.0077×10^{-11}	5.1818×10^{-10}	1.6789×10^{-9}	7.6676×10^{-10}	5.0283×10^{-10}	3.9963×10^{-10}
$d = 8$	2.5268×10^{-10}	1.8549×10^{-11}	3.3908×10^{-11}	4.9457×10^{-12}	2.8278×10^{-12}	4.8870×10^{-12}	1.5901×10^{-11}	3.3561×10^{-11}	5.0910×10^{-11}
$d = 9$	1.5238×10^{-11}	1.2366×10^{-10}	3.0521×10^{-8}	5.8051×10^{-11}	8.2174×10^{-10}	3.1848×10^{-11}	7.3581×10^{-10}	8.6837×10^{-11}	7.9491×10^{-11}

Table 3.5: Frobenius distance between $\mathcal{B}_N \mathcal{B}_N^\dagger$ and 2-by-2 identity matrix I for various d and κ values. The number of steps taken to cover every link is as follows: 3991 linear step and 9 circular steps. Note that, in our calculations $J = J_q^x = J_q^y = J_q^z = 1$ for all q and $\kappa = \kappa_q^x = \kappa_q^y = \kappa_q^5 = \kappa_q^6$ for all q (Eqs. 2.17−2.20) where κ have various values between 0.1 and 0.5.

	$\kappa = 0.1$	$\kappa = 0.15$	$\kappa = 0.2$	$\kappa = 0.25$	$\kappa = 0.3$	$\kappa = 0.35$	$\kappa = 0.4$	$\kappa = 0.45$	$\kappa = 0.50$
$d = 1$	6.9811×10^{-12}	1.5011×10^{-11}	1.6395×10^{-11}	1.2706×10^{-11}	5.7968×10^{-12}	3.1084×10^{-12}	1.2490×10^{-11}	2.1625×10^{-11}	2.9989×10^{-11}
$d = 2$	8.4484×10^{-13}	9.4426×10^{-13}	3.1654×10^{-12}	1.4375×10^{-11}	6.4673×10^{-13}	2.0686×10^{-11}	1.1691×10^{-11}	2.0996×10^{-11}	1.9276×10^{-11}
$d = 3$	4.8979×10^{-12}	3.1226×10^{-13}	8.1126×10^{-13}	3.3346×10^{-12}	1.7509×10^{-11}	9.7178×10^{-12}	1.6731×10^{-12}	1.9430×10^{-12}	3.5888×10^{-12}
$d = 4$	6.1821×10^{-12}	6.8167×10^{-13}	1.2406×10^{-12}	1.0707×10^{-11}	2.8480×10^{-13}	2.2007×10^{-11}	1.3800×10^{-11}	1.1008×10^{-11}	9.8008×10^{-12}
$d = 5$	5.6478×10^{-13}	4.3627×10^{-11}	5.5466×10^{-12}	1.1054×10^{-12}	7.0653×10^{-12}	2.2627×10^{-11}	5.1440×10^{-12}	2.2261×10^{-12}	2.3344×10^{-12}
$d = 6$	9.9971×10^{-13}	4.5689×10^{-13}	5.8483×10^{-12}	1.0776×10^{-11}	6.8154×10^{-13}	3.0991×10^{-11}	1.7377×10^{-11}	1.3294×10^{-11}	1.1106×10^{-11}
$d = 7$	9.0074×10^{-13}	1.5633×10^{-10}	7.5085×10^{-10}	1.8690×10^{-12}	7.4077×10^{-11}	2.9025×10^{-12}	3.2452×10^{-12}	8.8946×10^{-12}	1.4571×10^{-12}
$d = 8$	1.0161×10^{-11}	8.9676×10^{-13}	8.5276×10^{-11}	1.5088×10^{-12}	1.8823×10^{-12}	8.9688×10^{-13}	4.1219×10^{-12}	4.1975×10^{-12}	2.2304×10^{-12}
$d = 9$	8.2527×10^{-11}	1.1829×10^{-10}	2.6604×10^{-08}	2.4675×10^{-12}	7.0492×10^{-11}	1.2469×10^{-12}	5.0974×10^{-09}	3.7978×10^{-12}	3.4155×10^{-12}

Table 3.6: Frobenius distance between $\mathcal{B}_N \mathcal{B}_N^\dagger$ and 2-by-2 identity matrix I for various d and κ values. The number of steps taken to cover every link is as follows: 3801 linear step and 199 circular steps. Note that, in our calculations $J = J_q^x = J_q^y = J_q^z = 1$ for all q and $\kappa = \kappa_q^x = \kappa_q^y = \kappa_q^5 = \kappa_q^6$ for all q (Eqs. 2.17−2.20) where κ have various values between 0.1 and 0.5.

Chapter 4

SUMMARY AND CONCLUSIONS

In this chapter we highlight the main results and open problems presented in the thesis.

In the introduction chapter we gave a mathematical foundation for the existence of non-Abelian anyons and then gave examples of physical systems where non-Abelian anyons are realized. It also gives a brief description of topological quantum computation which shows the practical importance of the study of non-Abelian anyons.

In the second chapter we studied the Kitaev honeycomb model which is one the systems where non-Abelian anyons are realized. The Kitaev model is an exactly solvable model in terms of its eigenvalues and eigenstates. In this chapter, the model is solved after its Hamiltonian is expressed in terms of fermions which are defined on the honeycomb lattice. Resulting Hamiltonian has quadratic fermionic structure which can be solved exactly with the method explained in the text. Note that, this method also includes a simple numerical analysis. The ground states of the model are written by using Bloch-Messiah theorem which was also discussed in the text, and we concluded the chapter by showing that vortices of the Kitaev honeycomb model are Ising type non-Abelian anyons.

In the third chapter, we studied the non-Abelian Berry phase resulting from the adiabatic exchange of vortices of the Kitaev honeycomb model. We first introduced a way to move vortices adiabatically, then gave a brief introduction to the Berry phase. We also discussed some numerical techniques required to calculate it. The use of the Thouless' theorem gave us another way to write down the eigenstates of the quadratic fermionic Hamiltonians so that we were able to calculate the Berry phase numerically. All these theoretical tools are applied to calculate the non-Abelian Berry

phase resulting from the exchange of two vortices of the Kitaev honeycomb model.

Note that, exchanging of non-Abelian anyons is an essential part for topological quantum computation. In this thesis, we developed a theory of how to exchange non-Abelian anyons of the Kitaev honeycomb model and calculated the non-Abelian Berry phase resulting from the exchange of two non-Abelian anyons by using numerical tools. The method developed here can also be used to calculate the Berry phases for any finite dimensional systems with quadratic fermionic Hamiltonian numerically.

One of the results that we found here is that the energy eigenstates of the configuration that was used to calculate the Berry phase corresponds to fusion channels of some non-Abelian anyons in the configuration. This relation is explained in text by using arguments related to the symmetrical coordinates of the vortices on the lattice with respect to each other. However the relation between fusion channels and the energy eigenstates of the system is one of the open problems that can be addressed in a more general way by research in future.

We also studied the closeness of the calculated Berry phase to the expected Berry phase for various system sizes which is determined by the minimum distance d between vortices. It is observed that as d increases calculated values gets exponentially closer to expected ones with some oscillations. The maximum and minimum values of these oscillations are seen at the even and odd values of d respectively. Moreover, as d increases the ratio of the gap between two nearly-degenerate ground states to the gap between the first excited states and the nearly-degenerate ground-state space gets exponentially smaller with same types of oscillations. This ratio is an important quantity for justifying the validness of the adiabatic approximation. Therefore, as the adiabatic approximation becomes more valid we get better numerical values for the Berry phase, which is not surprising.

The reason of the oscillations seen on the odd and even values of d could be explained by the average oddness/evenness of the system along the trajectory. To be more precise, the number of fermions contained in the system could change from even to odd (or vica versa) while we move along the trajectory. The gap between

the nearly-degenerate ground states depends on oddness/evenness of the system such that odd systems have smaller gap as explained in the text. This also affects the validness of the adiabatic approximation too. By assigning, 1 and 0 to the even and odd systems respectively, we can calculate the average evenness/oddness of each configuration. A similar type of oscillation are seen there too. Therefore, we can say that adiabatic approximation is more valid for the odd systems than the even systems. However, the underlying relation between minimum distance d between vortices and evenness/oddness of the system needs further analysis.

From the point of its contributions to the other research, the thesis could be very helpful for the purpose of studying topologically ordered system at the microscopic scale. For example, since the Kitaev Honeycomb model can have both Abelian and non-Abelian phases depending on the values of coupling coefficients J and κ, it is possible to carry vortices from the non-Abelian phase to Abelian phase and to study their topological phase transition. Moreover, note that Ising type of non-Abelian anyons carry Majorana fermions. Therefore the method developed here can also be used to study the effect of brading or the effect of carrying vortices from to non-Abelian phase to Abelian phase to the internal structure of the Majorana fermions.

Overall, a detailed description of how to move vortices adiabatically could be valuable guide for experiments. However, the most important achievement of this thesis is that it presents a tool for studying the exotic statistical behavior of non-Abelian anyons in detail so that it can be used for testing predictions about the nature and behavior of non-Abelian anyons. In other words, the Kitaev honeycomb model can be considered now as a system where numerical experiments on the non-Abelian anyons can take place.

BIBLIOGRAPHY

[1] Dirac, P. A. M. *The principles of quantum mechanics*. Oxford University Press, 4th edition, (1982).

[2] Schiff, L. *Quantum mechanics*. McGraw-Hill Companies, 2nd edition, (1968).

[3] Messiah, A. *Quantum mechanics*. North-Holland Pub. Co, (1962).

[4] Merzbacher, E. *Quantum mechanics*. J. Wiley, 2nd edition, (1970).

[5] Sakurai, J. J. *Modern Quantum Mechanics*. Addison Wesley, 2nd edition, (2010).

[6] Messiah, A. and Greenberg, O. *Phys. Rev.* **136**, B248 (1964).

[7] Girardeau, M. *Phys. Rev.* **139**, B500 (1965).

[8] Mirman, R. *Nuo. Cim.* **18 B**, 110 (1973).

[9] Leinaas, J. M. and Myrheim, J. *Nuo. Cim.* **37 B**, 1 (1977).

[10] Laidlaw, M. and DeWitt, C. *Phys. Rev. D* **3**, 1375 (1971).

[11] Wu, Y.-S. *Phys. Rev. Lett.* **52**, 2103 (1984).

[12] Green, H. *Phys. Rev.* **90**, 270 (1953).

[13] Drühl, K., Haag, R., and Roberts, J. E. *Comm. Math. Phys.* **18**, 204 (1970).

[14] Kitaev, A. *Ann. Phys.* **321**, 2 (2006).

[15] Nayak, C., Stern, A., Freedman, M., and Das Sarma, S. *Rev. Mod. Phys.* **80**, 1083 (2008).

[16] Moore, G. and Read, N. *Nucl. Phys. B* **360**, 362 (1991).

[17] Nayak, C. and Wilczek, F. *Nucl. Phys. B* **479**, 529 (1996).

[18] Read, N. and Rezayi, E. *Phys. Rev. B* **59**, 8084 (1999).

[19] Slingerland, J. and Bais, F. *Nucl. Phys. B* **612**, 229 (2001).

[20] Rezayi, E. and Read, N. *Phys. Rev. B* **79**, 075306 (2009).

[21] Read, N. and Green, D. *Phys. Rev. B* **61**, 10267 (2000).

[22] Stern, A. *Nature* **464**, 187 (2010).

[23] Kitaev, A. *Ann. Phys.* **303**, 2 (2003).

[24] Freedman, M. H., Kitaev, A., Larsen, M. J., and Wang, Z. *Bull. Amer. Math. Soc.* **40**, 31 (2002).

[25] Sarma, S. D., Freedman, M., and Nayak, C. *Phys. Tod.* **59**, 32 (2006).

[26] Ivanov, D. *Phys. Rev. Lett.* **86**, 268 (2001).

[27] Tserkovnyak, Y. and Simon, S. *Phys. Rev. Lett.* **90**, 016802 (2003).

[28] Baskaran, G., Mandal, S., and Shankar, R. *Phys. Rev. Lett.* **98**, 247201 (2007).

[29] Chen, H.-D. and Nussinov, Z. *J. Phys. A* **41**, 075001 (2008).

[30] Vidal, J., Schmidt, K. P., and Dusuel, S. *Phys. Rev. B* **78**, 245121 (2008).

[31] Kells, G., Slingerland, J., and Vala, J. *Phys. Rev. B* **80**, 125415 (2009).

[32] Yao, H. and Kivelson, S. *Phys. Rev. Lett.* **99**, 247203 (2007).

[33] Yang, H.-Y., Laeuchli, A., Mila, F., and Schmidt, K. *arXiv:1006.5649* (2010).

[34] Lieb, E. H. *Phys. Rev. Lett.* **73**(16), 2158 (1994).

[35] Kells, G., Bolukbasi, A., Lahtinen, V., Slingerland, J., Pachos, J., and Vala, J. *Phys. Rev. Lett.* **101**, 240404 (2008).

[36] Blaizot, J. and Ripka, G. *Quantum Theory of Finite Systems.* MIT Press, 1st edition, (1986).

[37] Ring, P. and Schuck, P. *The Nuclear Many-Body Problem.* Springer, 3rd edition, (2004).

[38] Bloch, C. and Messiah, A. *Nucl. Phys.* **39**, 95 (1962).

[39] Lahtinen, V. and Pachos, J. K. *N. J. Phys* **11**, 093027 (2009).

[40] Bohm, A., Mostafazadeh, A., Koizumi, H., Niu, Q., and Zwanziger, J. *The Geometric Phase in Quantum Systems: Foundations, Mathematical Concepts, and Applications in Molecular and Condensed Matter Physics.* Springer, (2009).

[41] Wilczek, F. and Zee, A. *Phys. Rev. Lett.* **52**, 2111 (1984).

[42] Peskin, M. E. and Schroeder, D. V. *An Introduction To Quantum Field Theory.* Westview Press, (1995).

[43] Mathews, J. H. and Fink, K. K. *Numerical Methods Using Matlab.* Prentice Hall, 4th edition, (2004).

[44] Onishi, N. *Nucl. Phys.* **80**, 367 (1966).

[45] Thouless, D. *Nucl. Phys.* **31**, 211 (1962).

[46] Robledo, L. *Phys. Rev. C* **79**, 021302 (2009).

[47] Zumino, B. *J. Math. Phys.* **3**, 1055 (1962).

[48] Silvester, J. R. *Math. Gaz.* **84**, 460 (2000).